

**COOPERATIVE EFFECTS IN
VIBRATED GRANULAR
SYSTEMS**

Hector Adrian Pacheco Martinez, MSc.

Thesis submitted to the University of Nottingham
for the degree of Doctor of Philosophy

December 2013



IMAGING SERVICES NORTH

Boston Spa, Wetherby

West Yorkshire, LS23 7BQ

www.bl.uk

BEST COPY AVAILABLE.

VARIABLE PRINT QUALITY

Abstract

In this thesis we describe experimental studies carried out in three different granular systems.

Firstly, we describe the results of experiments and computer simulations carried out to test the validity of a randomly-forced model to describe the behaviour of a vertically vibrated, granular monolayer. We study how a single particle moves across a vibrated roughened surface and show that both a random force and viscous dissipation are needed to match the experimental data. We then simulate a collection of particles driven in this way and compare the structure factor $S(k)$ obtained from simulation with that measured experimentally. The small k behaviour of $S(k)$ reveals a quasi long-range structure which has not been observed previously.

Secondly, we study the behaviour of water-immersed granular beds. The first system consisted of spherical barium titanate particles contained in a rectangular cell which is divided into two columns, linked by two connecting holes, one at the top and one at the bottom of the cell. Under vibration the grains spontaneously move into just one of the columns via a gradual transfer of grains through the connecting hole at the base of the cell. We have developed numerical simulations that are able to reproduce this behaviour and provide detailed information on the instability mechanism. We use this knowledge

to propose a simple analytical model for this fluid-driven partition instability based on two coupled granular beds vibrated within an incompressible fluid.

In the second system to be studied a water-enhanced Brazil nut effect, which occurs when the vibrated granular bed is fully immersed in a liquid, will be describe. We use a bed of glass beads immersed in water and monitor the behaviour of a large steel intruder as the system is vibrated vertically. To aid our understanding, we have developed numerical simulations to model this system and provide detailed information about the fluid and grain motion. The mechanism responsible for the rapid rise of the intruder is shown to be fluid-enhanced ratcheting rather than simple differential drag.

Lastly, we describe experiments carried out in a levitation magnet to investigate the behaviour of spheres suspended magnetically in a viscous fluid. Under vibration the spheres attract and for sufficiently large vibration amplitudes the spheres are observed to spontaneously orbit each other. Data collapse shows that the instability occurs at a critical value of the streaming Reynolds number. Simulations are used to provide a detailed understanding of the cause of this instability.

Acknowledgements

I would like to take the opportunity to thank the people whose support has made possible this document.

Firstly, I would like to thank my supervisor Dr. Michael Swift for his support, patience and guidance throughout my degree. I am fortunate to have benefited from his knowledge, experience and drive during my research.

I would also like to thank Prof. Laurence Eaves for his endless support, words of advice and the interest shown on my degree. Dr. Roger Bowley and Dr. Richard Hill for the many useful discussions and their support and assistance during the experimental stages of my research.

Many thanks should also be extended to the administrative staff of the Physics Department and the technical staff at the School of Physics Workshop

I simply could not forget to thank my officemates Anwesha Fernandes, Leong Ting Lui, David Bray, Helen Wright, Kathryn Taylor, Pablo Lopez, Christian Clement, James Clewett, Jack Wade and Liang Liao for their support and friendship throughout all these years.

On a personal level I would also like to thank the amazing people who made my stay in Nottingham such a remarkable experience. To my adventure partners Yoanna Moguel, Daphne Klotsa, Lucy Goff, Mark Patton, Arianna Casiraghi, Daniel Rayneau-Kirkhope and my awesome friends and housemates

Eric Martinez, James Haigh, John Tullis and Richard Wall. You guys became my family away from home.

To the one and only Jara Imbers, I just cannot find words to fully express how thankful I am for your endless support, unlimited patience, useful advice and unconditional friendship throughout the past years. I am deeply indebted to you.

I am also grateful with my colleagues and friends in and out the Physics Department: Duncan, Fintan, Hengam, Robin, Richard, Mel, Shu Li, Denzil, Liz and so many more it would be impossible to include everyone in such a reduced space.

Finally I would like to thank my parents, my brother and sister-in-law, and my family. It would have been impossible to finish this experience without their unconditional support and love.

I dedicate this thesis to you all.

Publications

The following papers have been published as a result of this research:

1. P.J. King; P. Lopez-Alcaraz; H.A. Pacheco-Martinez; et al. *Instabilities in vertically vibrated fluid-grain systems*, European Physical Journal E, **22**, 219-226 (2007).
2. C.P. Clement; H.A. Pacheco-Martinez; M. R. Swift and P. J. King. *Partition Instability in water-immersed granular systems*, Physical Review E, **80**, 011311 (2009).
3. C.P. Clement; H.A. Pacheco-Martinez; M. R. Swift and P. J. King. *The water-enhanced Brazil nut effect*, European Physics Letters, **91**, 54001 (2010).

The following paper are in preparation:

1. H.A. Pacheco-Martinez; M. R. Swift and R. M. Bowley *Long-range structure of a randomly driven granular Monolayer*.
2. H.A. Pacheco-Martinez; R.J.A. Hill; M. R. Swift and R. M. Bowley *Hydrodynamic interaction of magnetically levitated spheres*.

Contents

Abstract	i
Acknowledgements	iii
Publications	v
1 Introduction	1
1.1 Granular Materials	1
1.1.1 Classical matter and Granular media	3
1.1.2 Fluid-Grain Systems	5
1.2 Thesis outline	9
2 Quasi-Long-range Structure of a 2-D Granular Gas	12
2.1 Introduction	14
2.1.1 Non-Equilibrium states	14
2.1.2 Granular Hydrodynamic Equations	16
2.1.3 The Random Force Model	19
2.1.4 Structural Properties of a Two-dimensional System	21
2.2 Experimental setup	24
2.3 Trajectory of a Single Particle	29
2.3.1 Experimental Procedure	30

2.3.2	Video Processing	31
2.3.3	Experimental Results	33
2.3.4	Discussion	36
2.4	Long-range Structure of a randomly-driven granular sub-monolayer	38
2.4.1	Experimental Procedure	39
2.4.2	Experimental Results	41
2.5	Computer Simulations of the long-range structure of a 2-D gas .	45
2.6	Discussion	48
2.7	Final Remarks	49
3	Fluid-Immersed Granular beds	51
3.1	Introduction	52
3.1.1	The Partition Instability	53
3.1.2	The Brazil Nut Effect	56
3.2	Vertical Vibratory Apparatus	57
3.3	Partition Instabilities	60
3.3.1	Experimental Details	61
3.3.2	Methodology	62
3.3.3	Experimental Results	64
3.3.4	Simulations	68
3.4	The Fluid-Enhanced Brazil Nut Effect	73
3.4.1	Experimental Details	74
3.4.2	Experimental Results	75
3.4.3	Simulations	78
3.4.4	Fluid-Enhanced mechanism	81
3.5	Summary	83

4	Dynamics of magnetically-levitated, fluid-immersed grains	85
4.1	Introduction	86
4.2	Dilute fluid-grain systems	91
4.2.1	Oscillatory fluids and Streaming flows	93
4.3	Experimental Setup	100
4.4	Levitated spheres	106
4.4.1	Initial Observations	107
4.4.2	Dynamics of a single, levitated particle	108
4.4.3	Dynamics of two levitated spheres	111
4.4.4	Streaming flow of levitated spheres	124
4.5	Final Remarks	128
5	Concluding Remarks	130
5.1	Chapter review	130
5.2	Future Work	133
A	Magnetic Levitation	135
A.1	Magnetostatics	135
A.2	Types of Magnetism	137
A.3	Diamagnetic levitation	139
	Bibliography	142

Chapter 1

Introduction

This thesis discusses some of the dynamical effects observed in both dry and liquid-grain systems subjected to vertical vibrations. The fields of granular dynamics and fluid dynamics are vast and the phenomena studied in this thesis are varied. The aim of this chapter is to provide a brief overview of the topic of granular materials. A more detailed background will be given as the particular subjects of study in each chapter are addressed. In the following section, some of the interesting phenomena observed in granular systems are reviewed to showcase the variety and complexity of granular behaviour. The chapter concludes with an outline of the structure of the thesis.

1.1 Granular Materials

Granular materials may be defined as a collection of discrete, macroscopic particles interacting through inelastic collisions. Even when the dynamics of each grain can be described by Newtonian physics the collective behaviour of a collection of grains can be complex. Although thermal fluctuations do not affect granular matter, its behaviour can be highly sensitive to the experimen-

tal conditions, to the presence of a surrounding fluid and its properties, and to parameters such as density, porosity and the size and shape of the particles. Granular materials are ubiquitous in nature where they are involved in many natural processes, some of which can be potentially dangerous such as avalanches and landslides and others which are vital to life such as seed propagation. In industry, many processes involve packing, sorting, storing, mixing and transporting some kind of material in the shape of grains, see for example Ennis *et al.* (1994). A few examples of such materials and processes are shown in Figure 1.1. Despite being the second most handled material in industry after water, handling granular materials remains one of the least understood areas in material processing plants.



Fig. 1.1: Examples of granular materials in agriculture, pharmaceutical and construction industries.

The undeniable importance of granulates in industrial processes may be the reason why engineers have studied this kind of material for a long time, however, this topic is relatively new in physics. The motion of a single grain can be fully described by Newtonian mechanics which may mislead one to think of granular media as a system easy to describe. For some further reading on granular systems we suggest the review articles by Jaeger(1996) and Kudrolli (2004).

1.1.1 Classical matter and Granular media

Granular systems have the remarkable ability to mimic some of the properties observed in classical solids, liquids and gases. However, the behaviour of a dry granular systems is heavily influenced by the inelastic collisions between individual grains. Granular materials have the ability to dissipate a large amount of kinetic energy very rapidly through these inelastic collisions. It is this characteristic which separates granular materials from other types of materials. The cause of a wide variety of phenomena observed in granular materials could be tracked to the way energy is dissipated within the material.

A pile of static grains can maintain a configuration in which the overall gravitational potential energy of the grains is not minimized. Static friction between adjacent grains usually results in unequal contact forces on each particle (Jaeger *et al.* 1996). As a result, these contact forces put the grains under different stress levels. When grains with similar stress level are in contact, they form “force chains”, see for example Figure 1.2. Within a given arrangement, however, the distribution of the magnitudes of the stresses along the force chains can be very broad. It is the static friction and the force chains which are responsible for the stability of the solid granular conglomerate, such as a sand pile. Force chains are responsible for the density of a granular bed being able to be within a range of values for a fixed number of grains. The force chains allow the void fraction of a bed of randomly packed spheres to vary between 0.36 and 0.45 (Onoda and Liniger 1990).

Avalanches are an example of granular materials behaving like fluids. When the slope of a granular pile exceeds the maximum angle of stability a flow of grains, which behaves very similar to a liquid flow, is triggered. Once the slope of the granular pile returns to the angle of repose the flow stops and the pile

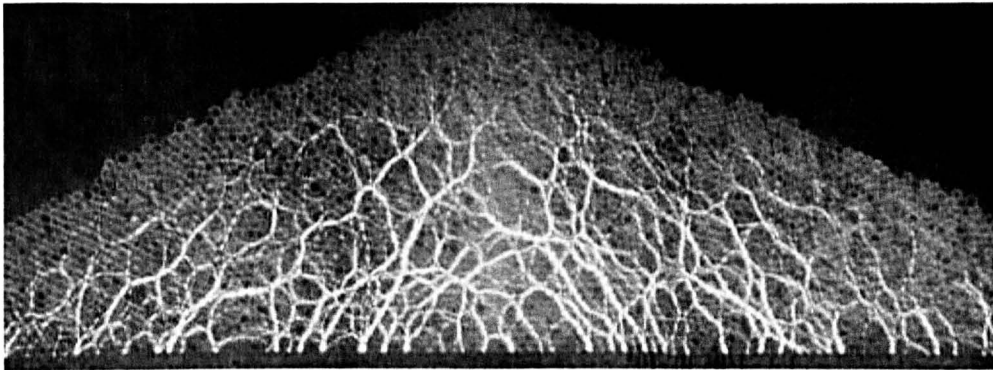


Fig. 1.2: A two-dimensional pile of photoelastic discs illustrating the stress chains within the structure of the pile. The pile is viewed between crossed polarizers, allowing one to see the underlying force structure. The bright regions correspond to the force chains described in the text. (Geng *et al.*, 2001)

takes on a solid behaviour again. Sheared induced flows are also present in granular materials. If subjected to strong enough shearing forces the grains will start to slide past each other deforming the shape of the granular material, however, the flow will remain confined to the surface layers of the pile.

Unlike normal liquids, grains stored in a container such as a silo, do not exhibit a height dependent pressure. The pressure at the base of the granular column does not increase with the height of the column. After the height of the column reaches a critical value, the extra weight is supported by the walls of the container due to contact forces between the grains and static friction with the side walls in what is known as the Janssen's effect (Janssen 1895). This effect is also responsible of the constant flow through a hole in the bottom of the silo, independent of the height of the grains above it.

A granular material can behave like a gas if it is sufficiently excited. Like a gas, an excited granular system consists of discrete particles and it is possible to compress it. However, unlike a classical gas, the collisions between grains are inelastic causing energy to be lost with each collision. This means that

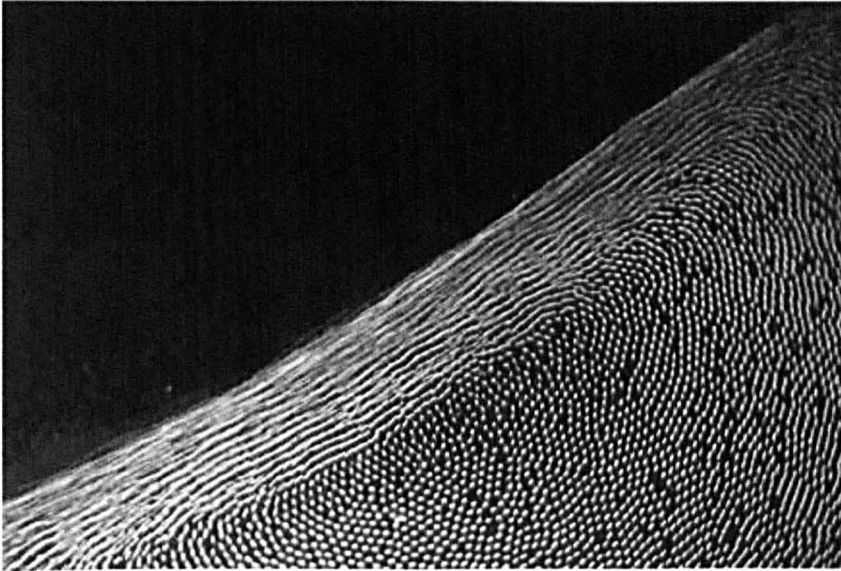


Fig. 1.3: Surface flow on a granular pile inside a rotating drum. (Photograph by Hubert Rague))

any description of the gas-like granular bed based on energy conservation fails to accurately describe the behaviour of the granular gas. Ordinary thermodynamic arguments are invalid and entropy considerations are outweighed by dynamical effects. It is possible to formulate an effective granular temperature. Analogously to molecular gases the granular temperature is defined in terms of the velocity fluctuations around the mean flow velocity (Cody *et al.* 1996).

1.1.2 Fluid-Grain Systems

Fluid-grain systems can be classified depending on the size of the grains within the fluid. Small particles form colloids. Particles in colloids are homogeneously distributed throughout the fluid and often have the appearance of solutions. Bigger particles produce suspensions in which the particles experience the influence of gravity and will sediment if no external energy is injected into the system. The grains in a suspension are also affected by properties of the fluid, either by drag effects or by hydrodynamic effects. To prevent sedimentation,

particles in suspensions can be made neutrally buoyant by matching the densities of the particles and fluid. In this case, motion of the particles relative to the fluid is generated through shear. The interaction among neutrally buoyant spheres in sheared suspensions of Newtonian and non-Newtonian fluids has been studied. Michelle *et al.* reported the formation of chains in a monolayer of neutrally buoyant particles under oscillatory shear flow of a visco-elastic fluid between two plates (Michele *et al.* 1977). In an extension of this study, it was found that the formation of chains occurred in the direction normal to the oscillation and it was suggested that this alignment could be the result of inertial or elastic effects (Petit and Gondret 1992).

Non-neutrally buoyant systems can be separated in two categories; systems in which the drag effects dominate and systems in which hydrodynamic effects dominate. When drag effects dominate, the particle effect on the fluid is not considered. This is the case for systems in which there are a large number of particles. Segregation has been observed in binary mixtures where two components have different densities. This segregation is the consequence of differential drag with the interstitial fluid, the result is the formation of stripes consisting on a single type of grains, as shown in figure 1.4, (Sanchez *et al.* 2004; Ciamarra *et al.* 2007). Separation has also been observed due to fluid drag effects in a vertically vibrated granular mixture. It was found that a mixture of bronze and glass can be separated perfectly if subjected to vertical vibration in the presence of air (Burtally *et al.* 2002).

Computer simulations showed that differential drag forces were the main mechanism behind the separation phenomenon, since differences in size and density between the components of the mixture cause the fluid drag force to affect the dynamics of the grains of each component differently (Biswas *et al.*

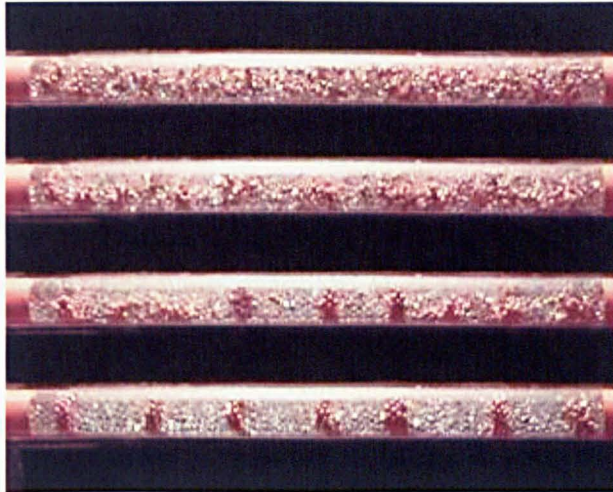


Fig. 1.4: Separation of granular materials due to differential drag. The system starts in a homogeneous, mixed state (Top) and evolves into a segregated state (Bottom). (Sanchez *et al.*, 2004)

2003). Separation is also observed in water immersed mixtures under vertical vibration (Leaper *et al.* 2005).

In very diluted systems where only a small number of particles are immersed in an oscillatory fluid flow, the hydrodynamic interactions between particles dominates and changes the behaviour of the specific granular system in interesting ways. Spherical particles have been observed to form patterns and exhibit collective behaviour (Voth *et al.* 2002; Wunenburger *et al.* 2002). Under vertical vibration spherical particles in a viscous fluid form time-periodic structures, chaotic fluctuating patterns or hexagonal lattices (Voth *et al.* 2002; Thomas and Gollub 2004). A short range repulsion and a long range attraction due to the fluid flow were used to explain the formation of these patterns. Small spheres in a water-filled container subjected to horizontal continuous vibration were observed to form a periodic pattern aligned perpendicular to the direction of oscillation (Wunenburger *et al.* 2002). Heavy spheres in a viscous fluid under horizontal vibration were also observed to align along the

direction perpendicular to the direction of vibration (Klotsa et al. 2007). It was also observed that two spheres would interact with each other and form a gap in between them when subjected to horizontal vibration (Klotsa et al. 2009). In these systems, the fluid establishes a steady secondary flow, termed the streaming flow. It has been proposed that this flow has an effect on the particles and forms the structures described above.

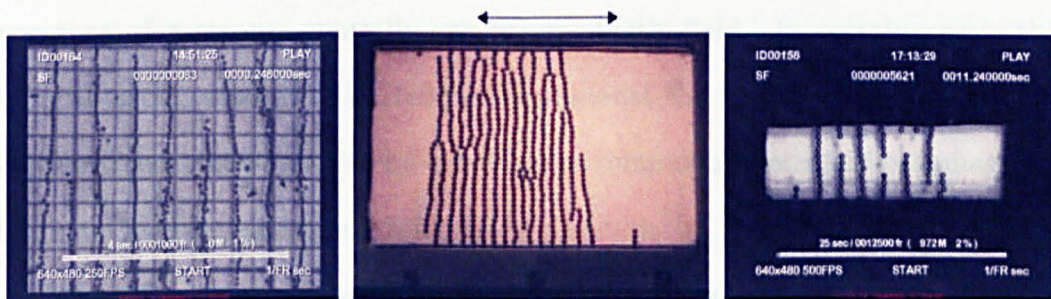


Fig. 1.5: Pattern formation. A collection of steel spheres immersed in a viscous liquid align perpendicularly to the direction of vibration to form chains. The direction of oscillation is given by the double arrow. The viscous liquid used in these experiments is an aqueous solution of glycerol. For further details see Klotsa *et al.* 2007

In this thesis we look at three granular systems where collective interactions between grains and their surroundings give rise to interesting phenomena. First, a collection of dry particles bouncing on a roughened surface will be studied. A system with these characteristics can be taken as a quasi-two-dimensional granular gas. Our motivation is to determine whether the Random Force Model (which will be introduced later) can be used to describe the dynamics of this type of systems. Later we will investigate larger collection of grains densely packed (also referred as *granular beds*) which are surrounded by an incompressible fluid such as water. Two particular phenomena will be studied; the instability observed in a partitioned container and the effect of the fluid on the rise of an intruder, a particle with different properties from the rest of the granular bed, in the well-known Brazil nut effect. In the final

system, the interactions between grains and the fluid surrounding them will be studied. The formation of chains and patterns by particles immersed in an oscillatory fluid have been reported in the past. Our approach involves the use of magnetic levitation to study these systems while preventing the interaction with the walls of the container or the effects of gravity. Magnetic levitation exploits the force on diamagnetic materials (e.g. water, glass, NaCl) in the presence of a strong, spatially-varying magnetic field. In certain cases, this force is strong enough to levitate bodies against the force of gravity. The concept and technique can also be extended to immersing bodies in paramagnetic fluids in the presence of a strong field.

The layout of the thesis is described in the following section.

1.2 Thesis outline

The topics addressed in this thesis involved the use of different techniques and experimental arrangements. Although the three systems deal with collections of grains under vibrations, each one has a particular background. For this reason, this document is divided into five chapters. In the first chapter we have given a brief introduction to the area of granular matter. In the remainder of this chapter we will describe the layout of the thesis. The following three chapters are self-contained and an introduction to their particular subject will be given at the begin of each chapter.

In Chapter 2 we will focus our attention on a vertically-excited, dilute monolayer of grains. A collection of vertically-excited grains moving close to the surface of the container can be considered as 2-dimensional granular gas. In the past, this type of system has been the subject of several studies. However, despite renewed interest to find a statistical description of the dynamics

of a granular gas, there is no consensus on whether they can be treated as homogeneous systems or their dissipative properties allow the formation of a more complex long-range structure. We present the results of an experimental study carried out to test the validity of the Random Force Model to describe the behaviour of a vertically vibrated, 2-dimensional granular gas. The chapter starts with an introduction covering some of the granular kinetic theories that have been developed to describe granular systems. We introduce the Random Force Model and review some of its predictions. The rest of the chapter describes the experimental study of a randomly-driven collection of grains. Firstly, the trajectory of a single particle across a vibrated roughened surface is recorded and its average displacement is measured as a function of time. From the experimental observations we found that viscous dissipation and a random force are needed to match the experimental data. Later, the structure factor, $S(k)$, and the pair correlation function, $g(r)$, for a collection of grains were also measured experimentally and compared with the results from simulations carried out within our research group. The experimental observations of $S(k)$ revealed a structure that, to our knowledge, have not been observed previously.

In Chapter 3 we describe the experimental work carried out to investigate two of the phenomena observed when a granular bed surrounded by fluid is subjected to vertical vibrations; the spontaneous migration of grains in a partitioned container and the effect of a fluid on the Brazil nut effect. The aim of these experiments is to provide a set of quantitative results which can be compared to the predictions of the simulation models developed within our research group.

In Chapter 4 we describe a series of experiments aimed to study the be-

haviour of spherical grains magnetically-levitated in an oscillatory fluid. To our knowledge this kind of experimental setup has not been used previously to study the hydrodynamic interactions in very dilute granular systems. We start the chapter with a review of the studies associated with pattern formation in granular systems in the presence of an oscillatory fluid. We continue with a brief review of basic concepts of magnetism and introduce diamagnetic levitation. Next, we describe our initial experimental observations when collections of grains were levitated magnetically in the presence of an oscillatory fluid. Several systems were investigated but our main studies will focus on the case of two particles. In the remainder of the chapter we will describe the details of the experimental study of two magnetically-levitated spheres.

Lastly, in Chapter 5 we will present a review of the main results of each chapter as well as the direction which future research could take.

Chapter 2

Quasi-Long-range Structure of a 2-D Granular Gas

Granular systems can exhibit states that resemble the solid, liquid and gaseous states of classical media. However, due to the dissipative nature of granular materials, the standard theories commonly applied to classical materials can not be used to describe their properties.

The present study will be focus on a vertically-excited, dilute monolayer of grains. Such a system can be considered to be a quasi two-dimensional granular gas. A number of experiments (Blair *et al.* 2003b; Olfen & Urbach 1998; Reis *et al.* (2006a & b, 2007a & b); Shattuck *et al.* 2009; Bordallo-Favela *et al.* 2009; Reyes & Urbach 2008) have been carried out on vertically vibrated granular monolayers with the aim of creating systems which are homogeneously excited. Even though the systems are uniformly agitated, dissipation in collisions can induce non-uniform spatial structures. In a nearly elastic system, Reis *et al.* found that the radial distribution function was identical to that of an equilibrium distribution of hard disks (Reis *et al.* (2006a & b, 2007a & b)). However, Bordallo-Favela *et al.* found that the short-range structure as

measured by the pair correlation function depends on the coefficient of restitution of the particles (Bordallo-Favela *et al.* 2009). Reyes and Urbach showed that the degree of dissipation also has a strong effect on the phase diagram but they did not investigate the long-ranged structure of the individual phases (Reyes & Urbach 2008). It has been proposed that vibrated monolayers can be modelled as a randomly-driven, two-dimensional dissipative gas (Melby *et al.* 2005). In the simplest form of the model, dissipation only arises from collisions between particles. Previous theoretical studies using kinetic theories or computer simulations have led to different predictions for both the structure (Peng & Ohta 1998; van Noije *et al.* 1999) and the velocity statistics (Ernst *et al.* 2006; Moon *et al.* 2001; van Zon & MacKintosh 2004 & 2005). Pugliesi *et al.* considered a generalisation of the model to include a term which acts as a viscous drag (Pugliesi *et al.* 1999). Melby *et al.* argued that both collisional and viscous dissipation may be present for grains vibrated on a roughened base (Melby *et al.* 2005). However, no quantitative confirmation of this picture has been attempted.

In this chapter we will present the results of an experimental study carried out to test the validity of the Random Force Model to describe the behaviour of a vertically vibrated, 2-dimensional granular gas. Our experimental study starts by recording the trajectory of a single particle across a vibrated, roughened surface and the average displacement is measured as a function of time. From these observations we have found that a random force is not enough to reproduce the experimental data; a viscous dissipative force is also needed to match the observations. The structure factor, $S(k)$, and the pair correlation function, $g(r)$, for a collection of grains were also measured experimentally and compared with the results from simulations carried out within our re-

search group. The experimental observations of $S(k)$ revealed a long-range structure that, to our knowledge, has not been observed previously.

2.1 Introduction

Since standard theories applied to classical materials can not be used to describe a granular system it is necessary to develop new theories or adjust those that already exist to take into account the complexities of granular materials. In this section we present a review of the theoretical approach to describing the dynamics of a dry granular system. Firstly, we highlight the effect of the inelastic collision in a granular system and introduce the concept of granular temperature as a way to characterise the average kinetic energy in a granular gas. Then, we review some of the granular kinetic theories derived from the Boltzmann equation of motion which incorporate the dissipation of energy due to collisions and the continuous injection of energy. Lastly, we conclude with a review of the Random Force Model, a model that has motivated various experimental studies on the structural properties of two-dimensional granular systems, including the present work.

2.1.1 Non-Equilibrium states

Vibrated granular systems are an example of a system out of equilibrium. The grains lose kinetic energy with every successive collision. If they are to stay in motion then an external source of energy is required. The amount of energy that is dissipated during each collision is determined by the coefficient of restitution (ϵ) which can be calculated from the relation between the velocities

of the grains before and after the collision,

$$v'_2 - v'_1 = \varepsilon(v_1 - v_2), \quad (2.1)$$

where v_1, v_2 are the normal components of the velocity before the collision and v'_1, v'_2 are the normal components of the velocity after the collision of the particle 1 and 2, respectively.

A way to quantify the energy of a granular system is by defining its granular temperature as the average kinetic energy per particle. If a collection of initially energetic grains, such as a granular gas in the absence of long-range forces, is left to evolve without an injection of kinetic energy the granular temperature will decrease with every collision in the system. Haff's law predicts how the granular temperature decays with time. According to this law the granular temperature at time t is (Brilliantov and Pöschel 2004):

$$T_t = T_0 \left[1 + \frac{4}{\sqrt{\pi}}(1 - \varepsilon) \frac{\phi T_0^{1/2}}{s^*(\phi)d} t \right]^{-2}, \quad (2.2)$$

where ϕ is the packing fraction (a measure of the density of the gas of grains) and $s^*(\phi) = (1 - \phi)^2 / (1 - 7\phi/16)$. Here t is the time and T_0 is the starting granular temperature at $t = 0$ and d is the diameter of the particles.

If the grains are weakly dissipative and only a small amount of energy is lost with each collision, Haff's law provides a good prediction for the decay of the temperature. However, if the grains are highly dissipative, large fractions of the grain's energy are lost with each collision which can cause the grains to strongly cluster together and under these circumstances Haff's law breaks down.

Haff's law is an example of applying hydrodynamic theory to granular media. Its failure at moderate to high dissipations demonstrates that a mean-

field theory treating the distribution of grains as homogeneous is inadequate; instead the spatial structure of the system must be considered.

2.1.2 Granular Hydrodynamic Equations

Equilibrium theories, such as those based on Maxwell-Boltzmann statistics, fail to describe granular systems because they do not account for the continuous dissipation and injection of kinetic energy that occurs in such systems. As a result, the general approach by physicists has been to modify the existing theories to incorporate collisional dissipation and energy injection. The difficulty arises in how to include these additional energy terms.

Kinetic theories are mostly derived from the Boltzmann equation of motion. The Boltzmann equation assumes that the state of a particle is separable from the system's other particles, in which case molecular chaos applies, so that there exists no correlation between grain velocities. For a steady state of fluidised inelastic hard spheres the Boltzmann equation is written as:

$$\frac{\partial f_i}{\partial t} + \mathbf{v} \cdot \frac{\partial f_i}{\partial \mathbf{r}} + \frac{\mathbf{F}}{M} \cdot \frac{\partial f_i}{\partial \mathbf{v}} = C(f_i) - E(f_i), \quad (2.3)$$

where f_i is the distribution function that describes a grain in terms of position \mathbf{r} , velocity \mathbf{v} and time t . The other terms comprise the forces acting on the particles between collision \mathbf{F} ; the mass of a grain M ; the rate of change of f_i due to collisions $C(f_i)$; and the rate of change of f_i due to energy injection $E(f_i)$.

Frequently an assumption to the Boltzmann equation is that the system is spatially homogeneous. However, it is well known that many granular systems are spatially homogeneous only on time average and not instantaneously. Furthermore, dissipation of energy during collisions in granular media leads to notable correlations in particle velocity even at reasonably low dissipation.

Some Specific Granular Kinetic Theories

The use of a Random Force acting on each particle is the easiest method to uniformly inject energy into a system. A solution to the Boltzmann equation can then be found to obtain the distribution of velocity. In practice it is a challenging task to describe the complete velocity distribution. Therefore, it is common practice to calculate only the high velocity tails of the distributions which has resulted in a variety of solutions for the asymptotic behaviour of the velocity distribution $P(v)$, where v is a component of the velocity \mathbf{v} .

Van Noije and Ernst proposed what has become the most commonly quoted approach (Van Noije and Ernst 1998). The system was assumed to be thermally heated by uncorrelated Gaussian white noise. The Boltzmann equation was approximated as the Enskog-Boltzmann equation for a uniform heated system. The high velocity tail of the distribution of velocity was calculated as a stretched-exponential of the form $P(v) = A \exp(-B|v|^{3/2})$.

Barrat *et al.* suggested in a later study that the velocity distribution is more complicated (Barrat *et al.* 2002). They reported that $P(v)$ crosses over from $A \exp(-B|v|^{3/2})$ for the large inelasticity regime to $A' \exp(-B'|v|^3)$ for the low inelasticity. This implies that for systems with nearly elastic collisions the cubic behaviour was dominant over observable statistics.

Ben-Naim *et al.* proposed an alternative approach (Ben-Naim and Krapivsky 2000). In their study, they used the Maxwell Model as an approximation for the Boltzmann equation. In this case the collision rate is independent of the particle's velocity so that the collision integral, $C(f)$, can be derived by just considering a collision between a pair of grains such that $C(f)$ contains both a single gain and a single loss term. The Maxwell Model is solved by ignoring the gain term and the high velocity tail of the velocity distribution is calculated

to be approximately exponential of the form $P(v) = A \exp(-Bv)$.

Another approach to solve the Boltzmann equation is described by Ben-Naim *et al.* (Ben-Naim *et al.* 2005). The Boltzmann equation is linearised by studying only the fastest particles. The collision rate is chosen to be a power of the relative difference in velocity between colliding grains. As the fastest grains are very rare, all other inbound grains are seen as stationary and the collisions of the system leads to a cascade effect; one collision causes two further collisions which in turn leads to four further collisions and so on. Due to this cascade effect, the kinetic energy contained per grain, in the form of the velocities, reduces in value. The theory assumes that the energetic grains are uncorrelated with the slow grains and so the Boltzmann equation can be linearised by taking the second grain's velocity to be zero. Solving the equation produces a power-law approximation for the high velocity tail of the distribution of velocities.

In the theories described previously, it is assumed that the granular system is homogeneous. Puglisi *et al.* proposed a theory that included spatial variation (Puglisi *et al.* 1999). The granular system is broken up into a number of boxes with fixed width containing a variable number of particles. Particles can move between boxes but the total number of grains in the system remains constant. The kinetic energy of the box is dependent on the number of particles held within and the distribution of velocity for each box is assumed to be Gaussian with standard deviation governed by the box's kinetic energy. The total velocity distribution of the system is thus equal to the sum of distribution of velocity for all the boxes and thereby incorporates the structure of the system.

In the majority of granular systems the energy injection is both time and

position dependent. If we consider the case of a shaken bed, kinetic energy is only transferred to those grains that are in contact with the base at the point in the cycle when the base is moving upwards. All other grains exchange energy through subsequent collision. For this reason it is difficult to represent these systems by granular kinetic theories. Instead the granular kinetic theories are tested against simpler systems where the driving energy injection can be considered to act at all times over all grains. One such theoretical granular system was proposed in by Williams and MacKintosh and is known as the Random Force Model (Williams and MacKintosh 1996).

2.1.3 The Random Force Model

The Random force model is defined as a set of confined identical grains, from now on referred to as particles, where kinetic energy is injected into the system by individually applying a random force, statistically distributed as a Gaussian, to each particle. The random force represents the overall effect of particles picking up successive packets of energy, identically distributed, over an infinitesimal period of time such that the Central Limit Theory applies.

Considering the simplicity of the Random Force Model and the level of study available in the literature it is surprising to find unresolved conflicts about the nature of these systems. Specifically, the velocity and structural properties of the two-dimensional case are still a cause of debate since it is still unclear whether or not a hydrodynamical description is applicable in these systems, as showcased at the beginning of this chapter.

The slight correlation of particle velocity with its neighbour after collision leads to clustering in these systems. The random force prevents the system from undergoing inelastic collapse by decorrelating the particles over time.

However, the tendency of particles to cluster puts into question any theories that suggest the system is homogeneous. Nevertheless much of the previous analysis of the Random Force Model assumes exactly that.

Regardless of the debate, these models are of particular relevance as several experiments have been performed using systems that can be considered as near approximations to the two-dimensional case. Reis *et al.* have performed several of such studies (Reis *et al.* 2006a; Reis *et al.* 2007a; Reis *et al.* 2007b). In their experiments a layer of identical spheres is placed between two glass plates, the lower of which is roughened. The plates are separated by just over a particle diameter to create a quasi-two dimensional system. Figure 2.1 shows their experimental setup.

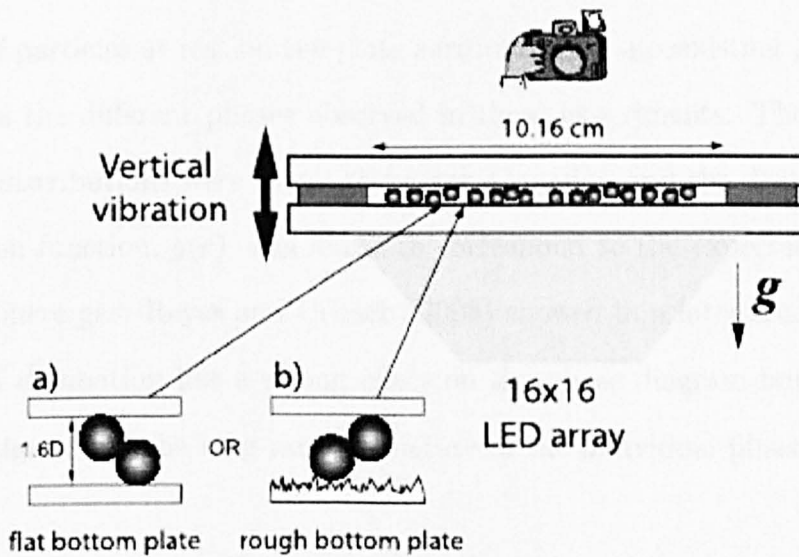


Fig. 2.1: Schematic diagram of the experimental apparatus used by Reis *et al.*. The grains were encased in between two glass plates, separated by a 1.905mm thick annulus (dark gray). The top glass plate was optically flat but the bottom glass plate could either be (a) optically flat or (b) rough by sand blasting. Image taken from Reis *et al.* (2007b).

During experiment the system is vertically vibrated and the roughened base acts as a source of random force for the particles. Of particular interest,

these researchers have measured the velocity statistics of particles and compared the results against the granular kinetic theory of Van Noije and Ernst (1998). More recently (Reis *et al.* 2009) there have been claims that the radial distribution function, $g(r)$, for these experimental granular systems was identical to that of an equilibrium distribution of hard disks. It was proposed that the experimental granular system broadly mimics an equilibrium systems as a result of all spatial gradients being removed.

Olafsen and Urbach (1998) conducted an experimental study of vertically excited granular monolayers. In their experiments the grains were vibrated until they were in motion in a gas-like state. As the dimensionless acceleration $\Gamma = A\omega^2/g$ was slowly decreased, the grains started to form clusters until one of these clusters became a nucleation point and the system collapsed into a cluster of particles at rest on the plate surrounded by a coexisting gas. Figure 2.2 shows the different phases observed in these experiments. The measured velocity distributions were found to be non-Gaussian and the density-density correlation function, $g(r)$, was found to correspond to the expected result for a hard sphere gas. Reyes and Urbach (2008) showed in a later study that the degree of dissipation has a strong effect on the phase diagram but there was no investigation of the long-range structure of the individual phases.

2.1.4 Structural Properties of a Two-dimensional System

The structure of a bed of particles can be quantified by a probability distribution called the structure factor, $S(k)$, which measures the Fourier transform of the correlations in positions between pairs of particles. The wave vector modulus k is inversely proportional to the distance such that large scale structure

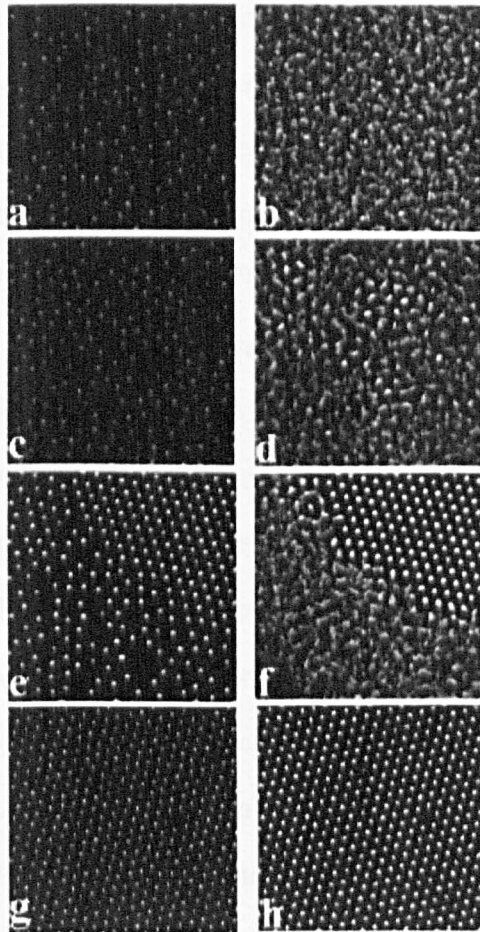


Fig. 2.2: Instantaneous (left column) and time-averaged (right column) photographs detailing the different phases of the granular monolayer as observed by Olafsen and Urbach (Olafsen and Urbach 1998). (a),(b) Uniform particle distributions typical of the gas phase ($\Gamma = 1.01$). (c) ($\Gamma = 0.8$) Clusters are visible as higher intensity points in a time-averaged image (d) denoting slower, densely packed particles. (e) A portion of a collapse ($\Gamma = 0.76$). (f) The time-averaged image shows that the particles in the collapse are stationary while the surrounding gas particles continue to move. (g),(h) In a more dense system, there is an ordered phase where all of the particles remain in motion.

is described by small scale k -space. The structure factor is a mathematical tool commonly used to interpret the interference patterns observed in diffraction experiments in crystallography and condensed matter physics. A specific definition of $S(k)$ will be given later in this chapter.

There is a general consensus amongst the literature that the structure factor of a two-dimensional granular gas varies as a power-law for small k of the form k^{-D_f} , but disagreement exists into the exact value of the exponent D_f . The earliest studies into the structure factor of the RF model were carried in the papers of Peng *et al.* (1998a & b). The small scale power-law correlations of $S(k)$ were measured to be $Ak^{-1.42}$ such that $D_f = 1.42$. Additionally, it was observed that the exponent D_f did not change with the coefficient of restitution but instead the scaling region reduced in length with decreasing dissipation. The suggested explanation for the power-law decay was that the system self-organized into a critical state where no characteristic spatial- or temporal-scales in the correlations existed.

Van Noije *et al.* (1999) explained the power-law decay of $S(k)$ using theory based on a hydrodynamical approach to a randomly driven inelastic hard sphere fluid. Their theory predicted that the system would exhibit three spatial regimes: dissipative, standard, and elastic, that determine the behaviour of spatial features at specific scales. The dissipative regime was stated to be dominated by the dissipation effects and represented features in $S(k)$ when $k \lesssim (1 - \varepsilon^2)/4l_0$ (where l_0 was the mean free path of a particle between collision and ε is the coefficient of restitution). Whereas the elastic regime was dominated by energy conduction and described $S(k)$ for $k \gtrsim \sqrt{1 - \varepsilon^2}/2l_0$.

The standard regime described the remainder of $S(k)$. Importantly the authors discussed whether or not these regimes could be seen in a system of a given size and concluded that the power-law decay of $S(k)$ was only appreciable when the system had lengths of $L > 4l_0/(1 - \varepsilon^2)$. Within the dissipative regime the structure factor was derived to obey $S(k) \propto k^{-2}$. This relation was compared with simulation data but accurate evaluation was not possible

due to the data quality. It was finally acknowledged that molecular chaos was violated for high inelasticity due to short range velocity-velocity correlations which were not incorporated in their theory.

In the following sections we describe the methodology and present the experimental results of a study carried out to test the validity of the random force model to describe the behaviour of a vertically vibrated granular monolayer. We begin by describing in detail the setup of our experiment, the vertical vibratory apparatus and the properties of the grains used in the experiments.

Part of our motivation consist in trying to model the experimental observations using the Random Force model. To this end, our study began by placing a single particle onto the roughened, vibrated surface of a tray and recording its trajectory. We continued our study by measuring the pair distribution function of a collection of grains under the same conditions. Finally, we obtained experimentally the structure factor, $S(k)$, of the system. Computer simulations were carried out within our group using the experimental parameters obtained from the motion of single particles. The corresponding results will be compared with the experimental observations at the end of this chapter.

2.2 Experimental setup

The experimental setup consisted of a collection of grains vibrated vertically on the roughened surface of a horizontal tray. To vibrate the tray we made use of a LDS permanent magnet shaker model V406 with a nominal maximum sine force rating of 196N. This shaker was firmly bolted onto a medium density fibreboard (MDF) base. To reduce the effects of undesired vibrations, the MDF base was attached to a large concrete block of approximately 250kg

using 8 bolts of adjustable length. These bolts were used to align the surface of the tray with the horizontal plane. An aluminium plate of 15 by 15cm horizontal cross-section and 1cm thickness was attached on top of the shaker. The distance between this plate and the casing of the shaker was varied using cylindrical aluminium spacers of 3cm height. A metal plate with a pair of capacitance cantilever accelerometers, ADXL105 and ADXL150, was fitted in between the aluminium spacers to monitor the motion of the shaker. The first accelerometer covers the range from 0 to 7g and the second from 0 to 70g, where g is the acceleration due to gravity. Figure 2.3 shows a schematic diagram of the vibratory apparatus.

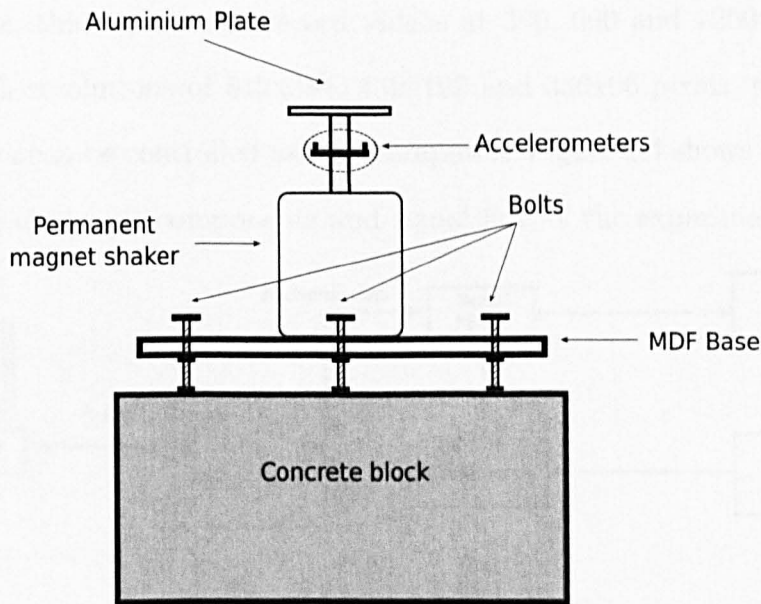


Fig. 2.3: Schematic view of the vibratory apparatus. The cell in which the experiments are conducted is placed on top of the aluminium plate. The permanent magnet shaker is levelled before each experiment by adjusting the bolts securing the medium density fibre (MDF) board to the concrete block.

A continuous sinusoidal wave was generated to drive the shaker using a Signal Generator Model DS345 by Stanford Research Systems. The frequency and peak-to-peak voltage of the driving signal was adjusted to the desired values

and sent through a device fitted with an on/off switch and a potentiometer to a Cambridge Audio Power Amplifier model P500. The potentiometer allowed a finer control over the maximum voltage of the signal fed to the shaker hence controlling the maximum acceleration experienced by the apparatus. The acceleration was monitored by the pair of accelerometers described previously. The signal from the accelerometers was sent through a 4-pole low-pass Bessel filter with a cut-off frequency of 800Hz . The output was displayed in a digital voltmeter which was calibrated so the voltages shown corresponded to the maximum dimensionless acceleration, Γ . A digital camera, Casio Exilim ex-F1, was used to take the images and high speed videos of our experiments. In high speed mode, the camera can record videos at 300, 600 and 1200 frames per second with resolutions of 512×384 , 432×192 and 336×96 pixels, respectively. This camera can be controlled using a computer. Figure 2.4 shows a schematic view of the electronic components and signal flow of the experimental setup.

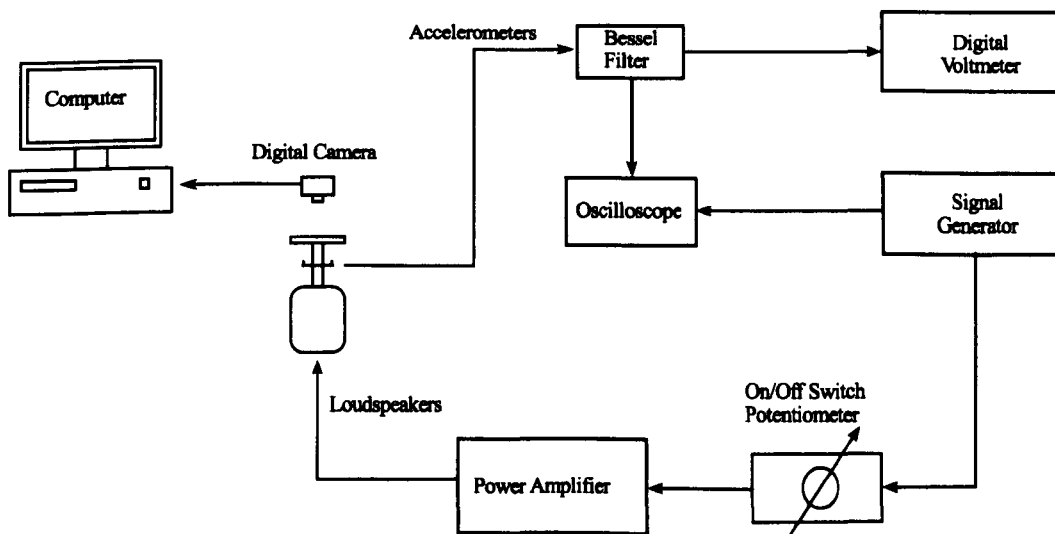


Fig. 2.4: A schematic diagram of the electronics and signal flow for the vertical apparatus. The driving sinusoidal wave from the signal generator is sent to the amplifier and then fed to the loudspeakers. The motion is monitored by the accelerometers and their output is displayed in a digital voltmeter and an oscilloscope.

The tray was built with a glass sheet of 15 by 15cm as a base. A sheet of emery paper was cut to match the dimensions of the glass sheet and carefully glued to its surface using a spray mounting glue. Special care was taken to ensure the removal of any air-pocket that could have formed between the glass and the emery paper. To form the borders of the tray we used a frame of rubber of width 1cm. The thickness of the rubber frame varied accordingly with the size of the particles used during the experiments. The free surface of the tray was a squared area of 13 by 13cm in which the particles were free to move. A further squared sheet of glass could be used to seal the tray if needed. Figure 2.5 shows a schematic diagram of the tray. For the experiments reported in this chapter there was no observable change on the surface of the emery paper due to the collisions with the particles when the cell was carefully checked under the microscope after the experiments. However, actual measurements of the properties of the emery paper before and after the experiments were not carried out. Table 2.1 contains a summary of the types of sandpaper used as roughened surface and the sizes of the inserts.

Particles made of glass, steel, plastic, bronze and lead were used in the experiments with different degrees of success. The glass and plastic particles were highly susceptible to become electrically charged. Furthermore, in the

Code	Grit Size
P100	162 μm
P220	68 μm
P400	35 μm

Table 2.1: Types sandpaper used in the experiment. The left column shows the ISO classification and the right column shows the typical size of the inserts.

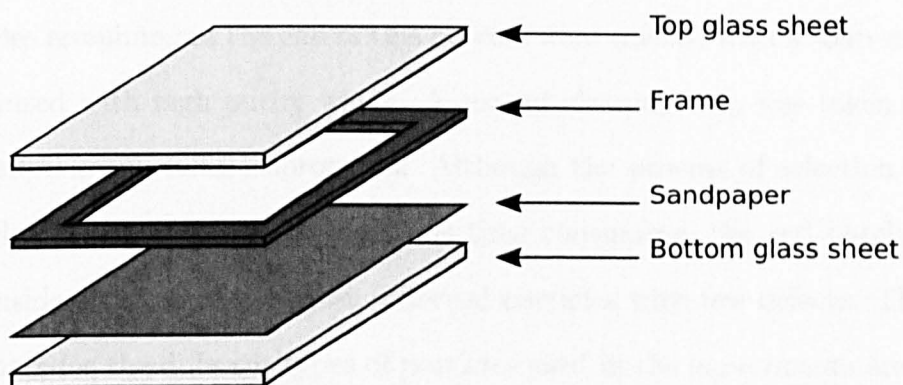


Fig. 2.5: A schematic representation of a typical tray. The surface of the bottom glass sheet is covered by a sheet of emery paper. The roughness of the surface was changed using different grades of paper. The majority of the experiments were carried out using a rubber frame. The top glass sheet could be removed and was used only when the experimental conditions required a close tray.

case of glass spheres, the images were difficult to analyse. The permanent magnet from the industrial shaker was strong enough to magnetize the steel particles. During experiments using steel spheres it could be observed that the particles formed chains which followed the lines of the magnetic field. Particles made of bronze or lead did not exhibit these problems, however, due to health and safety regulations regarding lead, the majority of the results presented in this chapter were obtained using bronze particles.

Bronze particles were sieved out to the desired range of sizes. The sieving process was repeated three times to ensure the size range was small. The particles were then poured on an inclined roughened surface. The particles that did not roll out smoothly to the bottom of the inclined plane were removed. This process was repeated several times until no particle was staying on the slope. Finally, the remaining particles were put under the microscope to search for imperfections such as rough surfaces, bumps or lumps, cracks or any other defect. Faulty particles were manually removed from the batch. The

particles remaining at the end of this process were washed with a soap solution and rinsed with high purity water. A second cleaning step was taken before each experiment using isopropanol. Although the process of selection of the particles and the cleaning process was time consuming, the end batch could be considered to contain almost spherical particles with few defects. The size and mass for the different types of particles used in the experiments are given in table 2.2.

Material	Diameter (mm)	Mass (Kg)
Bronze	0.8 (± 0.03)	2.4×10^{-6} (0.05×10^{-6})
Bronze	1.1 (± 0.05)	6.1×10^{-6} (0.03×10^{-6})
Lead	2.0 (± 0.10)	76.0×10^{-6} (0.7×10^{-6})

Table 2.2: Average diameter and mass for the particles used in the experiments described in this chapter. The standard error of these quantities is shown in brackets.

2.3 Trajectory of a Single Particle

In this section, experiments carried out to measure the trajectories of single spheres on a roughened, vibrating surface will be describe. The aim of these experiments is to determine the characteristics of the motion of a particle under our experimental conditions which will provide a starting point in the simulation of many-particle problems.

2.3.1 Experimental Procedure

Before starting each experiment care was taken to ensure that the tray was horizontally levelled. The tray was attached to the shaker and a small amount of grains were placed on top of it. The vibration was switched on and the amplitude and frequency were adjusted to the desired values for the experiment. If the grains were observed to be drawn to the edges of the tray, the bolts securing the MDF board to the concrete block were adjusted until the grains moved freely across the tray. The system was left to vibrate for a long period of time, usually about 30 minutes, to ensure that the grains would not drift towards the walls again. If no condensation of particles was observed during this period of time, the grains were carefully removed from the tray and the experiments could begin.

A lamp fitted with a 1000W halogen bulb was used to illuminate the tray. The lamp was positioned so the light illuminated the particle almost horizontally. Setting the light in this way was found to reduce reflections from the sandpaper surface. A digital camera capable of recording videos at up to 900fps (Casio Exilim Fx-1) was used to record the motion of the particles.

At the beginning of the experiment, a single particle was placed at the centre of the cell and the focus of the camera was adjusted accordingly. The vibration was switched on and the 6 by 6cm central region of the tray was filmed at 300 fps for 4 seconds. It was found during trials that, during this amount of time, most of the particles would have left the field of view of the camera. Furthermore, keeping the size of the video files small allowed an easier analysis of the recordings.

The procedure was repeated for 325 particles chosen randomly from a batch prepared as described in the previous section. The analysis of the video record-

ings using a computer program coded using Matlab will be explained in the following section.

2.3.2 Video Processing

A program in Matlab was used to analyse the high speed recordings of the motion of the particles to extract their trajectories. The program could be divided into four routines or stages. During the first routine, the frames of a single high speed video were extracted and saved into a *structure*-type variable along with all other information from the videos, such as number of frames, size of frames, etc. The second routine consisted of a series of steps to enhance the quality of the images. This stage of the analysis took advantage of the fact that light created a bright spot on top of the particles which could be easily identifiable. Each frame was converted to a grey-scale image. A threshold was set to convert the gray-scale images to black and white images. By carefully choosing this threshold, most of the background reflections in the images caused by the sandpaper were removed.

Using the Matlab function *centroids*, the position and size of the *particles* in each frame were acquired. Most of the remaining spots from the background were eliminated by discriminating the size of particle to be followed. The final stage of the programme tracked the motion of the particles. After locating the biggest object in the first frame, a small squared region centred on that particle was defined. The position of the particle between consecutive frames was compared.

To track the motion of the particle and record its trajectory, the programme scanned the squared region looking for the biggest cluster of pixels which corresponds to the location of the particle. The coordinates of the centre of the

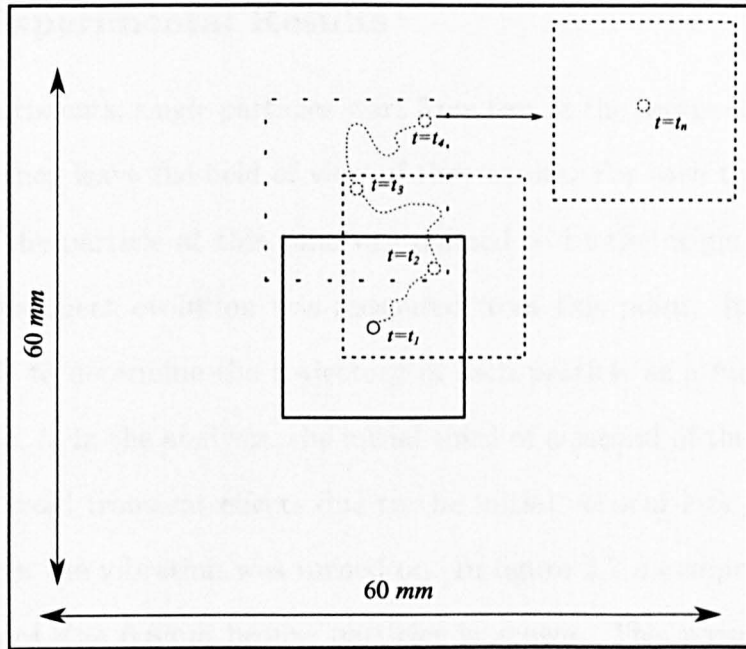


Fig. 2.6: To record the trajectory of a particle the programme scanned a squared region searching for the biggest cluster of pixels and the coordinates of the particle are recorded. In the next frame, the same squared region was scanned to locate the particle and record its new position then, a new region centred on this new coordinates was defined. The process is repeated until there is no cluster inside the region which is interpreted as the particle leaving the field of view of the camera.

particle were recorded. The start of the experiment, $t = 0$, was defined as the frame previous to the detection of a change in the position of the object and the origin of coordinates, $x = y = 0$, was defined as the position of the particle. In the next frame, the same squared region was scanned to locate the particle and record its new position then, a new region centred on this new coordinates was defined. The continuous discrimination on size and the analysis of just a small region around the last known position of the particle was necessary due to the possibility that some false *particles* were still present. A schematic representation of the tracking process is shown in figure 2.6.

2.3.3 Experimental Results

During experiments, single particles start from rest at the centre of the cell and move until they leave the field of view of the camera. For each trajectory, the position of the particle at this time was defined to be the origin, $x = y = 0$, and the subsequent evolution was measured from this point. In this way it was possible to determine the trajectory of each particle as a function of the elapsed time, t . In the analysis, the initial third of a second of the motion was ignored to avoid transient effects due to the initial vertical kick given to the particle when the vibration was turned on. In figure 2.7 a composition of the trajectories of $d = 0.8\text{mm}$ bronze particles is shown. The experiments were carried out at a frequency $f = 100\text{Hz}$ and dimensionless acceleration $\Gamma = 2.5$. The grit size of the sand paper was $68\mu\text{m}$.

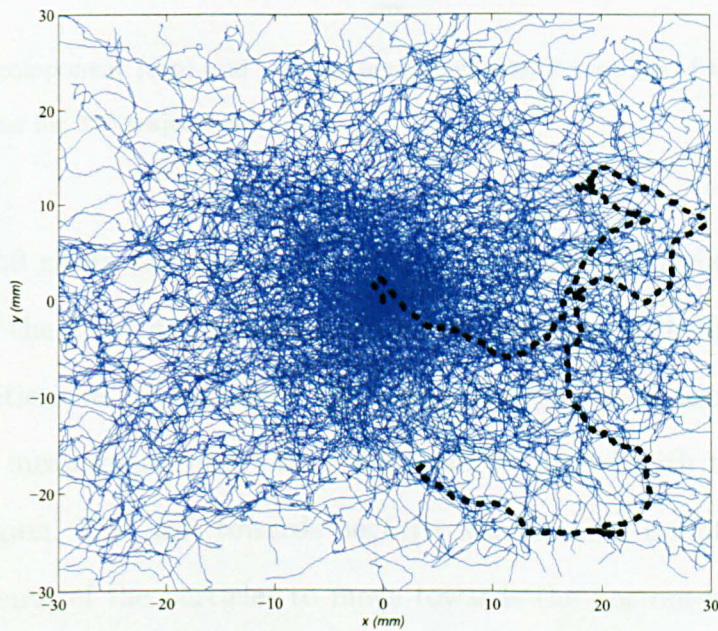


Fig. 2.7: Trajectories of 325 bronze particles of average diameter $d = 0.8\text{mm}$. One of such trajectories is plotted as a dashed line as an illustration. The experiments were carried out using sandpaper with a grit size of $68\mu\text{m}$.

From this image it is not obvious to observe a preferred direction of motion. The particles seem, at first glance, to follow a random trajectory through out the surface of the cell without an obvious bias towards any direction. In figure 2.8 the vertical and horizontal components of the trajectories are shown as a function of the elapsed time, t .

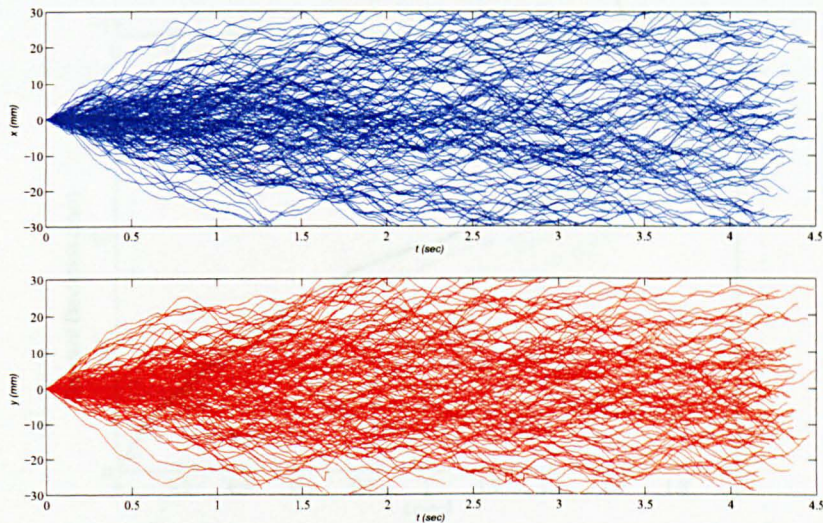


Fig. 2.8: x -component (top) and y -component (bottom) of position of the particle as a function of time for 325 trajectories.

Figure 2.9 shows the mean value (top), the standard deviation (middle) and ratio of the mean and standard deviation (bottom) of the horizontal and vertical positions of the particles. The calculation was done using 325 trajectories. The mean values of x and y are small compared with the size of the observed region. The drift towards negative values could be interpreted as a weak preference of the particles to move towards the bottom-left side of the cell. However there is no clear indication that this is the case. The standard deviations in the x and y direction are also shown in figure 2.9. It can be observed that both curves remain approximately equal for all times.

The particle's displacement between frames, Δx is calculated from the

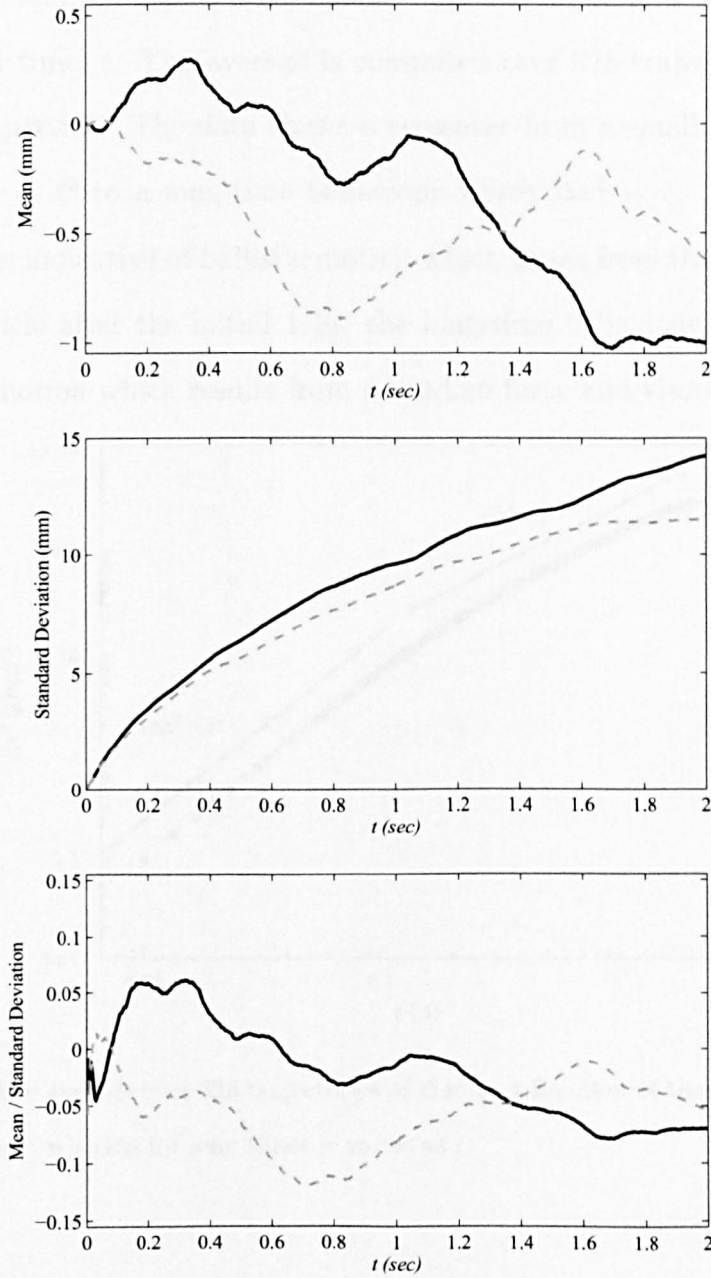


Fig. 2.9: Mean values (top), standard deviation (middle) and the ratio of the mean and the standard deviation (bottom) of the horizontal (continuous line) and vertical (dashed line) of the position of the particle as a function of the time, t . These quantities were computed over 325 trajectories for a $d = 0.8\text{mm}$ bronze particle moving on top of sandpaper with a grit size of $68\mu\text{m}$. The parameters of vibration were $f = 100\text{Hz}$ and $\Gamma = 2.5$.

trajectories and, in Figure 2.10, the average Δx^2 is plotted as a function of the elapsed time, t . The average is computed over 325 trajectories, each for a different particle. The data shows a crossover from a small-time behaviour where $\Delta x^2 \sim t^2$ to a long-time behaviour where $\Delta x^2 \sim t$. The short-time behaviour is indicative of ballistic motion which arises from the initial velocity of the particle after the initial 1/3s; the long-time behaviour is indicative of Brownian motion which results from a random force and viscous damping.

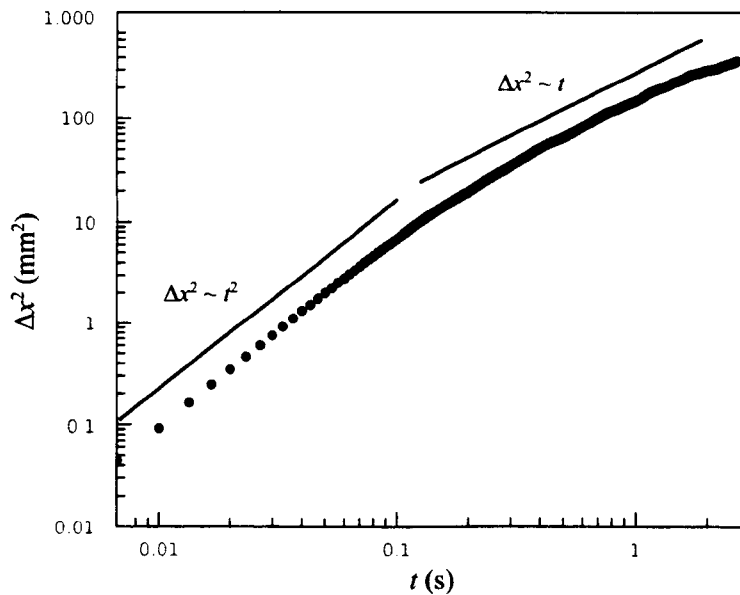


Fig. 2.10: The average over 325 trajectories of Δx^2 as a function of time. For small times Δx^2 varies as t^2 whereas for long times it varies as t .

2.3.4 Discussion

The simplest model that captures the features of the experimental data plotted in figure 2.10 can be obtained from the Langevin equation

$$m \frac{dv_\alpha}{dt} = -m \frac{v_\alpha}{\tau} + \eta_\alpha(t), \quad (2.4)$$

where τ is a time constant associated with the frictional forces acting upon the particles (drag effect), m is the particle mass, v_α is the particle's velocity

component in Cartesian direction α and $\eta_\alpha(t)$ is Gaussian white noise with correlator $\langle \eta_\alpha(t)\eta_\beta(t') \rangle = 2D\delta(t-t')\delta_{\alpha,\beta}$ ($\delta_{\alpha,\beta} = 0$ for $\alpha \neq \beta$ and $\delta_{\alpha,\beta} = 1$ otherwise). D is the diffusion constant and, in our case, is associated with the loss of energy through collisions. The effective viscous force, $-m\mathbf{v}/\tau$, is assumed to be proportional to the particle's speed. The displacement Δx^2 as a function of time, t , for a particle which starts with an initial speed $v_x(0)$ is

$$\Delta x^2 = \frac{2D\tau^3}{m^2} \left[t/\tau - (1 - e^{-t/\tau}) - \frac{1}{2}(1 - e^{-t/\tau})^2 \right] + \langle v_x(0)^2 \rangle \tau^2 (1 - e^{-t/\tau})^2. \quad (2.5)$$

where $\langle v_x(0)^2 \rangle$ is the initial x -component of the velocity averaged over independent trajectories. A similar expression to equation 2.5 holds in the y -direction.

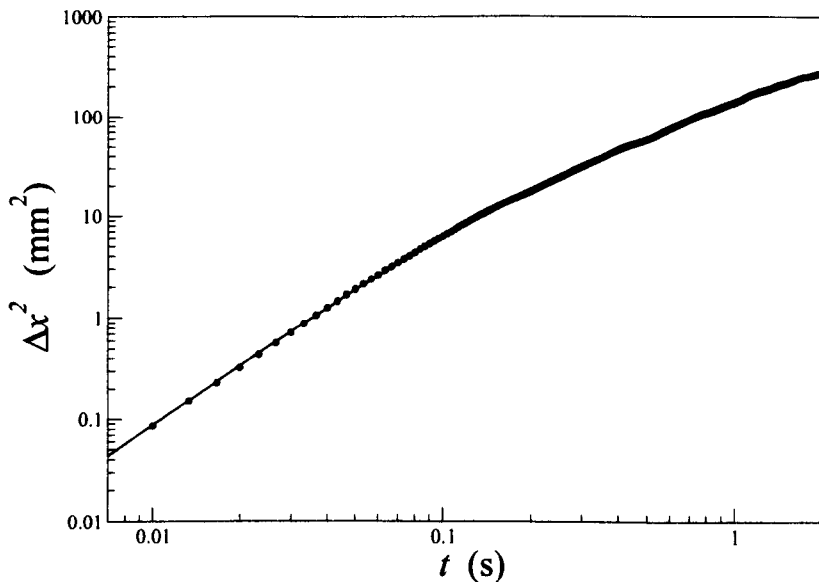


Fig. 2.11: The average over 325 trajectories of Δx^2 as a function of time. The solid line is a best fit to equation 2.5 which enables us to extract values of D and τ .

The solid line shown in figure 2.11 is the best fit of equation 2.5 to all the experimental data with τ , D and $\langle v_x(0)^2 \rangle$ left as fitting parameters. For

longer times than shown here a significant fraction of the particles move outside the field of view of the camera so this data is unreliable. The values of τ and D found from fitting the data are $\tau = 0.123\text{s}$ and $D = 2.9 \times 10^{-14} \text{kg}^2 \text{m}^2 \text{s}^{-3}$, with $\pm 3\%$ error. The fit is very good over the range shown which shows that the motion of a single particle driven by a roughened, vibrated surface can be described accurately by a random force model which includes viscous damping.

2.4 Long-range Structure of a randomly-driven granular sub-monolayer

We now consider the behaviour of a sub-monolayer of bronze particles vibrated on the same roughened surface. In particular we wish to investigate the long-ranged structure experimentally and compare it to that obtained from computer simulation of a randomly-forced gas. The long-ranged structure is best measured by considering the time-averaged, density-density structure factor, $S(\mathbf{k})$, defined by the equation

$$S(\mathbf{k}) = \frac{1}{N} \int \int \langle \rho(\mathbf{r}) \rho(\mathbf{r}') \exp(-i\mathbf{k} \cdot (\mathbf{r} - \mathbf{r}')) \rangle d\mathbf{r} d\mathbf{r}', \quad (2.6)$$

where $\rho(\mathbf{r}) = \sum_{i=1}^N \delta(\mathbf{r} - \mathbf{r}_i)$ and \mathbf{r}_i are the positions of the N particles.

In previous theoretical studies of the purely random-force model, the circular-averaged $S(k)$ has been shown to exhibit a power-law divergence for small k . However, to our knowledge, no attempt has been made to measure this quantity experimentally.

2.4.1 Experimental Procedure

For the experiments described in this section, the experimental setup consisted of bronze granules vertically vibrated on the roughened surface of the horizontal tray. The bronze granules varied in sizes but, otherwise stated, the results presented in this section were obtained using particles with mean diameter $d = 0.8 \pm 0.03\text{mm}$ and average mass $m = 2.4 \times 10^{-6}\text{kg}$.

The tray was mounted on the industrial shaker as described previously. Care was taken to ensure that the surface was horizontal and the same procedure describe in the previous section was followed so that the distribution of grains across the surface was homogeneous on the average. A 1000W halogen bulb was used to provide the illumination. The lamp was positioned to illuminate the tray forming an acute angle to reduce reflections from the roughened surface.

The shutter speed, aperture and focus of the digital camera were adjusted and it was programmed to take a snapshot every 5 seconds. The size of the observation window was 92mm by 92mm and the position of each particle could be determined to a resolution of 0.05mm.

A collection of grains were placed in the tray and the vibration was switched on. The tray was vibrated at 100Hz in the vertical direction and, for most of the experiments, the amplitude of vibration was chosen so that the maximum acceleration of the surface relative to gravity, Γ , was 2.5.

Image Analysis

The images were analysed using Matlab. The procedure was similar to that followed to measure the trajectories of single particles. The analysis started by enhancing the images. The RBG image was converted to a grey-scale image

in the first step of the image-enhancing routine.

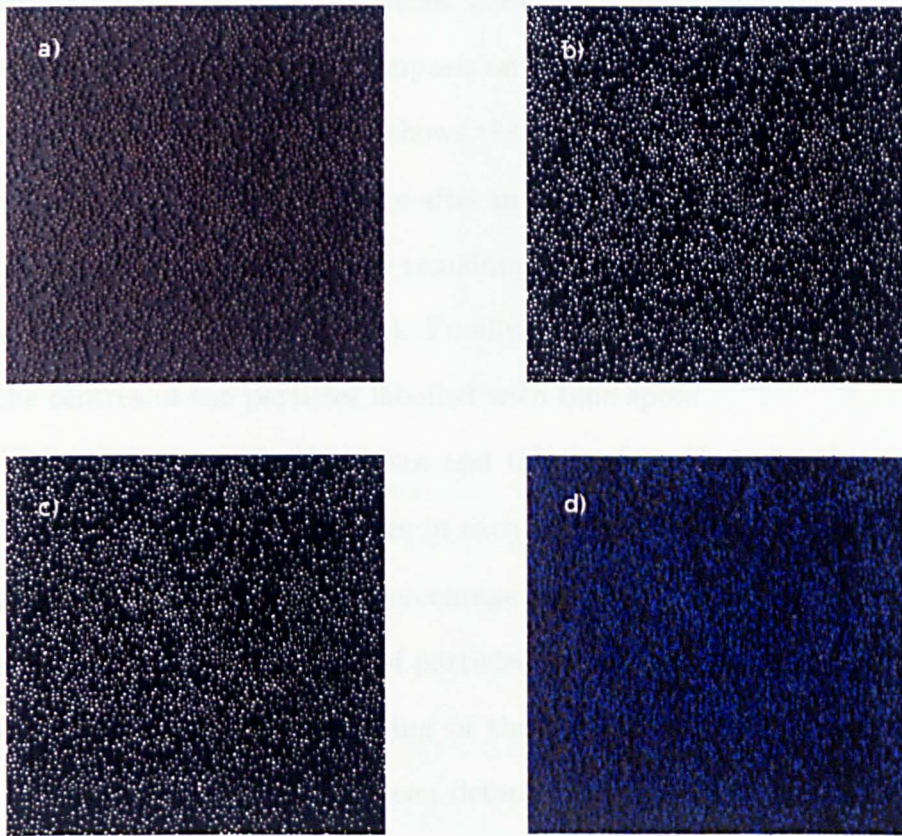


Fig. 2.12: Image Processing. The original image is shown in (a). The resulting images obtained during the enhancing routine are shown in (b) and (c). In b) the resulting black and white image after increasing the contrast and applying the intensity cut-off is shown. The remaining particles after elimination of the smaller objects is shown in figure c). The centres of the particles are shown as blue spots in (d).

Three parameters were controlled to locate the particles. From the camera's point of view, particles in close vicinity to each other could seem to overlap and be taken as a single object. To prevent this to happen, the contrast was increased and a threshold on the intensity of the signal (intensity of the reflection) was applied. These two steps allowed the identification of particles touching each other as separate objects. The third control parameter was the size of the particle. Applying a minimum limit on the size of the

particles removed most of the reflections coming from the surface of the tray. The centres of the remaining particles were found using the Matlab function *centroids*. Figure 2.12 shows a composition of images illustrating the particle recognition routine. Figure 2.12a shows the image taken by the camera, in b) the resulting black and white image after increasing the contrast and applying the intensity cut-off is shown. The remaining particles after elimination of the smaller objects is shown in figure c). Finally, figure d) shows the original image with the centres of the particles labelled with blue spots.

Due to limitations of the camera and the experimental setup, it was not possible to identify all the particles in each image. However, typically only 1 % of particles were missed. This percentage is an estimated obtained by direct comparison between the number of particles identified by the programme and the one obtained by visual counting of the particles every hundred images. Once the particle positions had been determined, $S(k)$ and the pair correlation function, $g(r)$, were calculated assuming periodic boundary conditions, as explained in the next section. The time-average was carried out using 1000 images.

2.4.2 Experimental Results

To calculate the pair correlation function, $g(r)$, only the particles within the central squared region shown in figure 2.13 were considered to mimic periodic boundary conditions. For each particle located in this region, a circular area of radius $r_{max} = l/4$ (where l is the length of the square image) was defined and the number of particles at a particular distance $r_{ij} \lesssim r_{max}$ were counted.

The pair correlation function, $g(r)$, obtained from experiment is shown in figure 2.14. In this figure it is possible to see that the small- r behaviour of

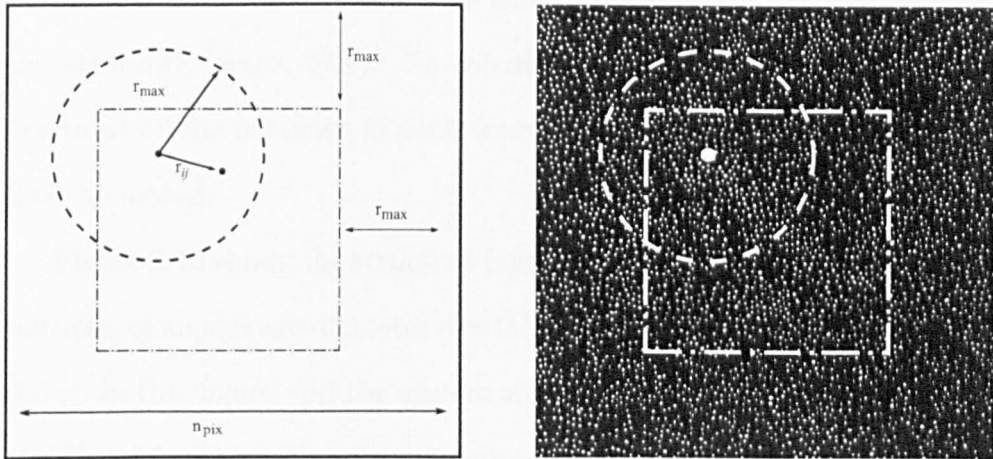


Fig. 2.13: The pair correlation function, $G(r)$, was obtained for a square region at the centre of the tray of size $l/4$, where l is the size of the image. A circular region of radius r_{max} was defined for each particle within the dash-bordered region and the distances with every other particle within the circle was measured.

$g(r)$ closely resembles that of an equilibrium hard-sphere gas. However, the long-ranged structure only shows up as a weak decay for large values of r .

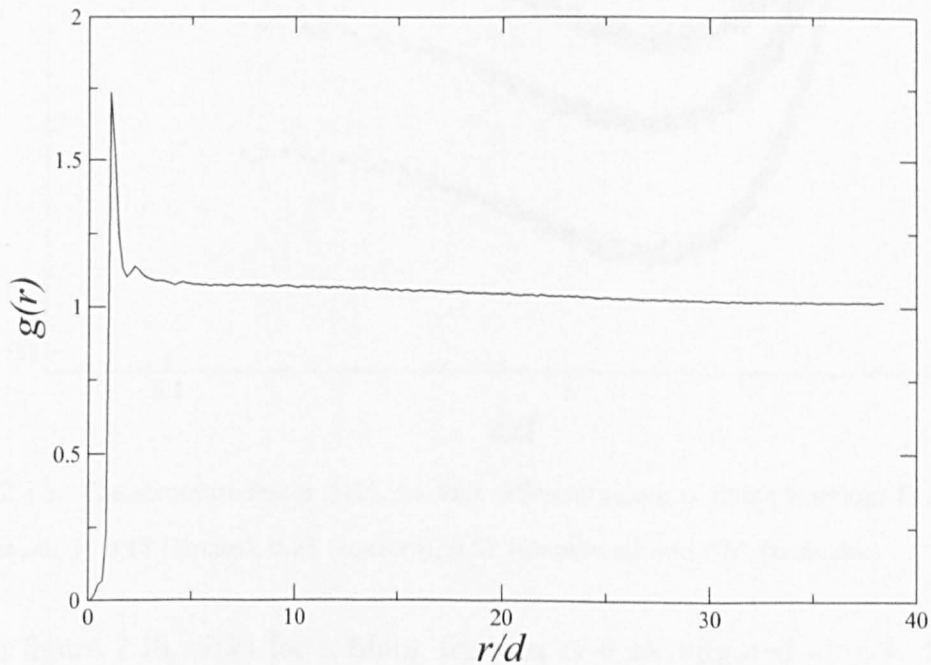


Fig. 2.14: The experimentally determined correlation function $g(r)$. The long-ranged structure only shows up as a weak decay in $g(r)$ for large r .

As mentioned previously, the long-range structure is best measured by the structure factor, $S(k)$. To calculate $S(k)$, the Fourier transform of the positions of the particles in each frame was taken and the average over time was calculated.

Figure 2.15 shows the structure factor for four areal filling fractions. Bronze particles of an average diameter $d = 0.8\text{mm}$ were used for the set of experiments shown in this figure and the system was vibrated with a frequency $f = 100\text{Hz}$ and $\Gamma = 2.5$. The behaviour appears to be the same; the curves can be moved to collapse the behaviour for small values of k . Currently this feature remains unexplained and future work will be needed in order to understand this result.

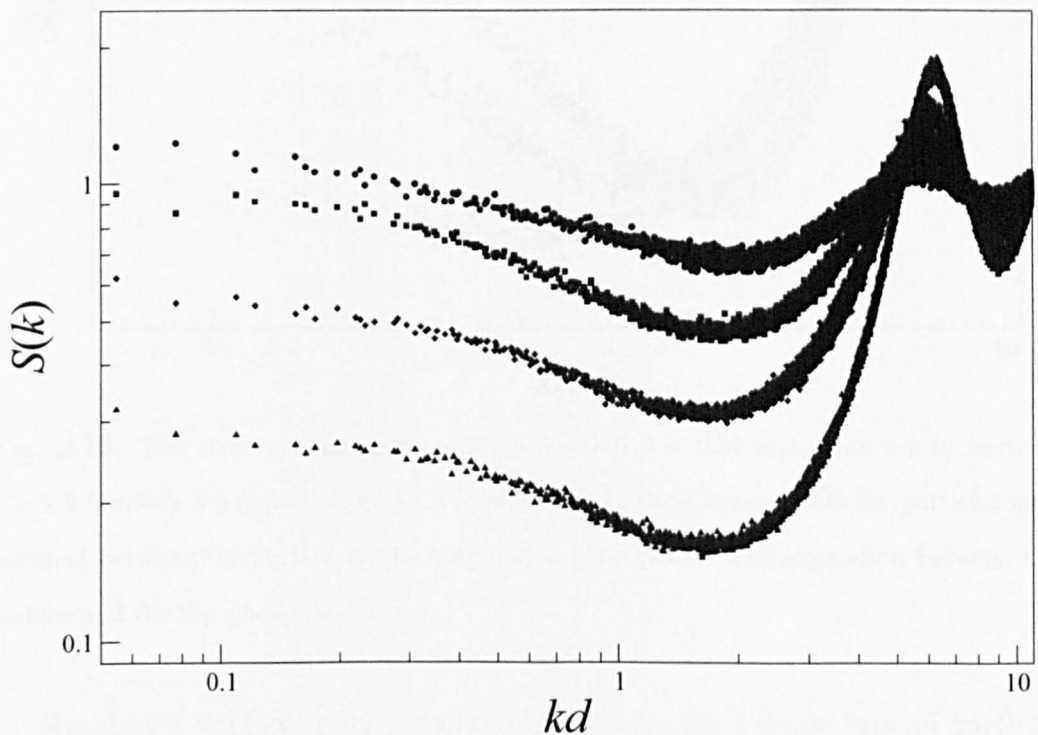


Fig. 2.15: The structure factor $S(k)$, for four different values of filling fraction. From top to bottom, ϕ : 0.13 (circles), 0.25 (squares), 0.37 (diamonds) and 0.51 (triangles).

In figure 2.16, $S(k)$ for a filling fraction of 0.25, vibrated at $f = 100\text{Hz}$ and values of $\Gamma = 2.5, 5.0,$ and 7.5 is shown. In these experiments the grains were confined by an upper flat glass plate, 3mm above the emery paper. As

Γ increases, the long-ranged structure (the slope displayed by $S(k)$ for small values of k) was found to decrease. For the largest value of Γ , $S(k)$ is almost featureless, closely resembling that of an equilibrium hard-sphere gas. Similar results were found by Reis *et al.* (2006b) from measurements of their pair correlation function.

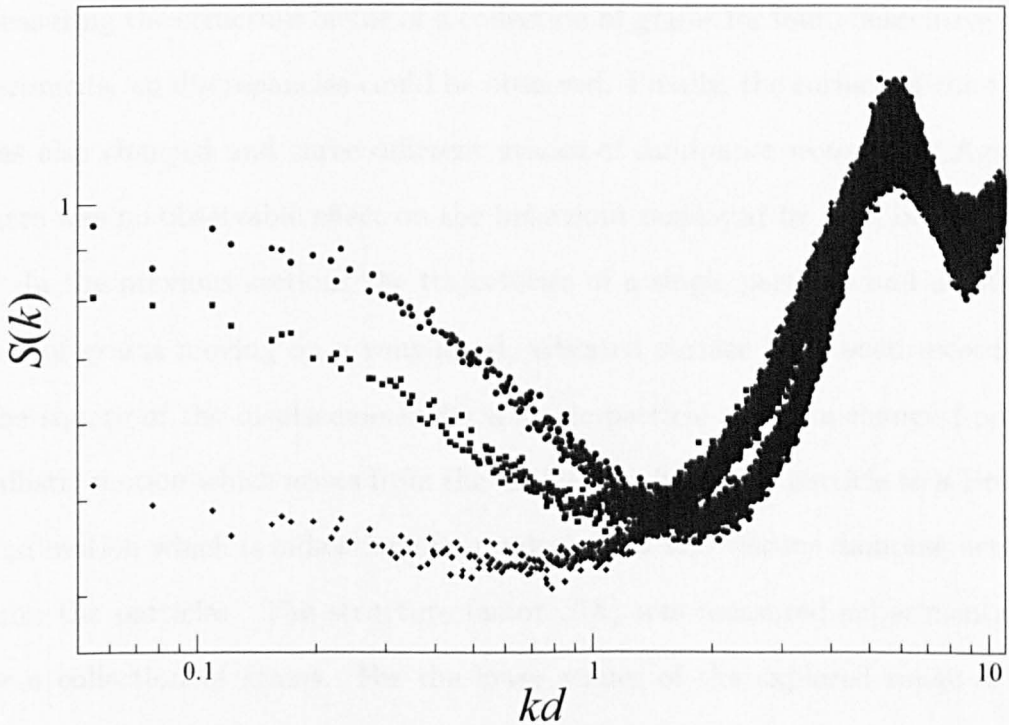


Fig. 2.16: The structure factor for a filling fraction $\phi = 0.25$ and, from top to bottom, $\Gamma = 2.5$ (circles), 5.0 (squares), and 7.5 (diamonds). In these experiments the particles were confined between the surface of the tray and a glass plate. The separation between the surface and the top plate was 3 mm.

For clarity, we have only presented the results for a single type of particle. However, the corresponding $S(k)$ and $g(r)$ for bronze particles of average diameter $d = 1.1\text{mm}$ and lead shots of average diameter $d = 2.0\text{mm}$ were also calculated.

The results for these particles were consistent with the ones presented in this section. The effect of the continuous motion of the particles on a rough-

ened surface was also explored, as follows. There was the possibility that the characteristics of the surface of the particles were being affected by the continuous interaction with the sandpaper. The particles bounce repetitively on the roughened surface and their surface could be eroded, this could have had an effect on the interaction during collisions between particles. However, after measuring the structure factor of a collection of grains for four consecutive experiments, no discrepancies could be observed. Finally, the surface of the tray was also changed and three different grades of sandpaper were used. Again, there was no observable effect on the behaviour displayed by $S(k)$ or $g(r)$.

In the previous sections the trajectories of a single particles and a collection of grains moving on a roughened, vibrated surface have been recorded. The square of the displacements for a single particle shown a change from a ballistic motion which arises from the initial velocity of the particle to a Brownian motion which is indicative of a random force and viscous damping acting upon the particles. The structure factor $S(k)$ was measured experimentally for a collection of grains. For the lower values of the explored range of Γ , $S(k)$ exhibited some features for small values of k which suggests a long-range structure. However, the experimental evidence is not conclusive since these features are observed to weaken as k decreases.

2.5 Computer Simulations of the long-range structure of a 2-D gas

In order to compare the experimental results with the random-force model, soft-sphere molecular dynamics simulations were carried out by other members of the Granular Dynamics Group at The University of Nottingham. The

modelled system consisted of N spherical particles of the same size and density as those in the experiments. The particles were assumed to move in two-dimensions within a 92mm by 92mm region. In the absence of collisions, each particle was set to obey the Langevin equation (equation 2.4) with the values of τ and D taken from the fit of the experimental data. Particle interactions were modelled using a linear repulsive force and dash-pot damping; the damping parameter was chosen so that the coefficient of restitution was 0.5. For simplicity, particle rotation and tangential friction were ignored.

In figure 2.17 shows the structure factor, $S(k)$, for a system of 2274 particles of mean diameter 0.8mm, contained within the square region, giving an areal filling fraction of 13%. In this figure, the experimental data is plotted as solid circles and the solid line represents the corresponding simulated data. It is possible to observe that the agreement between the experiment and simulation is good. The short-ranged order gives rise to the peak in $S(k)$ at $kd \sim 2\pi$ while the small k behaviour is a measure of the long-ranged structure. For comparison, the upper dashed line shows $S(k)$ from a simulation in which there is no viscous dissipation ($\tau \rightarrow \infty$); the lower dashed line shows $S(k)$ for an equilibrium hard sphere gas of the same filling fraction. It can be seen that the long-ranged structure of the experimental system lies between these two ideal limits.

Computer simulations revealed that the rise in $S(k)$ as k decreases (for $kd < 1$) was a remnant of the purely random force model; the levelling of at very low k arises from the presence of viscous damping. As $\tau \rightarrow 0$ the computed $S(k)$ tended towards that of an equilibrium hard-sphere gas.

There was good agreement between the theoretical and experimental results for low values of filling fraction. In figure 2.18 the structure factor obtained

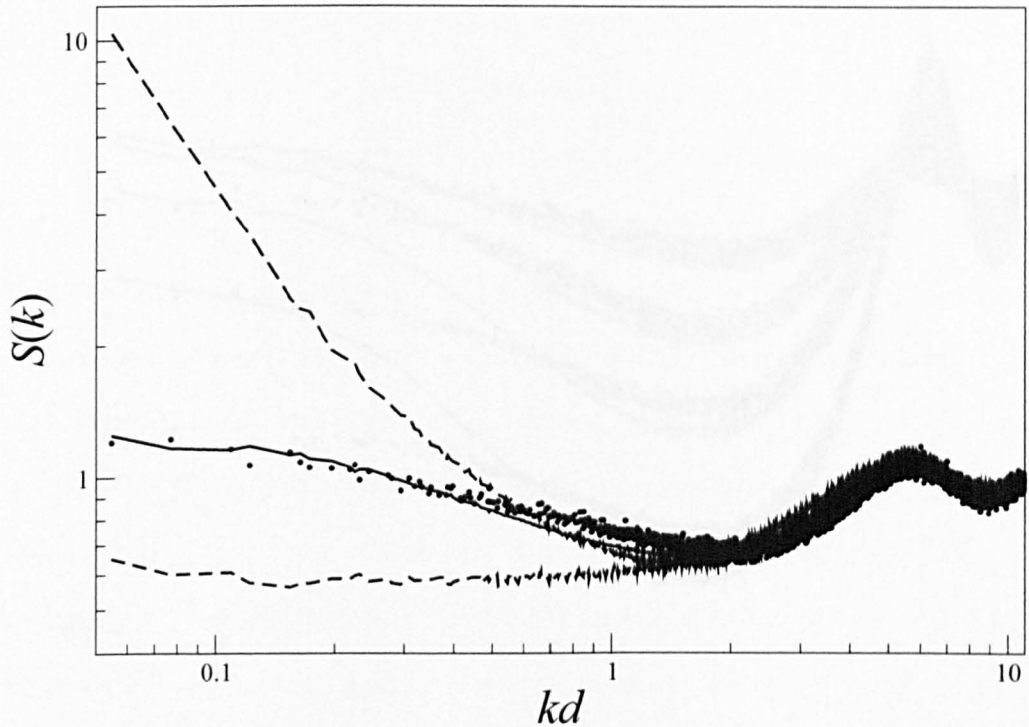


Fig. 2.17: Structure factor $S(k)$ as a function of k for a filling fraction of 0.13. The points show the experimental data and the solid line shows the results of the simulation using the values of D and τ obtained from Fig. 1. The upper dashed line shows $S(k)$ obtained from a simulation in which the viscous force is absent. The lower dashed line shows the corresponding $S(k)$ for a hard sphere gas.

from experiments and simulation for four filling fractions is shown. The same values of D , τ and the coefficient of restitution were used for each simulation. Although the simulations and experimental results show the same qualitative features there is a systematic disagreement for small values of kd as the filling fraction increases.

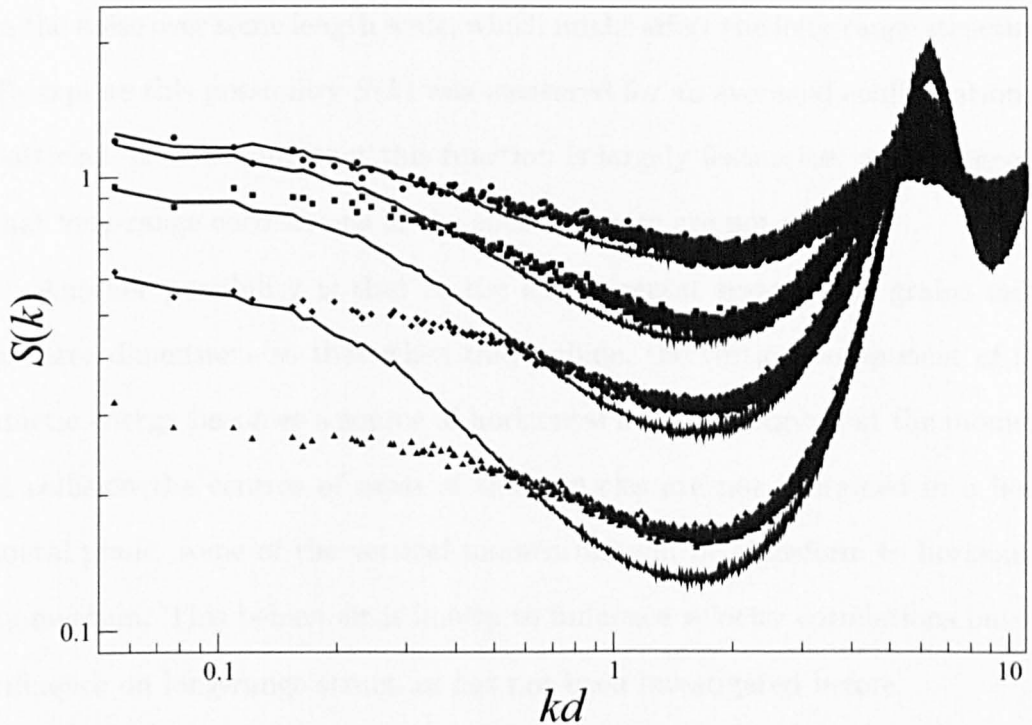


Fig. 2.18: The structure factor, $S(k)$, for four different values of filling fraction: ϕ : 0.13 (circles), 0.25 (squares), 0.37 (diamonds) and 0.51 (triangles). The solid lines show the simulated data for the corresponding filling fraction. The agreement between simulation and experiment weakens as the filling fraction increases.

2.6 Discussion

The behaviour of $S(k)$ in the simulations can be understood by considering the single particle motion. As the filling fraction increases, the distance between collisions decreases, and the particle motion between collisions is dominated by the random force rather than the viscous dissipation. As a result there is a steeper slope in $S(k)$ for larger filling fractions as more of the purely random force behaviour is revealed. However, this behaviour which is predicted by the simulations is not observed experimentally. This disagreement suggests that an additional feature which becomes important as the filling fraction increases has been omitted from the model.

One possibility is that the roughened surface introduces spatial correlation

in the noise over some length scale, which might affect the long-range structure. To explore this possibility $S(k)$ was measured for an averaged configuration of particles. It was found that this function is largely featureless which suggests that long-range correlations in the effective noise are not present.

Another possibility is that in the experimental system, the grains move in three dimensions so that when they collide, the vertical component of the kinetic energy becomes a source of horizontal kinetic energy; if at the moment of collision the centres of mass of the particles are not contained in a horizontal plane, some of the vertical momentum will be transform to horizontal momentum. This behaviour is known to influence velocity correlations but its influence on long-range structure has not been investigated before.

2.7 Final Remarks

In this chapter the trajectories of single particles moving on a roughened surfaces have been described. Using high speed video recording and computer particle tracking it was found that, for particles starting at rest, the ballistic motion exhibited at the beginning of their trajectories changed to a long-time behaviour with characteristics of Brownian motion. The long-time behaviour of the motion was the result of a random force and a viscous damping acting simultaneously on the particles.

Later, the structure factor, $S(k)$, of a collection of grains vertically vibrated on a roughened surface was also measured experimentally. It was observed that the behaviour for small- k did not fit the predictions of the random force model nor did it have the characteristics of a hard sphere gas. Computer simulations were performed using the information obtained from the study of the trajectories of single particles. Adding a viscous damping term to the random

force model, the simulations reproduced the experimental measurements with good agreement for low values of filling fraction.

Chapter 3

Fluid-Immersed Granular beds

In this chapter we describe experimental work carried out to investigate some of the phenomena observed when a granular bed surrounded by a fluid is subjected to vertical vibrations. In particular we study the spontaneous migration of grains in a partitioned container and the influence of a fluid on the Brazil nut effect. The aim of these experiments is to provide a set of quantitative results to be compared with the predictions of the simulation models developed within our research group.

We start this chapter with an introduction to the subjects of study, namely, the Brazil Nut effect and the partition instability. We follow with a section providing a detailed description of the general setup used in both of our experiments. The remainder of the chapter is then divided into three sections; the experimental details of the partition instability study will be given in the first section along with the experimental observations and results. At the end of this section, the experimental results will be compared with predictions of computer simulations carried out within our research group. The second section will cover the experimental details of the Brazil nut experiment. Again, the results from our experiments will be compared against simulations at the

end of the section. Lastly, we present a summary containing the main findings of our study taking into consideration both the experimental and simulation results.

The work described in this chapter has produced the following articles: P.J. King; P. Lopez-Alcaraz; H.A. Pacheco-Martinez; et al. *Instabilities in vertically vibrated fluid-grain systems*, European Physical Journal E, **22**, 219-226 (2007); C.P. Clement; H.A. Pacheco-Martinez; M. R. Swift and P. J. King. *Partition Instability in water-immersed granular systems*, Physical Review E, **80**, 011311 (2009) and C.P. Clement; H.A. Pacheco-Martinez; M. R. Swift and P. J. King. *The water-enhanced Brazil nut effect*, European Physics Letters, **91**, 54001 (2010).

3.1 Introduction

A seemingly simple granular system such as a collection of grains stacked under the effect of gravity can exhibit interesting phenomena. For example, through the formation of stress chains, regions of the material become isolated from the load of the surrounding grains; the distribution of stresses within a granular pile is not homogeneous. If the grains are contained by boundaries, the stress chains transfer the load to the boundaries. When energy is injected to the particles, by vibrating the containers for example, a richer set of phenomena can be observed. The behaviour of the granular bed will depend on several factors including the specific geometry of the vessel as well as the properties of the fluid surrounding the grains, if present. The phenomena studied in this chapter, namely the partition instability and the Brazil nut effect, will be introduced in the remainder of this section.

3.1.1 The Partition Instability

It has been shown that the inelastic nature of granular materials provides a mechanism for the partition instability (Eggers 1999). It is commonly observed that within a collection of kinetically active grains, dense regions will experience dissipative collisions more frequently and, as result, the grains moving in these regions will lose energy more rapidly than those in less dense regions. The system will spontaneously condense in the more dense regions making them become even more dense as they rapidly lose energy. This is the phenomenon of inelastic collapse (Goldhirsch and Zenetti 1993; McNamara and Young 1994). Related behaviour of this type is dramatically displayed by grains contained within a vertically vibrated box which is divided by a vertical partition either of finite height or containing a small elevated hole (Eggers 1999; Van der Meer *et al.* 2002; van der Weele *et al.* 2001). If there are more grains on one side of the partition, then those grains will experience greater dissipation and be less kinetically active; they will bounce less high than those on the other side of the partition where there are fewer grains. This difference in kinetic energy may cause a net flow of grains over the partition, or through the hole, from the minority side to the majority side, see figure 3.1 for an example of this behaviour. Under the appropriate conditions of vibration all of the grains may move to one side of the partition (Eggers 1999; Van der Meer *et al.* 2002; van der Weele *et al.* 2001). Similar behaviour has also been observed within vibrated granular mixtures. Furthermore for particular vibratory conditions this instability may lead to periodic oscillatory motion of the grains from one partition to the other (Hou *et al.* 2008; Lambiotte *et al.* 2005; Viridi *et al.* 2006).

Our aim is to investigate a second mechanism which can give rise to a spatial

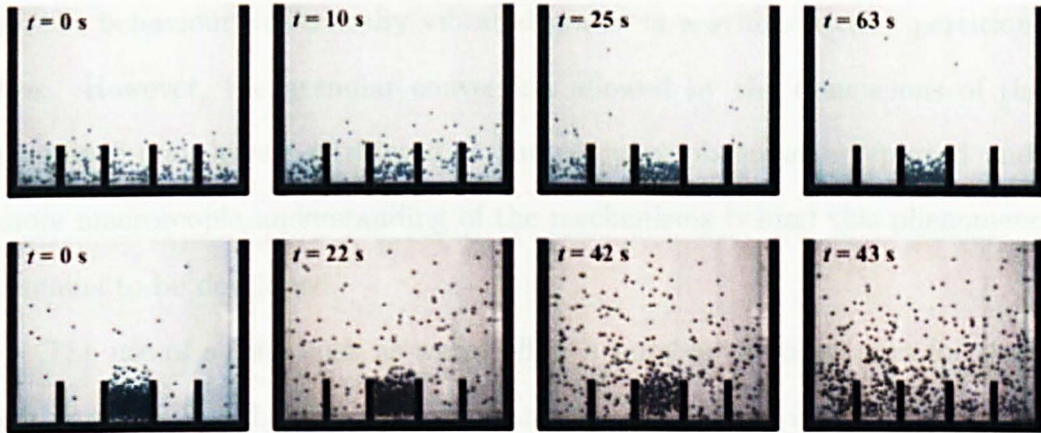


Fig. 3.1: Maxwell demon experiment for a 5-compartment cell. Top: Four stages in the clustering experiment. The particles do not cluster directly into one compartment but go through a two-cluster transient state which can be seen at $t = 10\text{s}$ and $t = 25\text{s}$. Bottom: Breakdown of the cluster when the strength of vibration is increased. The cluster is seen to survive up to $t = 42\text{s}$ and suddenly collapses. After just one second the distribution of particles is uniform. Image taken from Van der Weele (2008).. No details of the driving conditions were provided.

instability, namely, the interaction between fine grains and a background fluid. This process may be illustrated using a fluid immersed granular bed within a vertically-vibrating partitioned cell with two connecting holes, one at the top and one at the bottom of the cell. A gradual transfer of grains through the connecting hole at the base of the cell will result in the granular bed to move into just one of the columns.

Ohtsuki *et al.* (1998) studied one such system. In their experiments, fine grains surrounded by air were vibrated within a partitioned container. They observed that the presence of air influences the height difference between the beds on either side of the container. Chen and Wei (Chen *et al.* 1998) have suggested that this height difference may be caused by the same air-driven mechanism used to explain Faraday heaping as described by Pak *et al.* (1995). Akiyama *et al.* (1991) have carried out a detailed study of the influence of air

on the behaviour of vertically vibrated grains in a symmetrically partitioned box. However, the granular convection allowed by the dimensions of their container may have contributed to the complex phenomena reported and a more macroscopic understanding of the mechanisms behind this phenomenon remains to be developed.

The use of a fluid such as water offers a number of advantages for studying partition instabilities. Firstly, water enables larger particles to be used, making the observation of the granular dynamics considerably simpler than for air. In a non-turbulent fluid flow, the effects of fluid drag on the granular dynamics scales approximately as $\rho_g d^2 / \eta$, where ρ_g is the density of the granular material, d is the grain diameter and η is the dynamic viscosity of the surrounding fluid (Leaper *et al.* 2005). At room temperature (20°C), water is about 50 times more viscous than air. This suggests that similar effects may be observed in water for particles approximately 7 times larger in diameter than for the equivalent behaviour exhibited by fine particles in air.

The increased damping due to the presence of a liquid such as water (Gondret *et al.* 2002) reduces the granular temperature of a thrown bed maintaining the porosity, ϕ , closer to the value appropriate to a random packing of spheres. This makes comparison with the theory which more straightforward than would be the case for a fluid such as air. Another advantage is that water eliminates the effects of static electricity which often slow and otherwise modify the dynamics of dry granular systems when they are shaken vigorously for long periods, particularly within an insulating box (Leaper *et al.* 2005).

3.1.2 The Brazil Nut Effect

In the *Brazil nut effect* (BNE) a large heavy object, often referred to as an *intruder*, rises to the top of a bed of smaller particles under the influence of vertical vibration (BNE) (Harwood 1977; Williams 1976). Various mechanisms have been proposed as candidates to explain this behaviour. The *ratcheting* mechanism (Bridgewater *et al.* 1969; Rosato *et al.* 1987; Williams 1977) proposes that small grains fall beneath the large particle as the vibrated bed expands. When the bed comes back to its rest state the intruder is elevated by the smaller particles that have fallen beneath it. Another mechanism, the “convection-driven” mechanism, notes that the entire granular bed moves in vertical convection rolls, with broad upward moving regions at the centre of a shaken container and narrow downward moving regions along the edges (Ráktai 1976; Knight *et al.* 1993; Cooke *et al.* 1996, Poschel and Herrmann 1995, Gallas *et al.* 1996). In the convection-driven case, segregation occurs because the larger intruder particle cannot re-enter the downward flow and thus remains at the top of the bed. Both of these mechanisms tend to segregate large particles above smaller ones.

Recent studies have investigated the effects of a fluid such as air on the Brazil nut effect. It was observed that the presence of an interstitial fluid dramatically influences the motion of the intruder through a fine granular bed (Möbius *et al.* 2001; Naylor *et al.* 2003; Yan *et al.* 2003). Möbius *et al.* showed that the presence of air strongly influences the rising of the intruder. Naylor *et al.* demonstrated that not only the presence of air but also the motion of air coupled to the granular bed plays a key role in the intruder’s behaviour. The effects of air pressure have been investigated by Yan *et al.*.

The influence of air on granular segregation has also been investigated

both in experiment (Burtally *et al.* 2002) and simulation (Biswas *et al.* 2003; Wylie *et al.* 2008). Under vertical vibration almost complete segregation may occur with one component rising to the top or forming a sandwich structure. Similar effects have been observed for larger grains in water (Leaper *et al.* 2005). Under horizontal vibration, where the role of gravity can be ignored, segregation into a striped configuration occurs (Sanchez *et al.* 2004).

In all these cases the basic mechanism responsible for the BNE or segregation is the fact that the fluid provides a differential drag force which influences the two components differently.

3.2 Vertical Vibratory Apparatus

The experimental work described in this chapter required to subject a container to carefully controlled vertical vibrations. For this effect we used a vertical vibratory apparatus. The apparatus consisted of two long-throw electromagnetic transducers (8-inch loudspeakers by Peerless) mounted facing each other on a rigid frame constructed from medium density fibreboard (MDF). A horizontal surface was created on top of the diaphragms using expanded polyurethane foam. A rigid, horizontal metal plate was attached to each of these surfaces and four metal pillars were used to join both plates creating a rigid frame joining the loudspeakers which ensured vertical motion during vibration. Figure 3.2 shows a schematic view of the apparatus. The loudspeakers were wired in anti-phase to obtain a one-direction motion when the external driving signal was applied. The motion of the loudspeakers was monitored using a pair of capacitance cantilever accelerometers, Analog Devices ADXL105 and ADXL150, attached to the top transducer. The accelerometers covered the ranges from $0 - 7g$ and $0 - 70g$ respectively, where g is the acceleration due to gravity.

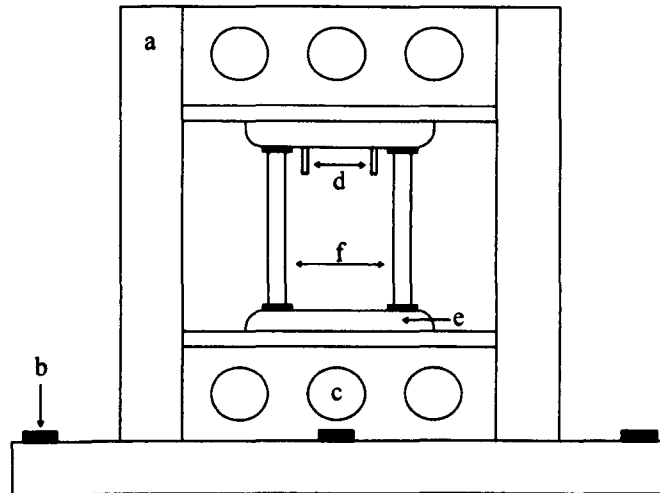


Fig. 3.2: A schematic representation of the vertical vibratory apparatus. The MDF frame (a) is firmly bolted to a concrete block using variable-length bolts (b). A set of holes (c) were cut in the MDF frame to prevent resonance. The aluminium frame (f) is fixed to the polyurethane foam surface of each loudspeaker (e). The motion of the loudspeakers was monitored by two accelerometers (d).

Vibrational motion from the loudspeakers can be transmitted to the MDF frame. To reduce the effect of such vibrations the MDF frame was bolted to a set of two concrete blocks weighing approximately 250kg each. The concrete blocks were separated by a layer consisting of a cork sheet and a butyl matting. A further set of layers of these materials was placed between the bottom concrete block and the floor of the laboratory to remove any resonant modes from the concrete blocks. Furthermore, four heavy lead block were also put on top of the frame to reduce the effects of unwanted resonant modes. A picture of this apparatus is shown in figure 3.3.

A continuous sinusoidal wave was generated to drive the transducers using a Signal Generator Model DS345 by Stanford Research Systems. The frequency and peak-to-peak voltage of the driving signal was adjusted to the desired values and sent through a device fitted with an on/off switch and a potentiometer to a custom-made power amplifier. The potentiometer allowed

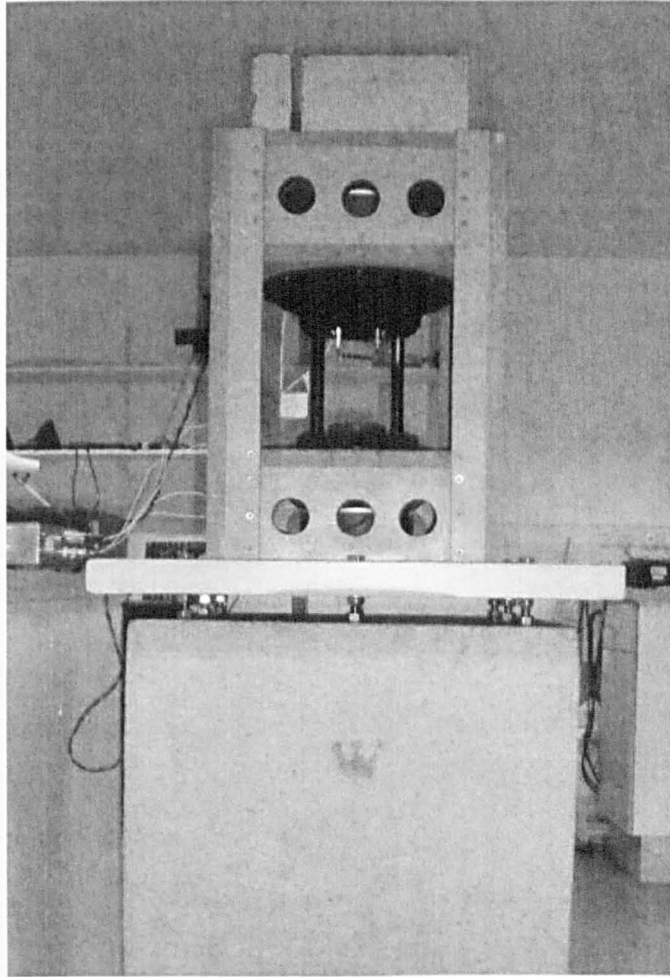


Fig. 3.3: Picture of the vertical vibratory apparatus. The transducers can be seen mounted in a MDF frame which is bolted to a concrete block. Additional lead weights are placed on top of the frame to prevent resonant modes from the transducers.

a finer control over the maximum voltage of the signal fed to the transducers hence controlling the maximum acceleration experienced by the apparatus. This acceleration was monitored by the pair of accelerometers described above. The signal from the accelerometers was sent through a 4-pole low-pass Bessel filter with a cut-off frequency of 800 Hz. The output was displayed in a digital voltmeter which was calibrated so that the voltages shown corresponded to the maximum dimensionless acceleration, Γ . Figure 3.4 shows a schematic view of the electronic components and signals of the experimental setup.

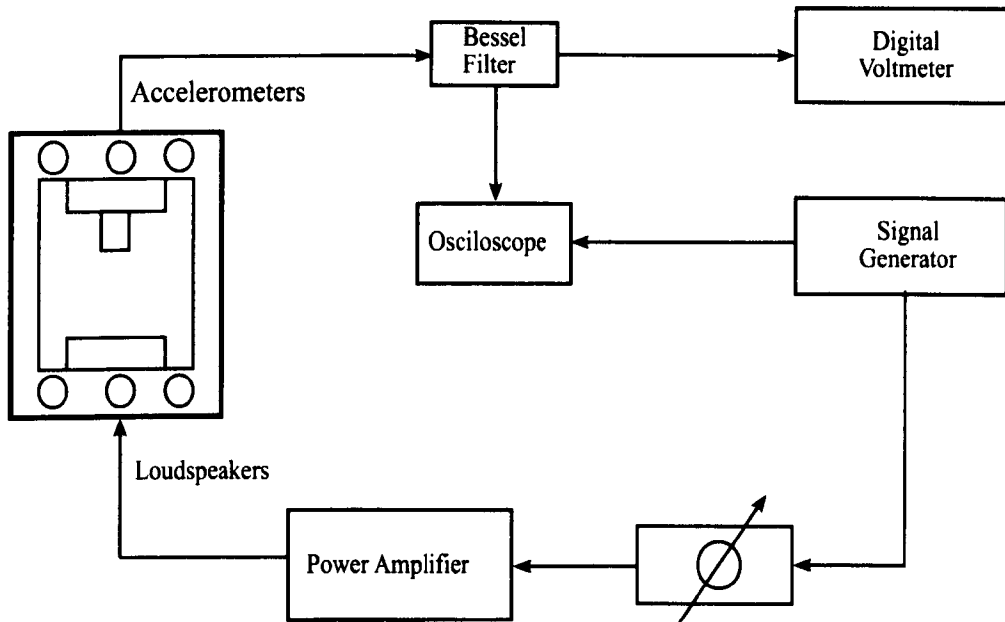


Fig. 3.4: A schematic diagram of the electronics and signal flow for the vertical apparatus. The driving sinusoidal wave from the signal generator is sent to the amplifier and then fed to the loudspeakers. The motion is monitored by the accelerometers and their output is displayed in a digital voltmeter and an oscilloscope.

3.3 Partition Instabilities

It is commonly observed that a system of grains under vertical vibration exhibits spatial instabilities (Van der weele 2008). In particular grains held in a space which is partitioned into segments linked by connecting holes may move into just one segment, the phenomenon of the partition instability (Eggers 1999; Van der Weele 2008; Van der Meer *et al.* 2002; Akiyama 1991; Akiyama 1993; Maeno 1996; Ohtsuki 1998; Chen 1998; Akiyama 2001).

Under the appropriate set of conditions a system of fluid-immersed grains within a vibrated partitioned cell will migrate into just one of the segments thorough a linking gap at the base of the container. In this section we present the results of our experimental study of the partition instability. In order to better understand the mechanism responsible for this behaviour, the ex-

perimental results are compared with the predictions of numerical-simulation studies carried out within the Granular Dynamics Group at the University of Nottingham.

3.3.1 Experimental Details

To conduct the set of experiments described in this section, a rectangular, water-tight cell was constructed from PMMA. A central partition of 2mm thickness was introduced to divide the cell in two identical columns of 90mm height and 10mm by 10mm cross section. Both columns are linked by two gaps spanning the depth of the cell and located at the bottom and the top of the central partition. The bottom gap was 4mm in height and 10mm in depth and allowed grains to move freely from one column to the other while the top gap, 7mm in height and 10mm in depth, allowed the free flow of fluid between the two columns. Figure 3.5 shows a schematic representation of the cell. A photograph of the experimental setup is shown in figure 3.6. The granular bed consisted of spherical barium titanate grains of density 4500 kg m^{-3} and diameters spanning the range $600\text{--}850 \mu\text{m}$ to avoid gross crystallisation effects.

A Kodak EktaPro EM high-speed camera was used to record the experiments. This camera is able to record video at up to 1000 frames per second as well as to capture still images. The camera is connected to a Kodak processor which output is displayed on a monitor. The footage can be played back at a speed as low as 1 frame per second. This feature allowed a detailed analysis of the motion of the particles in the experiments. The recordings can be downloaded to a computer using a special USB cable fitted with a video-to-data converter and a video capture program such as Pryme or Ulead Capture Studio. Recording videos at high speed requires the use of spotlights. To pre-

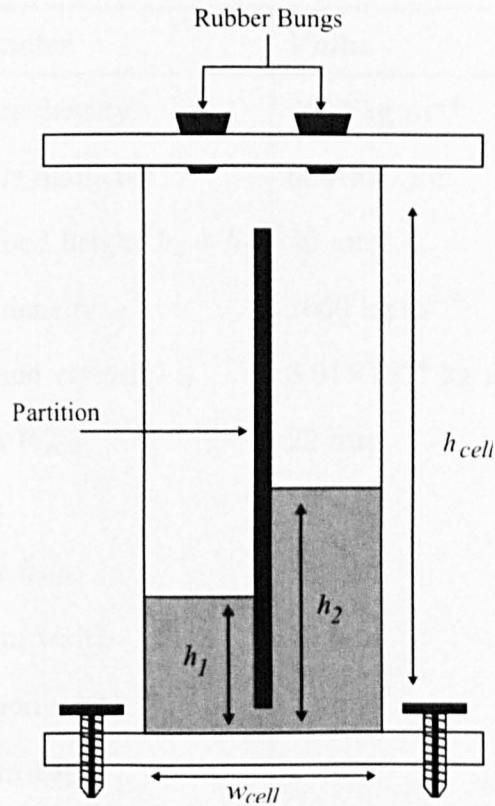


Fig. 3.5: Schematic representation of the partitioned cell. The granular bed is shown as a shaded region. The cell is firmly attached to the frame joining the vibrating loudspeakers. The dimensions of the cell are given in Table 3.1

vent the cell to overheat, fans were used to blow cool air around the vibratory apparatus.

3.3.2 Methodology

Before each set of experiments the barium titanate spheres and the partitioned box were cleaned to ensure they were free of pollutants. The spheres were washed with a isopropyl-alcohol and then rinsed with ultra high purity (UHP) water. They were left to dry and then washed with acetone and rinsed a second time with UHP water. Finally, the spheres were placed in an oven to dry. The inner walls of the cell were cleaned with soap and rinsed thoroughly with UHP

<i>Parameter</i>	<i>Value</i>
Particle density	4500 kg m ⁻³
Particle diameter	600–850 μm
Total bed height $h_1 + h_2$	40 mm
Fluid density ρ	1000 kg m ⁻³
Dynamic viscosity η	8.91×10^{-4} kg m ⁻¹ s ⁻¹
Width W_{cell}	22 mm
Depth	10 mm
Height h_{cell}	90 mm
Column width	10 mm
Partition width	2 mm
Bottom gap	4 mm
Top gap	4 mm
f	15 Hz
Γ	2.25–3.50

Table 3.1: Parameters for experimental partition system.

water. A solution of water and propyl-alcohol was used to rinse the cell a second time and then it was left to dry.

The grains were inserted into the cell through one of two upper holes. The cell was then filled with water of density 1000 kg m⁻³ and viscosity $\eta = 8.91 \times 10^{-4}$ kg m⁻¹s⁻¹, the dissolved air has been pumped out prior experiments. The cell was shaken to release any air bubbles trapped within the grains and then refilled and sealed with bungs so that no visible air bubbles are contained within its volume. The total amount of grains was such that $h_1 + h_2 = 40$ mm and they were distributed between the two columns so that the beds are given

an initial height difference of $h_2 - h_1 = 4\text{mm}$. See figure 3.5 for reference. In this thesis we present those experimental results that were used to test the computer simulations presented latter in this chapter. However, a wide range of parameters were explored experimentally. Two geometries were studied, the rectangular box described in this chapter and a U-shaped tube. Both geometries exhibited qualitative similar behaviours but the U-tube geometry is more challenging to simulate. The frequencies explored ranged from $f = 10$ to 35Hz and were limited by the capacity of our experimental setup.

During experiments the cell was vibrated sinusoidally with frequency f in a direction aligned to within $\pm 0.2^\circ$ of vertical in a manner that ensures accurate one dimensional motion (Leaper *et al.* 2005). The motion is monitored using cantilever capacitance accelerometers which display the dimensionless maximum acceleration $\Gamma = A\omega^2/g$. Here A is the amplitude of vertical vibration, $\omega = 2\pi f$ is the angular frequency and g is the gravitational acceleration.

Vibration is applied and the height of the granular beds in the left and right columns are studied as a function of the total time of vibration, the heights being measured through the use of a high speed camera. This camera, usually operated at 1000 frames per second, also allows the study of granular motion within each cycle.

3.3.3 Experimental Results

As the system is vibrated we find that over time the particles migrate through the lower hole from the shallower bed into the taller bed. Eventually almost all the grains occupy just one of the columns, with only a small percentage of grains inhabiting the gap and the base of the opposite column. Figure 3.7 illustrates the flow of grains within the partitioned cell for vibration parameters

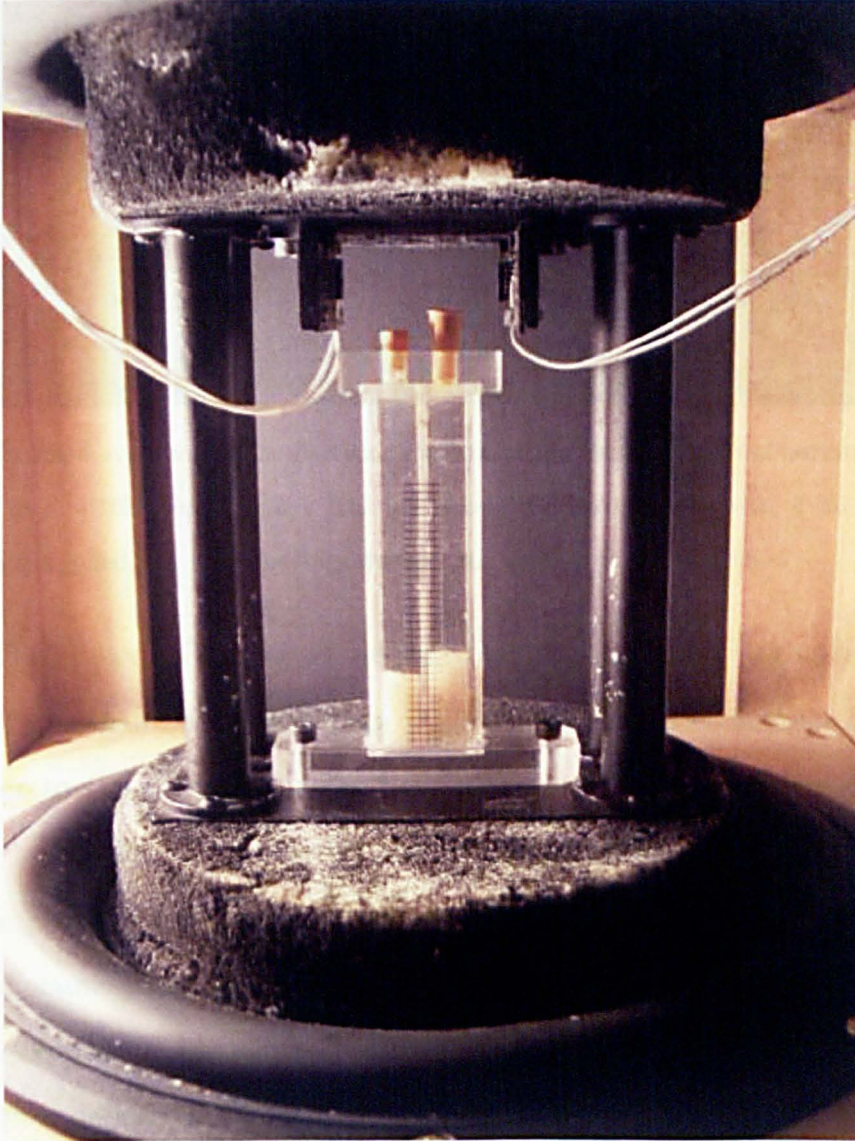


Fig. 3.6: A photograph of the experimental setup before starting the experiment. The box is firmly attached to the loudspeakers and the accelerometer can be seen above the box.

of $f = 15\text{Hz}$ and $\Gamma = 2.5$.

By analysing footage from a high speed camera we have observed in detail the motion of grains between columns within each cycle. In the first part of the cycle the grains are thrown and particles are drawn from the shallower to the deeper bed whilst both beds are in flight. In the second part of the cycle as the two beds land a smaller number of particles are forced back towards

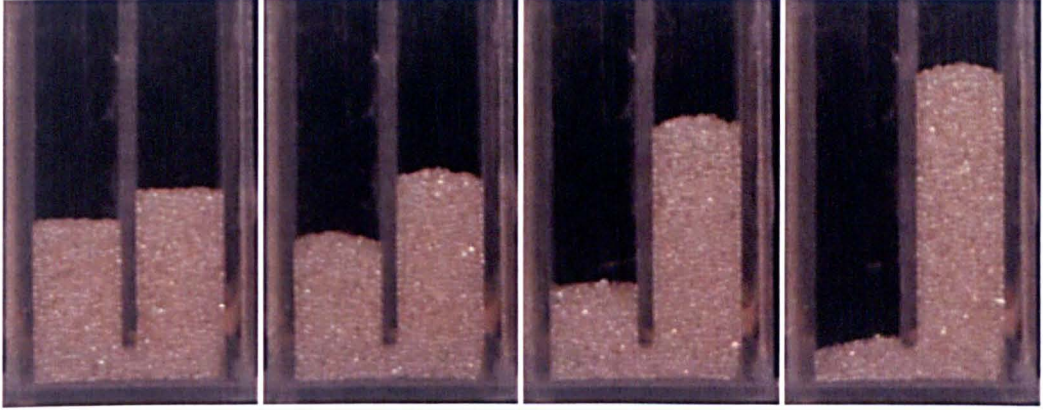


Fig. 3.7: Time evolution of the partition experiment for water immersed barium titanate particles at $f = 15\text{Hz}$ and $\Gamma = 2.5$. The initial height difference is $h_2 - h_1 < 4\text{mm}$. When vibration is applied, the particles migrate from the shorter to the taller bed

the shallower bed. On average we find that the motion of grains is greater during flight than on landing, thus the particles gradually migrate from the shallower to the deeper granular bed. After some time the flow of grains moving backwards and forwards between the columns evens out. Since there is no net granular movement over the vibration cycle and the system is said to be in “dynamic equilibrium”. This is, over the course of one cycle, the grains move backwards and forwards from one column to the other at the same rate.

We have defined $\Delta h = |h_1 - h_2|$ as the magnitude of the difference in height between the two granular columns. Figure 3.8 plots Δh against time, t , for barium titanate in water vibrated at $f = 15\text{Hz}$ and dimensionless accelerations in the range $\Gamma = 2.25 - 3.5$. The plot shows that the transfer of grains into the deeper bed initially accelerates as Δh increases and then continues at an almost constant rate until almost all the grains have been transferred to the deeper bed. Subsequently the net transfer of grains decelerates until a steady state is reached in which a small number of grains move backwards and forwards between the two columns. The last experimental points we plot are at $\Delta h = 32\text{mm}$ as beyond this point the results become erratic and no

measurements were carried out.

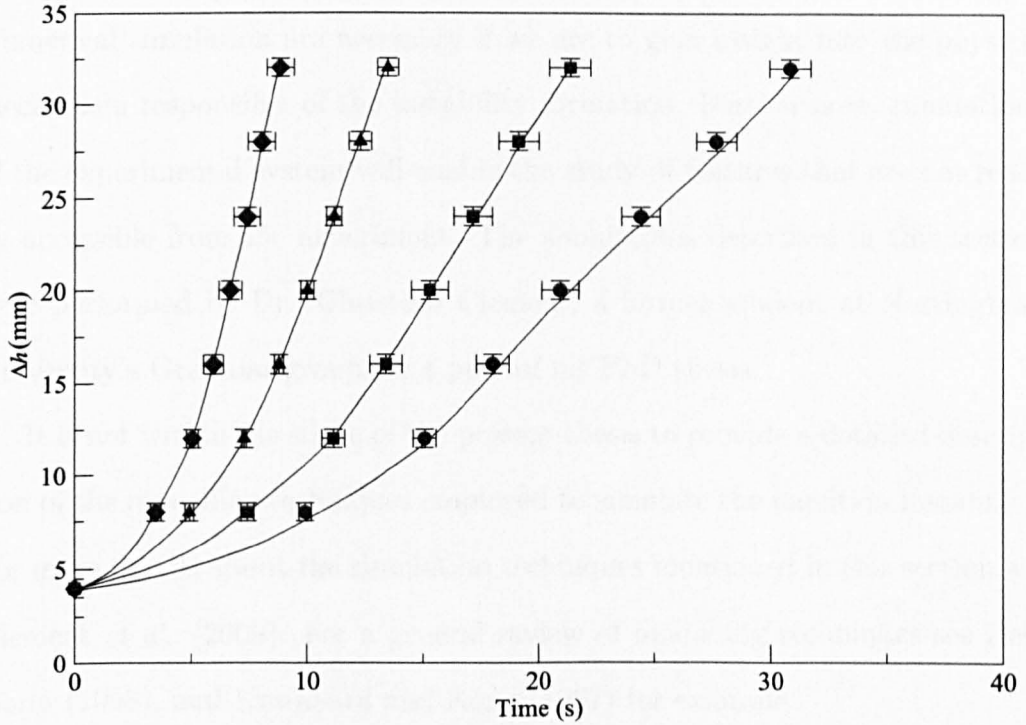


Fig. 3.8: Variation of the height difference Δh as a function of time for a collection of water-immersed barium titanate grains. The experiments were conducted at a frequency $f = 15\text{Hz}$. The dimensionless acceleration are, from right to left, $\Gamma = 2.25$ (circles), $\Gamma = 2.50$ (squares), $\Gamma = 3.00$ (triangles) and $\Gamma = 3.50$ (diamonds).

We find that as Γ is increased the total time taken for the grains to migrate into one column reduces due to the increased amount of mechanical energy within the beds driving the grain transfer process. This strong dependence on Γ results from the non-linear flight dynamics of the bed within the fluid and the variation of bed porosity with vibratory conditions.

If the experiments are performed with the gap through the partition at the top of the cell closed, there is no transfer of grains from the shallower to the deeper granular bed. In fact if vibrated for a long period of time the granular beds then end up of equal height.

3.3.4 Simulations

Numerical simulation are necessary if we are to gain insight into the physical mechanism responsible of the instability formation. Furthermore, simulations of the experimental system will enable the study of features that are not readily accessible from the experiment. The simulations described in this section were performed by Dr. Christian Clement, a former student at Nottingham University's Granular group, as a part of his PhD thesis.

It is not within the scope of the present thesis to provide a detailed description of the modelling techniques employed to simulate the partition instability. For more details about the simulation techniques mentioned in this section see Clement *et al.* (2009). For a general review of modelling techniques see Hermann (1998), and Kuwabara and Kono (1987) for example.

Fluid Springs Model

The particle interactions are modelled within a Molecular Dynamics framework using the Damped-Hertzian collision model. The fluid is modelled using the Navier-Stokes equations. In these simulations, a two-way coupling between the grains and the fluid is considered. In this approach the fluid particle coupling is achieved by introducing a body forcing term into the Navier-Stokes equation rather than through providing a boundary condition for the fluid flow. The basic idea of this model is to allow the fluid to exist both inside and outside the particles. The particles are therefore treated not as boundary conditions to the flow but by a volume forcing term, \mathbf{f} , in the Navier-Stokes equation. The particles are distributed throughout the partitioned cell which is held stationary and the grains are allowed to settle under the influence of gravity. The vibrations are switched once the particles have settled on the base of the

partitioned cell. The dimensions of the cell in simulation are the same as those in the experiment with the exception of the depth of the box which was reduced to 2.5 mm to minimize the computing time.

As was the case in the experiments, the columns are given an initial height difference of $\Delta h = 4\text{mm}$. Figure 3.9 plots Δh against time for a vibration with frequency $f = 15\text{Hz}$ and dimensionless accelerations $\Gamma = 2.25, 2.5, 3.0$ and 3.5 . In this figure, the experimental results are compared with the predictions of the Fluid Springs model. It can be observed that there is a good agreement between simulation and experimental results, especially for the higher values of Γ . For $\Gamma = 2.25$, the simulation results differs significantly. One likely explanation is that the barium titanate grains used in the experiment are not perfectly spherical as it is assumed in the simulations and are prone to jam within the bottom gap. At this low values of Γ it is possible that there is not enough agitation to keep a smooth granular flow through the connecting gap.

Instability Mechanism

We now consider the possible mechanism for the partition instability. The resistance to fluid flow through the bottom gap is much bigger than the resistance through either bed. Under vibration each granular column is thrown independently and will develop a pressure gradient (an under-pressure) proportional to its height. The pressure drop under the deeper bed early in flight will be greater than beneath the shallower bed causing grains to move in the direction of the deeper bed. Later in flight the changing pressure reduces the speed of the grains but it does not reverse the direction of grain motion. A second possibility is that the coupling between the two columns is such that the resistance to fluid flow through the lower hole is far less than that through

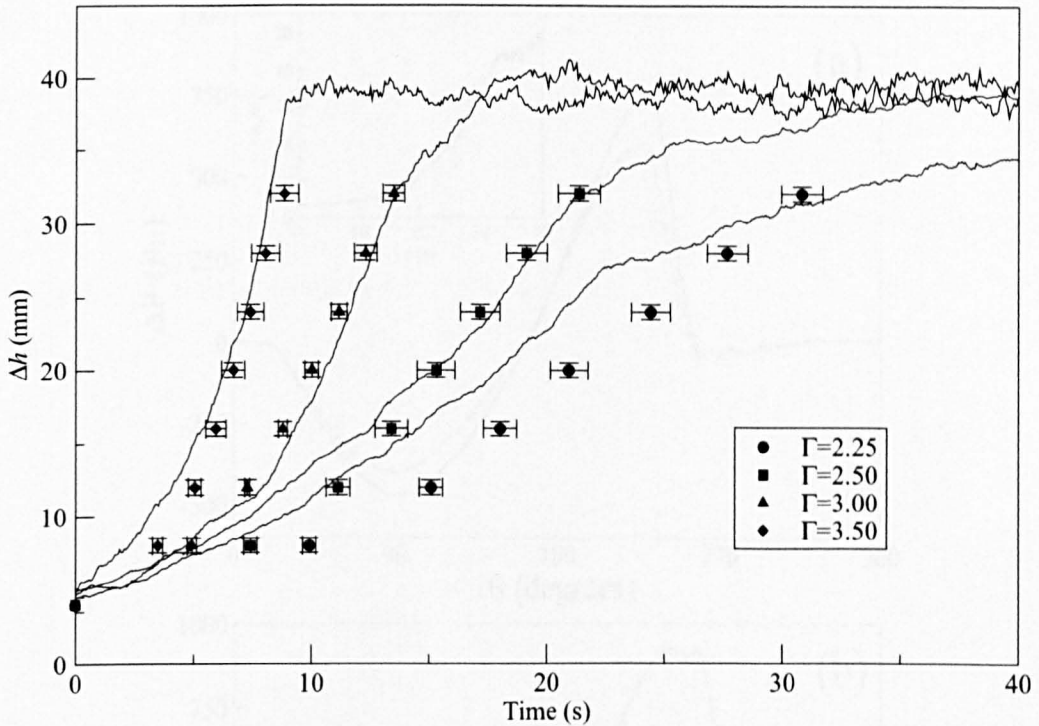


Fig. 3.9: Variation of the height difference Δh as a function of time. The solid lines are the simulation data for vibration parameters $f = 15\text{Hz}$ and, from left to right, $\Gamma = 2.25$, 2.5, 3.0, and 3.5. The corresponding experimental data is plotted as points.

either bed. Both columns experience a common under-pressure which can only be achieved if more fluid flows through the shallower bed rather than through the deeper bed. This fluid flow also transports grains towards the deeper granular column.

In order to test which, if either, mechanism is dominant we determine from simulation the pressure beneath each column for vibrational parameters $f = 15\text{Hz}$ and $\Gamma = 2.5$. Figures 3.10 (a) and (b) show the pressure drop across the bed on each side of the partition at times $t = 10\text{s}$ and $t = 30\text{s}$. The inset in Fig. 3.10 (a) shows the variation of h_2/h_1 with time t . The variation of pressure throughout a cycle shows that ΔP is approximately the same on both sides of the partition. For example, by $t = 30\text{s}$ the height ratio is $h_2/h_1 \approx 15$ while the ratio of pressures on the two sides $\Delta P_2/\Delta P_1$ is only

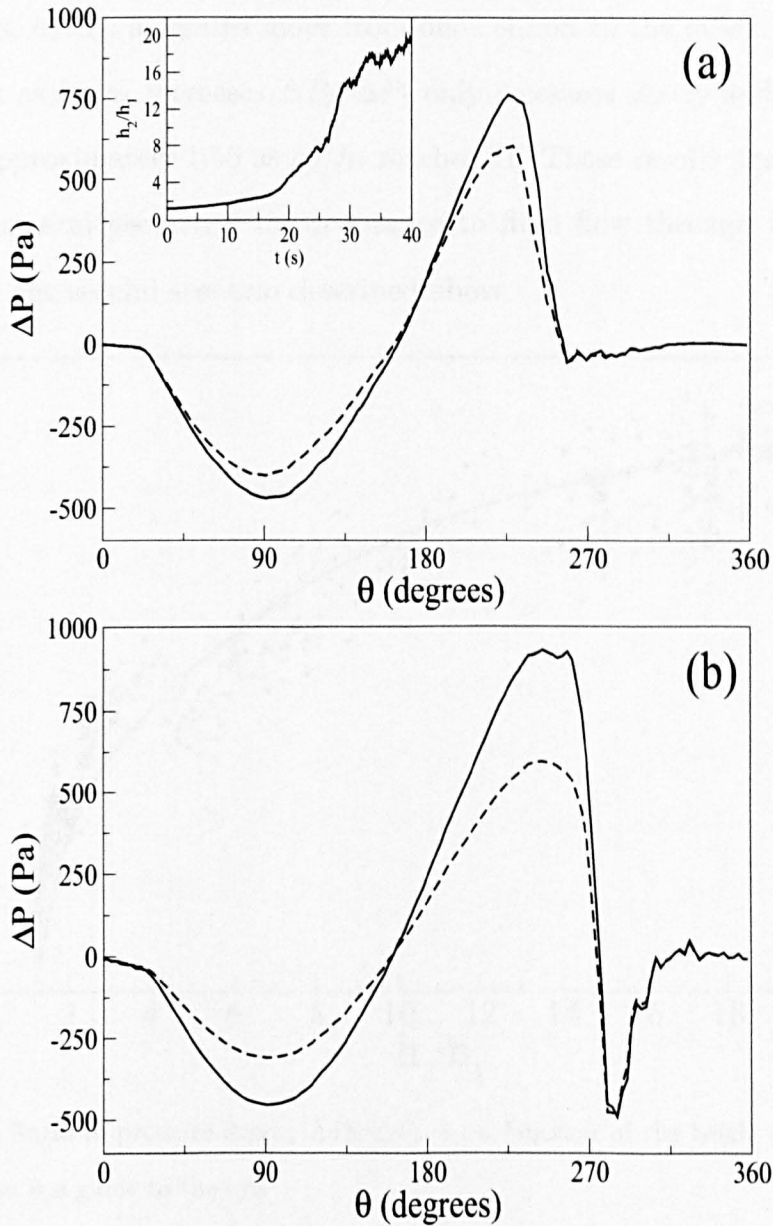


Fig. 3.10: Under-pressure drop across the bed on each side of the partition plotted against the phase angle θ for the deep column (solid line) and the shallow column (dashed line). The vibration parameters are $f = 15\text{Hz}$ and $\Gamma = 2.5$ and the figures show data at times (a) $t = 10\text{s}$ and (b) $t = 30\text{s}$. The data was averaged over 5 cycles. The insert in (a) shows the height ratio h_2/h_1 against time, t .

1.5. Furthermore, the pressure curves throughout a cycle on either side of the partition can be scaled onto each other. Figure 3.11 plots the ratio of pressure drops, $\Delta P_2/\Delta P_1$, across each bed against the ratio of the heights of the two

bed depths, h_2/h_1 , as grains move from one column to the other. The figure shows that as h_2/h_1 increases $\Delta P_2/\Delta P_1$ only increases slowly and eventually levels at approximately 1.55 as h_2/h_1 reaches 21. These results show that, for our experimental geometry, the resistance to fluid flow through the bottom gap is low, the second scenario described above.

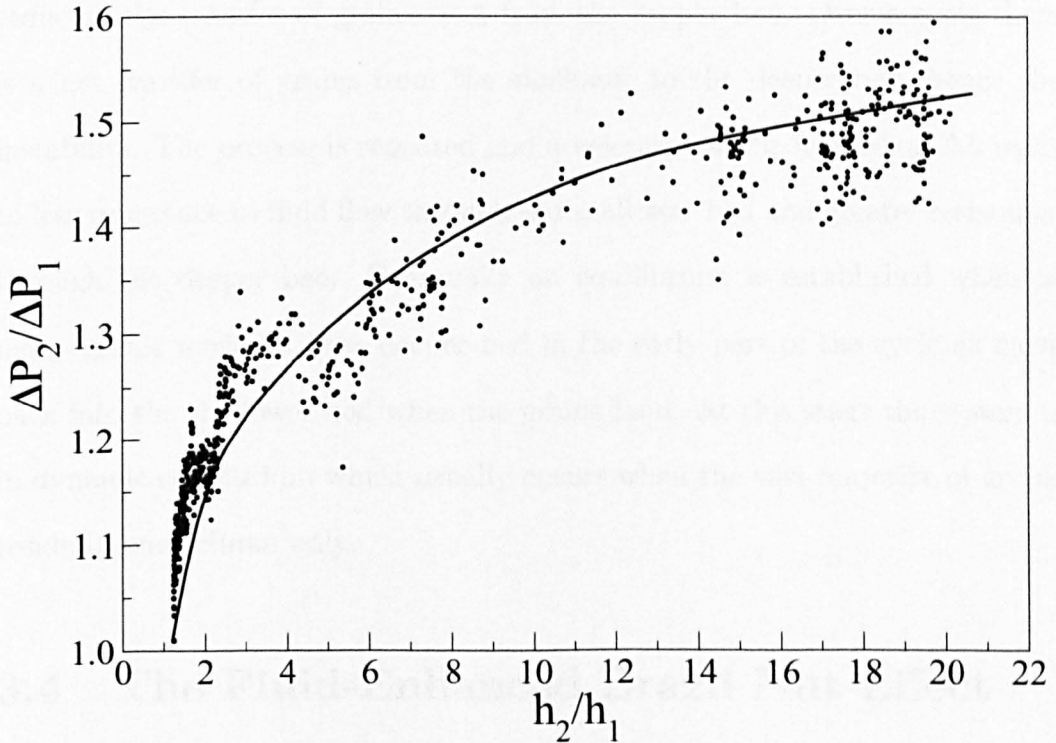


Fig. 3.11: Ratio of pressure drops, $\Delta P_2/\Delta P_1$, as a function of the height ratios h_2/h_1 . The solid line is a guide to the eye.

The simulation results enables a better understanding of the mechanism that drives the grain transfer. When the beds are thrown, an under-pressure develops across the base of the container and thus fluid flows downwards through the beds to fill the space left beneath. The shallower bed provides less resistance to the downward flowing fluid and thus fluid is drawn from the shallower side through the hole to the deeper side. The fluid accelerates grains in the direction of the flow, from the shallower to the deeper bed. As the beds

begin to fall in the second half of the cycle an over-pressure develops beneath the beds and the fluid flow is reversed. Fluid is forced upwards through the beds to fill the void above. Again the shallower bed provides less resistance to the upward moving fluid so fluid now flows through the channel from the deeper bed to the shallower bed. However, the shallower bed lands first, thus reducing the transfer of grains back from the deeper bed. Over a cycle there is a net transfer of grains from the shallower to the deeper bed, hence the instability. The process is repeated and accelerates as the increasing Δh leads to less resistance to fluid flow through the shallower bed and greater resistance through the deeper bed. Eventually an equilibrium is established when as many grains move into the deeper bed in the early part of the cycle as move back into the shallower bed when the grains land. At this stage the system is in dynamic equilibrium which usually occurs when the vast majority of grains reside in one column only.

3.4 The Fluid-Enhanced Brazil Nut Effect

It is commonly observed that a large dense intruder may rise to the surface of a vibrated granular bed, a collection of small light grains. This phenomenon is known as the Brazil nut effect. In this section we describe an experimental study of the fluid-enhanced Brazil nut effect. This effect can be observed when the granular bed is fully immersed in a liquid. Our experimental system consist of a bed of glass beads immersed in water and a large steel intruder. The motion of the steel intruder is closely monitored as the system is vibrated vertically. The experimental parameters are used to develop numerical simulations of this system to aid understanding of the rising mechanism. The simulations described in this section were performed by Dr. Christian Clement, a former

member of the Granular Dynamics group at the University of Nottingham, during his PhD studies.

3.4.1 Experimental Details

The experiments are conducted in a water-tight cell constructed from soda glass of dimensions $40\text{ mm} \times 10\text{ mm}$ in the horizontal plane and 43 mm tall. The bulk of the granular bed is made up of host glass spheres of density 2500 kg m^{-3} with mean radii of 1 mm and a spread of sizes in the range $0.85\text{ -- }1.15\text{ mm}$ to avoid crystallisation. We use a steel “Brazil nut” (spherical steel ball bearing) of density 7750 kg m^{-3} and radius 3.5 mm . The grains are inserted through one of two upper holes in the box until the bed has a height of 26 mm . The cell is then filled with water of density 1000 kg m^{-3} and dynamic viscosity $8.91 \times 10^{-4}\text{ kg m}^{-1}\text{ s}^{-1}$. The cell is thin enough that we are able to visually follow the steel intruder motion within the bed through the front wall. The cell is shaken to remove any air bubbles trapped within the granular bed. More water is then added and the cell is sealed using bungs so that no visible air bubbles are contained within its volume. After each run the cell is removed from the vibratory apparatus and the steel ball is returned to the base of the cell. A schematic of the cell is shown in Fig. 3.12.

During experiments the box is vibrated sinusoidally with frequency f in a direction within $\pm 0.2^\circ$ of vertical in a manner which ensures accurate one-dimensional motion (Leaper *et al.* 2005). The vibration is monitored using cantilever capacitance accelerometers which display the dimensionless maximum acceleration Γ . The motion of the steel particle is monitored through the use of a high speed camera. This camera, usually operated at 1000 frames per second, also allows the study of the granular motion within each cycle.

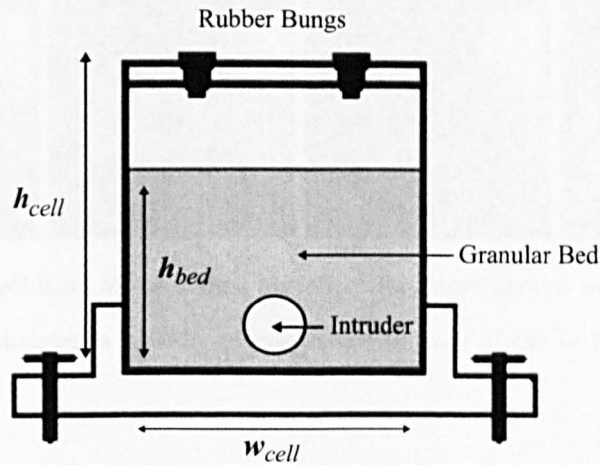


Fig. 3.12: Schematic diagram of the cell used in the Brazil nut experiments. The height of the cell is $h_{cell} = 43\text{mm}$ and the width of $w_{cell} = 40\text{mm}$. The granular bed has a depth of $h_{bed} = 26\text{mm}$.

3.4.2 Experimental Results

Figure 3.13 illustrates how a steel Brazil nut rises through a fluid-immersed glass bed when vibrated with parameters $f = 15\text{ Hz}$ and $\Gamma = 3.5$. The intruder is carefully placed in position with the aid of a weak magnet so it initially begins on the cell base away from the front and back walls. On the application of vertical sinusoidal vibration the intruder rises rapidly through the bed until it eventually emerges through the bed surface. Once the Brazil nut reaches the top of the bed it does not then re-enter the granular bulk. By visual inspection of the footage we note that the Brazil nut remains away from the front and back walls during rising.

Figure 3.14 plots the gap between the lowest point of the intruder and the base of the cell, H , against time, t , for vibration parameters $f = 15\text{ Hz}$ and $\Gamma = 3.5, 4.0$ and 4.5 . H was measured at the beginning of each cycle when there is no gap between the cell base and the bottom of the bed and the cell is moving upwards with velocity $\dot{z}_c = A\omega$. We define this position of the

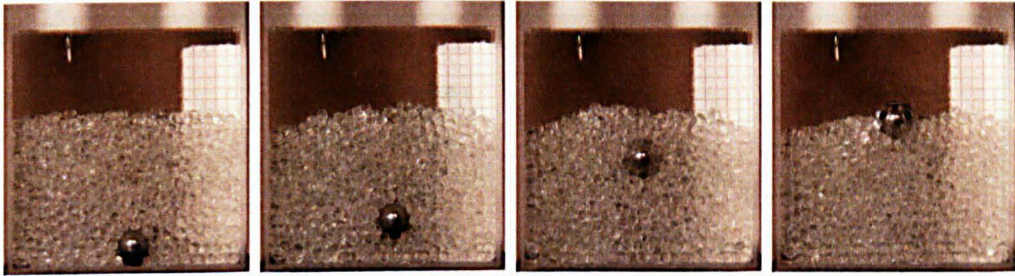


Fig. 3.13: Time evolution of the Brazil nut effect for experimental parameters $f = 15\text{Hz}$ and $\Gamma = 3.5$. The intruder is initially placed at the bottom of the bed and away from the walls.

cell to correspond to a phase angle $\theta = 0^\circ$. The error bars were obtained from averaging the intruder trajectories over five independent runs. From this figure we can see that under vibration the large intruder will rise through the bed until it eventually breaks the bed surface. For all the vibratory conditions we have investigated we find that the vertical motion of the Brazil nut accelerates as it moves upwards through the bed. As Γ is increased the speed with which the intruder rises increases due to the greater amount of energy input into the intruder and bed.

Under the vibratory conditions that we have investigated, there is very little convective motion of the bed in the absence of the intruder. With the intruder present, the upward motion of the Brazil nut drives two vertical convection rolls within the cell. This shows that, in our system, the intruder does not rise due to convective effects alone. We have also carried out experiments in the absence of the liquid. We find that, under the same vibratory conditions, the bed is highly fluidised and the intruder either rises slowly or remains within the bed. Clearly, the presence of the liquid has a strong effect on the intruder's behaviour.

During the experiments it was noted that the rise times were sensitive to the cleanliness of the granular bed. Consequently, great care was taken to clean

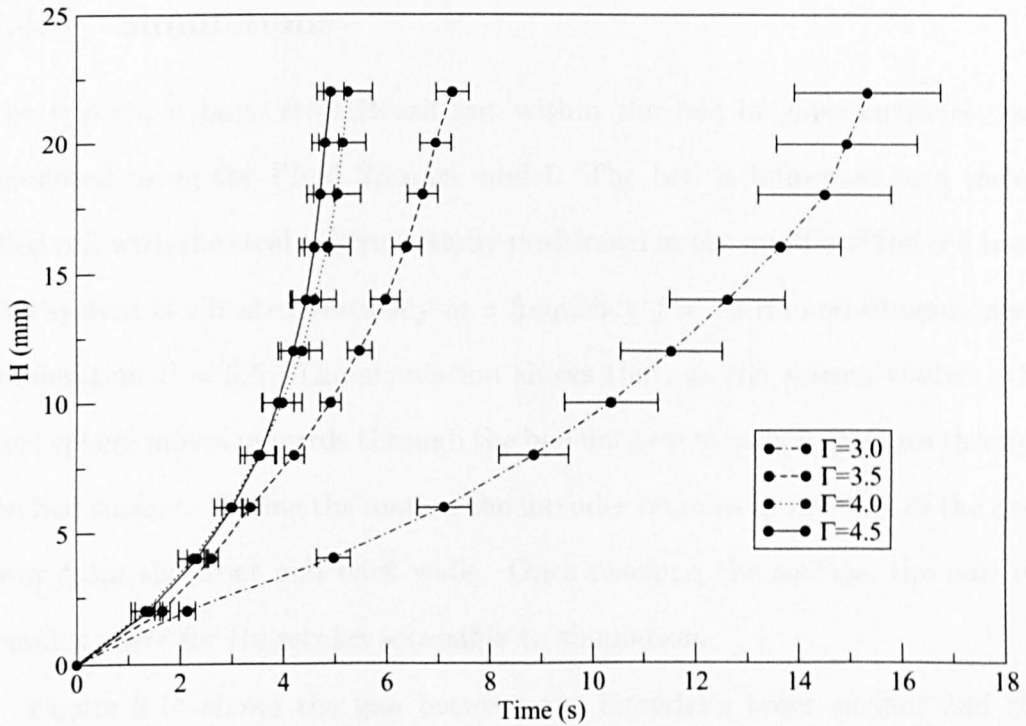


Fig. 3.14: Gap H between the intruder and the bottom of the cell plotted against the time t for a frequency $f = 15\text{Hz}$ and dimensionless accelerations, from right to left, $\Gamma = 3.0$, 3.5, 4.0 and 4.5. The error bars correspond to the standard error over five independent experiments.

the grains and cell prior to each experimental session. It was also observed that there was some dependence of the rise time on the position of the intruder in the cell between the front and back faces. Intruders that are in contact with one of these faces rise typically about 15% faster than those initially positioned in the middle. In our experiments we try to start with the intruder away from these walls.

We now perform numerical simulations of the experimental system. This allows us to obtain detailed information about the intruder mechanism that is otherwise unattainable from experiments.

3.4.3 Simulations

The system, a large steel Brazil nut within the bed of glass particles, was simulated using the Fluid Springs model. The bed is immersed in a water-filled cell with the steel sphere initially positioned in the middle of the cell base. The system is vibrated vertically at a frequency $f = 15$ Hz and dimensionless acceleration $\Gamma = 3.5$. The simulation shows that, as the system evolves, the steel sphere moves upwards through the bed until eventually it emerges through the bed surface. During the motion the intruder remains in the bulk of the bed, away from the front and back walls. Once reaching the surface, the particle remains there for timescales accessible to simulation.

Figure 3.15 shows the gap between the intruder's lower surface and the cell base, H , plotted against time, t , for vibration parameters $f = 15$ Hz and $\Gamma = 3.5, 4.0$ and 4.5 . H is recorded at the beginning of each cycle of vibration when $\theta = 0^\circ$. The simulation data presented in Figure 3.15 was averaged over five independent runs as in the experiments. Here we observe that the Brazil nut rises upwards through the bed for all of the vibration amplitudes considered. As in experiments, when Γ is increased the overall rise time of the intruder reduces. Figure 3.15 shows that the simulation results give very good agreement with those obtained in experiments.

During the experiments it was noted that the rise times were sensitive to the cleanliness of the granular bed. Consequently, great care was taken to clean the grains and cell prior to each experimental session. Similarly, the simulations are sensitive to the friction parameter μ .

As was noted within experiments, the Brazil nut rises at a faster rate when in contact with either the front or back cell wall. Figure 3.16a plots the gap, H , as a function of time, t , for the steel intruder when it is either fixed to the

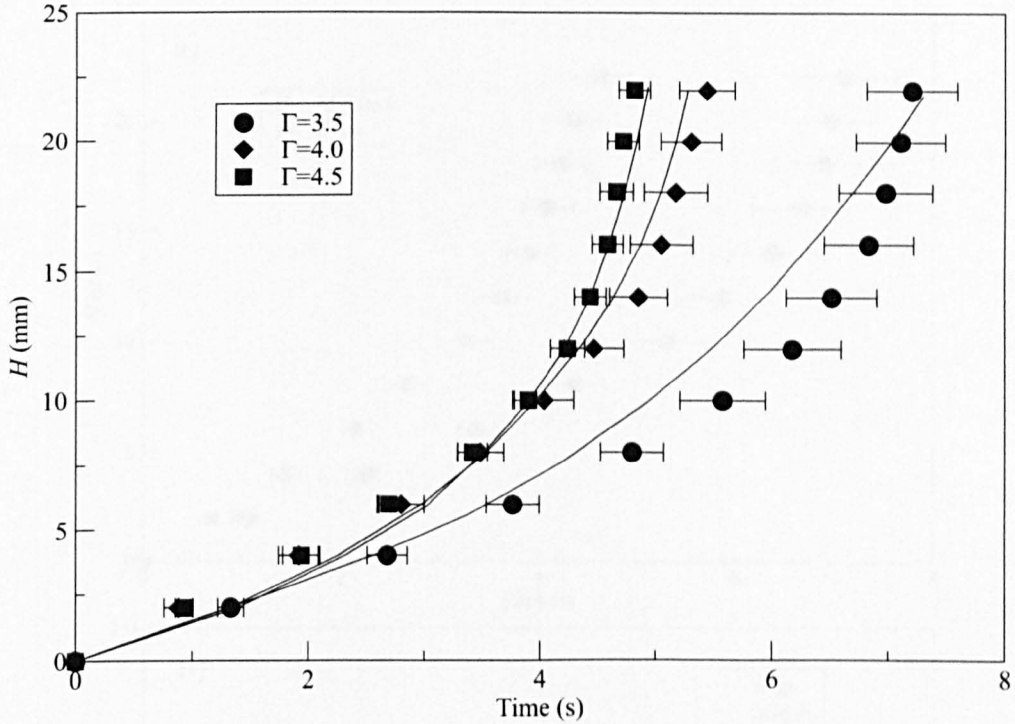


Fig. 3.15: Simulation results for the intruder gap H as a function of time, t , using the Fluid Springs model to simulate a steel intruder in a water-immersed glass bed. The solid lines are polynomial fits to the experimental results in Figure 3.14. The error bars show the standard error over five independent runs.

front wall or fixed in a plane half way between the front and back cell walls. The error bars again show the standard error calculated from five independent runs. Figure 3.16a shows that the Brazil nut rises considerably faster when it was forced to move close to the front wall without actually being in contact with it. This could be because the glass grains within the granular bed are able to move downwards past the large intruder easier when the intruder is fixed to the front surface.

Figure 3.16(b) plots the normalised intruder position between the front and back walls, y_{norm} , against time, t . We evaluate the normalised position using $y_{norm} = (y_I - r_I) / (L_y - 2r_I)$, where y_I is the position of the intruder within the cell along the y -axis, r_I is the radius of the intruder and L_y is the length

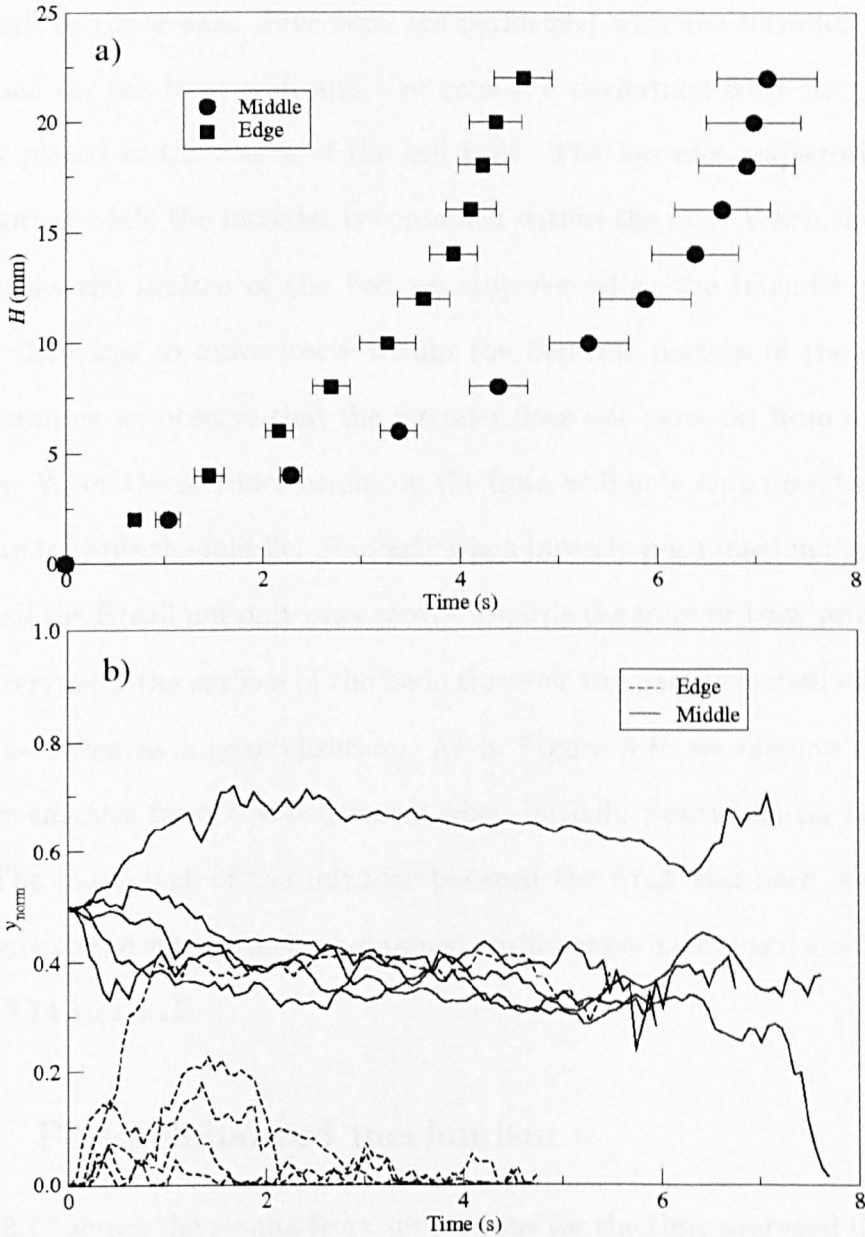


Fig. 3.16: Effect of the initial position of the intruder in simulations. a) Simulation results for the intruder gap H as a function of time for an intruder ascending next to the front wall of the cell (squares) or half way between walls (circles). b) Normalized position of a free intruder, y_{norm} between the front and back walls. The intruder is initially placed on the front wall (dashed lines) or half way between the front and back walls. For both cases, the Fluid Spring Model was used to simulate the system with vibration parameters $f = 15\text{Hz}$ and $\Gamma = 3.5$.

of the cell in the y -axis. Five runs are performed with the intruder initially positioned on the front wall and five runs are performed with the intruder initially placed in the centre of the cell base. The intruder trajectories have been plotted while the intruder is contained within the bed. When the Brazil nut reaches the surface of the bed we stop recording the intruder position as it is then free to move freely within the bed-free portion of the cell. In both instances we observe that the intruder does not move far from its initial position. When the intruder begins on the front wall only once does the Brazil nut move towards the middle. Similarly when initially positioned in the middle of the cell the Brazil nut only once moves towards the front or back wall, which occurs very near the surface of the bed. However the past two observations are not to be taken as a generalization. As in Figure 3.16 we observe that the intruder emerges from the bed faster when initially positioned on the front wall. The movement of the intruder between the front and back walls may contribute to the standard error obtained within experiments and simulations, figures 3.14 and 3.15.

3.4.4 Fluid-Enhanced mechanism

Figure 3.17 shows the results from simulations for the time-averaged fluid and granular flow around the Brazil nut when in flight for vibration parameters $f = 15$ Hz and $\Gamma = 3.5$. The flows were recorded once every vibration cycle at a phase angle of $\theta = 90^\circ$. The results were averaged over 101 cycles of vibration, the duration for which the intruder remains within the bed.

Figure 3.17(a) shows the fluid flow while Figure 3.17(b) shows the corresponding granular flow. Figure 3.17(a) shows that as the intruder is thrown fluid is forced upwards and away from the space above the intruder while si-

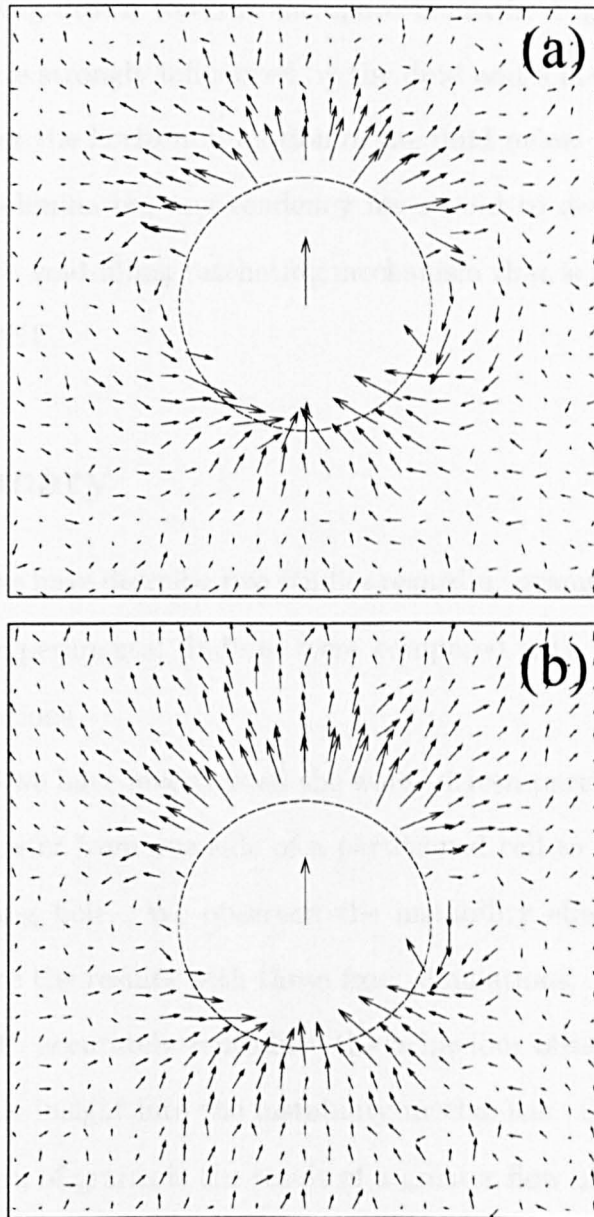


Fig. 3.17: Computer simulation results. Average (a) fluid and (b) grain motion relative to the centre of mass of the steel intruder using the Fluid Springs model. Both results were obtained at a phase angle of $\theta = 90^\circ$ when the granular bed is moving upwards relative to the cell. The vibration parameters were $f = 15$ Hz and $\Gamma = 3.5$. The flows were averaged over 101 vibration cycles, the time taken for the intruder to reach the surface. The arrows in the centre of the Brazil nut shows the sphere velocity relative to the cell of 94 mm s^{-1} at this stage of the cycle. The magnitude of the fluid and grain velocity vectors are drawn to the same scale.

multaneously being drawn towards the space beneath. Figure 3.17(b) shows that the grains are strongly influenced by the fluid and follow a similar trajectory. In particular the horizontal motion of the fluid below the intruder drags grains sideways eliminating any tendency for a void to develop beneath the intruder. It is this void-filling ratcheting mechanism that is responsible for the fluid-enhanced BNE.

3.5 Summary

In this Chapter we have describe two studies regarding granular beds immersed in water. The experimental findings were compared with the predictions of numerical simulations.

In section 3.3 we have investigated the water-driven partition instability, in which grains transfer from one side of a partitioned cell to the other through a lower connecting hole. We observed the instability effect in experiments and then compare the results with those from simulations. The Fluid Springs Model was able to accurately reproduce the behaviour observed in the experiment and provide insight into the instability mechanism. Our results suggest that the migration of grains is the result of a greater flow of fluid through the shallower column of grains as the beds are thrown by the vibration.

In section 3.4 we have shown experimentally that the presence of a liquid can dramatically influence the behaviour of a dense intruder in a vibrated granular bed. Specifically, a large steel intruder was observed to rise rapidly to the surface of a bed of water-immersed glass particles when subjected to vertical vibration. To gain insight into this behaviour, we modelled the effect using simulations and found that a fluid-grain coupling technique based on a microscopic fluid-particle model was able to capture the process, both quali-

tatively and quantitatively. The simulations allowed a detailed investigation into the mechanism.

At the beginning of each vibration cycle the steel and glass particles are thrown upwards. Due to its larger mass and size, the steel intruder is slowed less by the fluid drag than the glass spheres. As the intruder is thrown upwards the void beneath it, that would be created due to the relative motion, is quickly filled with grains dragged by the fluid. Later in the cycle the intruder falls, reversing the direction of fluid flow, which in turn decelerates the motion of the grains beneath it. However, due to the grains' inertia, this flow is insufficient to return them to their original position. This rearrangement is also strengthened as it is easier for the grains to move into a low density region, rather than in the opposite direction. The net result is that the intruder draws fluid and grains beneath it as it is thrown and later in the cycle lands on these particles increasing its vertical position. It is this fluid-enhanced ratcheting mechanism that causes the Brazil nut to rise rapidly through the bed.

Chapter 4

Dynamics of magnetically-levitated, fluid-immersed grains

In the previous chapter we studied densely-packed collections of grains immersed in an oscillatory fluid in the presence of gravity. In this chapter we describe a series of experiments aimed at studying very dilute collections of grains in an oscillatory fluid, in particular we will focus our attention on the behaviour of spherical grains immersed in an oscillatory fluid flow. The grains are magnetically levitated so the effects of gravity are removed. To our knowledge this kind of experimental setup has not yet been used to study the hydrodynamic interactions in very dilute granular systems.

We start the chapter with a review of the studies associated with pattern formation in granular systems in the presence of a fluid. We continue with a brief review of basic concepts of magnetism and diamagnetic levitation. After these introductory sections we describe the initial experimental observations

when collections of grains are levitated magnetically in the presence of an oscillatory fluid. Several systems were investigated but our main studies will focus on the case of two particles. In the remainder of the chapter we will describe details of the experimental study of two magnetically-levitated spheres.

4.1 Introduction

In recent years there has been an increasing interest in the collective behaviour and pattern formation in granular matter (Aranson 2006), which can be enhanced by the presence of a fluid. The formation of ordered structuring of spherical particles immersed in an oscillatory fluid flow has been reported in the literature (Wunenburger 2002, Voth 2002, Thomas and Gollub (2004)). This section reviews some of the earlier experiments which have served as motivation for a series of studies, including the work described in this chapter.

Wunenburger *et al.* (2002) performed experiments in which small metal spheres were placed in a water-filled cell which was undergoing horizontal, sinusoidal vibration. The dimensions of their cell were $100 \times 100 \times 10 \text{ mm}^3$, as shown in Figure 4.1 (a). The grains were a polydisperse mixture of roughly spherical bronze particles with diameters d in the range $d=280\text{-}630\mu\text{m}$. The frequency of the driving pulse was in the range of $f=10\text{-}20\text{Hz}$ and the amplitude was in the range of $A=0.7\text{-}3.5\text{mm}$. Because the spheres were not neutrally buoyant they would sink to the bottom surface and oscillate with respect to the fluid once the vibration was switched on. If we define the Reynolds number to be $Re = 2\pi fdA/\nu$, where ν is the kinematic viscosity of the liquid, we get an estimate for the Reynolds number in these experiments in the range of $Re = 1 - 280$.

At the beginning of the experiments, the spheres were clustered together

in the middle of the cell, as shown in Figure 4.1 (b). When the vibration was switched on, the spheres were observed to form equally spaced chains oriented perpendicularly to the direction of oscillation; a top view is shown in Figure 4.1 (c). Wunenburger *et al.* found that the periodic pattern of chains shrinks and expands; the distance between the chains increases and decreases depending on the vibratory conditions, regardless that the initial configuration has the particles always clustered together in the centre of the cell. Wunenburger *et al.* did not provide an explanation of the exact mechanism behind the formation of the pattern and it was left as an open question.

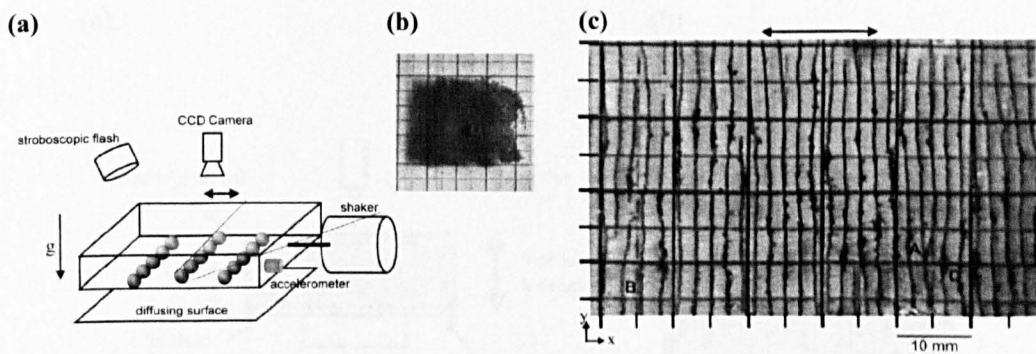


Fig. 4.1: (a) The experimental setup used by Wunenburger *et al.* (2002). (b) Top view of the initial configuration of the particles which is a clump in the middle of the cell. (c) Top view of the chains of particles formed in water, perpendicular to the vibration axis (horizontal) as indicated by the double-headed line. All images were taken from Wunenburger (2002).

Using the experimental arrangement shown in figure 4.2 (a), Voth *et al.* (2002) observed clusters and hexagonal lattices of lead spheres. In figure 4.2 (b) their experimental observations are shown. In their experiments a cell filled with a viscous mixture, a solution of water and glycerol, and stainless steel spheres, 0.8mm in diameter, are vibrated vertically. The Reynolds numbers for Voth *et al.*'s experiments were in the range $Re = 2 - 10$.

The spheres would bounce on the vibrating base of the cell under the in-

fluence of gravity and fluid-induced interactions in the plane perpendicular to the axis of vibration made the spheres cluster together and form various structures. A top view is shown in Fig. 4.2(b). We can identify an attraction and a repulsion between the spheres in that plane as they cluster but sit at a distance from each other. Thomas and Gollub (2004) investigated the same system theoretically and discussed the chaotic fluctuations in the positions of the spheres after the clusters were formed. After varying the number of particles, they concluded that the inter-particle forces are not simply pairwise additive but there are nonlinear hydrodynamic interactions between the spheres.

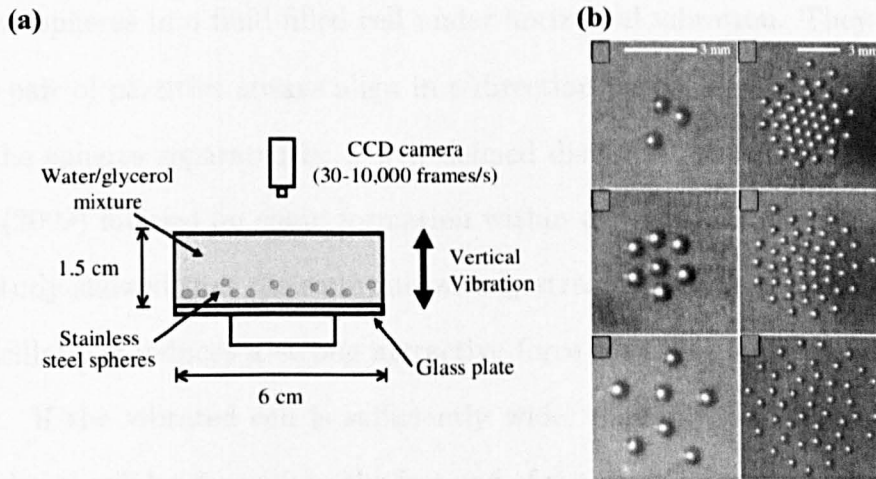


Fig. 4.2: (a) The experimental arrangement used by Voth *et al.* (2002). (b) Top view of the lattice structures formed by steel spheres in a viscous fluid in a vertically-vibrated container. The interactions are in a plane perpendicular to the vibration axis which is in and out of the page. All images are taken from (Voth 2002).

In both experiments macroscopic dense spheres are subjected to vibrations and, as a result, they form structures perpendicular to the direction of oscillation. More specifically, in Wunenburger *et al.* (2002) there is an attraction between the spheres which leads to the formation of a chain oriented perpendicular to the axis of oscillation. In Voth *et al.* (2002), there is an attraction and a repulsion in the plane perpendicular to the oscillation which

leads to the formation of lattice structures. The values of the Reynolds number in both experiments lie in the intermediate regime where the flows are both viscous and inertial. In their explanation of these phenomena both groups discussed the existence of a non-zero, time-averaged flow which exists at non-zero Reynolds numbers in oscillatory flows (Riley 1966, Riley 2001). However, experimentally, three-dimensional fluid flows are difficult to track and visualise and direct observation or measurement of flows was beyond the scope of their studies.

In a more recent work, Klotsa *et al.* (2007) examined a system containing just two spheres in a fluid-filled cell under horizontal vibration. They studied how a pair of particles always align in a direction perpendicular to oscillation with the spheres separated by a well defined distance. More recently Klotsa *et al.* (2009) focused on chain formation within experiments and simulations. This study showed that the returning steady streaming flows perpendicular to the oscillations induces a strong attractive force towards the free ends of the chains. If the vibrated cell is sufficiently wide, roaming single particles and short chains will be drawn into the free end of the chain augmenting its length.

Pattern formation in oscillatory fluids can be observed in other systems apart from granular materials. Beysens *et al.* (2008) observed ordering phenomena of bubbles within an oscillating fluid. Their experiments investigated the liquid-vapour phase transition of hydrogen during high frequency ($f = 10\text{--}25$ Hz) and low amplitude (0.3–0.47 mm) vibrations in a weightless environment. Gravity effects were removed using a strong magnetic-field gradient. The experiments were performed near the liquid-vapour critical point. It was observed that, as the system was vibrated, vapour bubbles nucleate and grow in the liquid phase. When these bubbles grew to a sufficient size, the bubbles

would move with a different velocity to the oscillating fluid. The bubbles then ordered themselves in planes perpendicular to the vibration motion.

Similar effects may be reproduced in experiments using fluid-immersed diamagnetic particles held within a strong inhomogeneous field. The magnetic field is adjusted so that the particles become weightless at some height within the magnet. When the cell is shaken, the particles experience a drag relative to the fluid and streaming flows will form. Figure 4.3 shows a snapshot of shaken water-immersed bismuth particles within a strong magnetic field in one of the earliest experiments on this kind of system carried out within our research group. It was observed that the bismuth particles organise themselves into distinct layers perpendicular to the oscillation motion.



Fig. 4.3: Snapshot from experiments showing layer formation. The bismuth particles are $50\ \mu\text{m}$ in diameter and immersed in water. The experiments were performed within the Oxford Instruments superconducting magnet with a maximum central field of 17 T and maximum field gradient of $BdB/dz = 1470\ \text{T}^2\ \text{m}^{-1}$ which will be described in detail later. The oscillations are in the vertical direction which is perpendicular to the granular layers.

4.2 Dilute fluid-grain systems

The flow of a fluid through a granular bed can be described by phenomenological expressions for the flow through porous media. In 1856, Darcy was the first to formulate a simple relation between the pressure drop and the flow rate across a porous column (Darcy 1856). Extensions and additions to this model have been made in order to account for a wider range of applicability (Forcheimer 1901, Brinkman 1947 and Ergun 1952).

However, for dilute suspensions where the grains are fewer and the hydrodynamic interaction between each particle and the fluid is important, these

phenomenological expressions are not applicable because they describe the granular bed as one entity. A microscopic description is required to describe the interaction of the particles with the fluid.

The motion of the fluid in fluid-particle systems is governed by the Navier-Stokes equation,

$$\rho \left(\frac{\partial \mathbf{u}}{\partial t} + (\mathbf{u} \cdot \nabla) \mathbf{u} \right) = -\nabla P + \eta \nabla^2 \mathbf{u} + \mathbf{f}, \quad (4.1)$$

Where \mathbf{f} is a non pressure force such as gravity. If the fluid is incompressible, the mass conservation equation takes the form,

$$\nabla \cdot \mathbf{u} = 0 \quad (4.2)$$

Because the Navier-Stokes equation is nonlinear in \mathbf{u} , approximations need to be made depending on the system under investigation. A common practice is to determine which term is dominant in the equations and make approximations for the limiting cases. For this effect the Reynolds number is introduced. The Reynolds number, Re , is the dimensionless parameter which measures the ratio of inertial forces to viscous forces.

In the creeping flow limit, at low Reynolds numbers, viscous forces dominate and the Navier-Stokes equation is simplified to the linear Stokes equation by omitting the inertial term.

$$\nabla P = \eta \nabla^2 \mathbf{u} + \mathbf{f} \quad (4.3)$$

At high Reynolds numbers, if the flow is assumed to be inviscid, the viscous term can be dropped from the Navier-Stokes equation and Euler's equation govern the flow,

$$\rho \left(\frac{\partial}{\partial t} + \mathbf{u} \cdot \nabla \right) \mathbf{u} + \nabla P - \mathbf{f} = 0, \quad (4.4)$$

When the flows are irrotational, $\nabla \times \mathbf{u}$, it can be shown that the velocity distribution can be determined by a linear equation. In steady flows Bernoulli's theorem can be obtained by integrating Euler's equation along a streamline to provide a solution for the pressure distribution. In real fluids the values of the Reynolds numbers are in the intermediate and high regions and therefore both viscosity (even if it is very small) and inertia are equally significant and neither can be neglected. Numerical techniques are required to solve the Navier-Stokes equation.

Unsteady flows where the time derivatives of the flow field do not vanish, such as an object accelerating from rest through a fluid or time-periodic flows are more complex and only specific limits can be solved analytically. The systems described in this chapter lie within this case.

The boundary layer hypothesis states that in the presence of a solid boundary, two regions of flow can be identified: a thin layer close to the boundary called the boundary layer, and a region beyond (Prandtl 1905). Under this hypothesis, the Reynolds number is high enough that the viscosity effects are only significant in the boundary layer, which is thin compared to the characteristic size of the boundary, and the rest of the flow is assumed to be inviscid.

4.2.1 Oscillatory fluids and Streaming flows

When a solid boundary or object oscillates within a fluid it produces a periodic fluid flow. Let us consider a rigid sphere oscillating in the presence of a viscous fluid with a velocity $U \cos(\omega t)$, measured relative to the fluid. If no-slip conditions for the surface of the sphere are assumed, the motion of the

object will produce a flow field. In the limiting case of zero Reynolds number the flow is time-reversible and the flow field generated during the first half of the cycle will be cancelled by the flow field generated in the second half. As a result, there will be no net average flow. However, for moderate Reynolds numbers the viscous as well as the inertial forces in the Navier-Stokes equation have to be considered. Near the surface of the sphere vorticity is generated at the boundary layer as in the case of zero Reynolds number but the flow fields of the two parts of the cycle do not cancel each other. This is the case of a nonlinear system for which the average velocity field over a cycle is not zero.

This non-zero, time-averaged flow is called *steady streaming* and can be produced by an oscillatory, non-conservative body force or through the action of Reynolds stresses in the main body of the fluid, produced by no-slip boundaries. Nonlinear fluid phenomena of this kind have already been reported by Faraday in 1831. Later, in 1884, Rayleigh gave a theoretical explanation of the streaming produced by standing waves between two plane walls. The same steady flow pattern was later confirmed experimentally by Andrade (1931a&b) and Schlichting (1932). These observations constitute the basis for a series of experiments, theoretical approaches and, more recently, computer simulations on the subject of streaming flows.

In this thesis we are particularly interested in the streaming flow generated when a solid boundary, such as an spherical object, oscillates in an incompressible fluid. We will refer to this flow as an *steady streaming* flow. In three dimensional flows, the motion of an isolated single sphere subjected to an oscillating fluid flow has been studied both analytically and numerically. Lane (1995) and Riley (1966) used boundary-layer approximations and perturbation theory and Wang *et al.* (1965) used inner-outer expansions. More

recently, Mei (1994) and Alassar and Badr (1997) used finite-difference for the time advancement and matched asymptotic expansions for the near and far velocity fields and a series truncation method, respectively, to study the flow of a single sphere. In recent years, a few experimental studies have dealt with 3D flows around an oscillating sphere such as those by Kotas *et al.* (2007) and by Otto *et al.* (2008). Related experiments have reported the interactions and the patterns formed in oscillatory flows with a large number of particles where steady streaming is present, and it has been proposed that these phenomena are the result of hydrodynamic interactions (Voth 2002, Wunenburger 2002, Thomas and Gollub 2004). In the literature there are four dimensionless parameters that are commonly used to relate the properties of the fluid with those of the particles: the Reynolds number Re , the inverse Strouhal number ϵ , the streaming Reynolds number Re_s , and M^2 . They are defined as:

$$\begin{aligned} Re &= \frac{2A\omega r}{\nu}, \quad \epsilon = \frac{A}{r} \\ Re_s &= \epsilon Re = \frac{2A^2\omega}{\nu}, \quad M^2 = \frac{Re}{\epsilon} = \frac{2r^2\omega}{\nu}. \end{aligned} \quad (4.5)$$

Here the radius of the sphere is r , the amplitude of the oscillation is A , the angular frequency is ω and the kinematic viscosity of the fluid is ν . Only two of these ratios are independent: the Reynolds number (Re) which gives a measure of the ratio of inertial forces to viscous forces and consequently quantifies the relative importance of these two types of forces for given flow conditions and the inverse Strouhal number (ϵ) which gives a correlation between flow rate and frequency.

The theoretical studies have found that the shape of the steady streaming flow depends on the location of the specific problem in the parameter space depicted in Figure 4.4. For example, for low amplitudes, $\epsilon \ll 1$, Riley (1966)

found that a pattern similar to that shown in Figure 4.5(a) occurs for $M^2 \gg 1$ and $Re_s \ll 1$ but it changes to (b) when $M^2 \ll 1$.

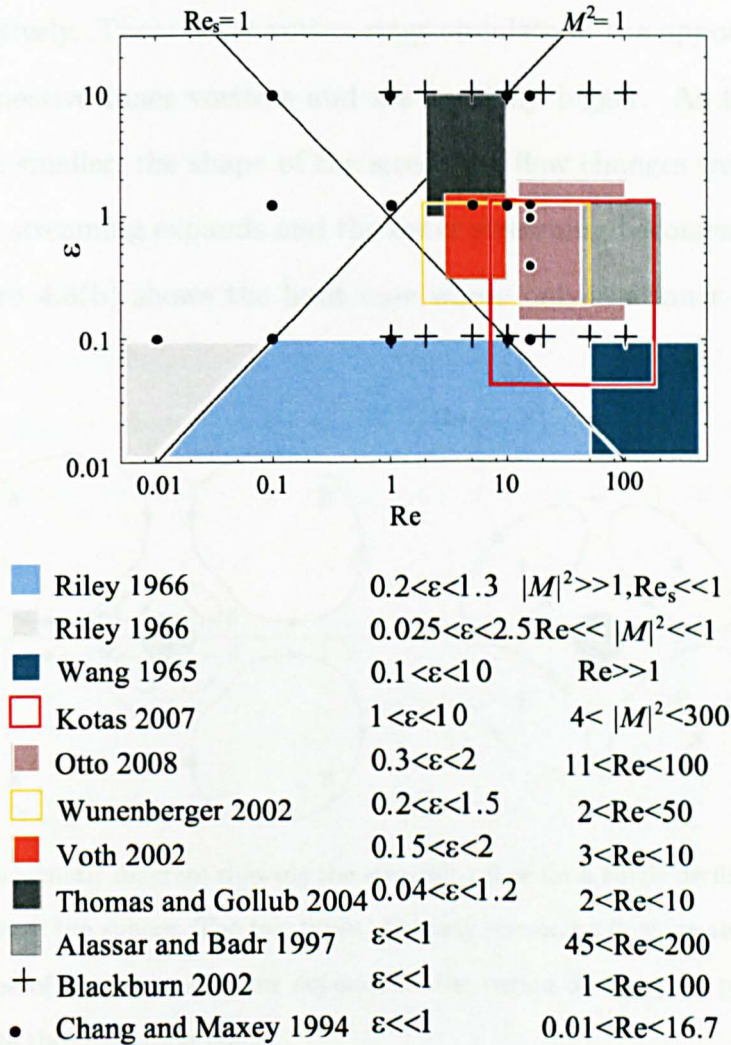


Fig. 4.4: Parameter space showing the regions where various studies have been conducted for a single sphere oscillating in a fluid. The figure was based on Fig. 1 in Otto *et al.* 2008.

Figure 4.5(a) shows the streaming flow for a sphere oscillating horizontally as indicated by the double arrow on it. Four vortices can be observed close to the surface of the sphere, $\alpha, \alpha', \beta, \beta'$. These four vortices are cross-sections through two vortex rings labelled $\alpha\alpha'$ and $\beta\beta'$. In other words, α and α' are the cross-sections of a single vortex ring $\alpha\alpha'$. The vortex rings are the consequence

of the non-slip boundary condition between the surface of the sphere and the fluid. This non-zero average flow is usually referred to as the *inner streaming*. The inner vortex rings $\alpha\alpha'$ and $\beta\beta'$ will generate the outer vortex rings AA' and BB' , respectively. These outer vortex rings circulate in the opposite direction to their respective inner vortices and are spatially bigger. As the Reynolds number gets smaller, the shape of the streaming flow changes from (a) to (b) as the inner streaming expands and the outer streaming becomes increasingly weak. Figure 4.5(b) shows the limit case where only the inner streaming is present.

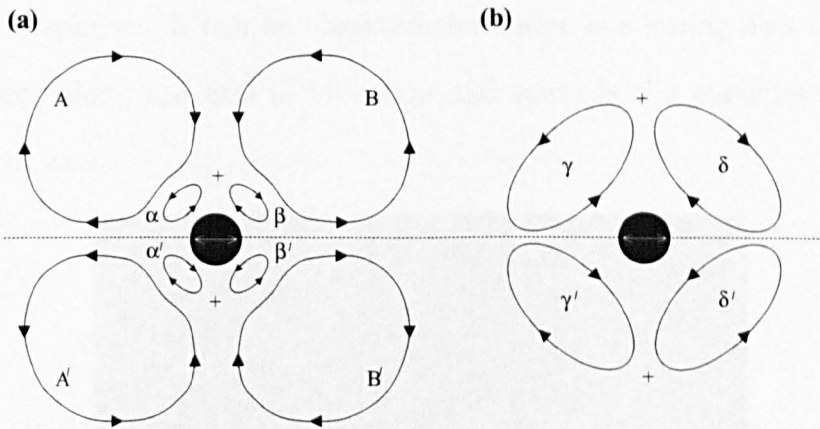


Fig. 4.5: A schematic diagram showing the streaming flow for a single oscillating sphere in the plane through the sphere. The two types of steady streaming flow are shown in (a) and (b). The shape of the streaming flow depends on the region of the space parameter. The crosses indicate the stagnation points.

Experimentally, the study of three-dimensional steady streaming flows is not a simple task since the visualization of such flows can prove to be challenging. Hence, it is not surprising that not many experimental studies have been carried out. In the experimental study performed by Kotas *et al.* (Kotas *et al.* 2007) the flow around a single oscillating spheroid at finite Reynolds numbers was visualized and recorded for various vibratory conditions. In their experiments, different shapes of spheroids were glued to a metal rod which was

connected to a shaker and then vibrated vertically in a fluid-filled container. The aim of the study was to extract the three-dimensional streaming flows and measure the inner steady streaming.

Klotsa *et al.* (Klotsa *et al.*, 2007) observed that spheres undergoing horizontal vibrations aligned perpendicularly to the direction of oscillation and, in some cases, a gap could appear between the particles. They carried out experiments with a pair of stainless steel spheres in a horizontally-shaken cell filled with a mixture of water and glycerol. Figure 4.6 is a snapshot taken during their experiments and shows the resulting streaming flow produced by the pair of spheres. It can be observed that there is a strong flow away from the spheres along the axis of vibration and towards the particles along the orthogonal axis.

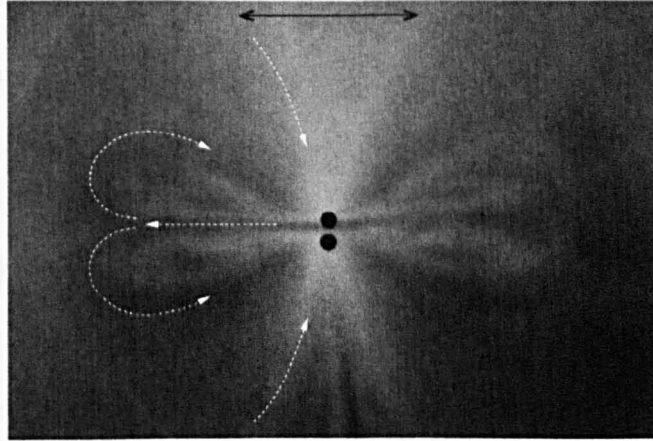


Fig. 4.6: Flow pattern induced by a pair of 1mm diameter spheres. The spheres were immersed in a glycerol-water mixture. The white arrows indicate the direction of the streaming flow for the left side of the cell; the flow pattern in the right side is a mirror image. The black double-headed line indicates the direction of oscillation. Image taken from Klotsa *et al.* (2007).

In a development of their work (Klotsa *et al.*, 2009), a collection of spherical particles were placed in the same cell. When the cell was vibrated, the

particles were observed to form chains perpendicular to the direction of oscillation. They studied this phenomenon experimentally and through computer simulations, their observations are shown in figure 4.7. Figure 4.7 a) shows the evolution of the chain formation during a typical experiment. Figure 4.7 b) show the corresponding evolution in simulations which seems to agree with their experimental observations. They concluded that the mechanism responsible for the attraction of two spheres, the formation of chains and the repulsion between adjacent chains was caused by the steady streaming flows. Isolated spheres are brought together along a line perpendicular to the direction of oscillation. Each sphere has a flow pattern as shown in figure 4.5. As the spheres approach each other the outer vortex loops of opposite circulation interact and cancel, leaving only the inner vortices which create the gap between the spheres. The repulsive interaction observed between chains can be traced to the streaming flow generated by each chain as depicted in figure 4.7 c). In the plane containing the spheres it can be observed that the flow is always away from the chain and it is this flow which tends to push the chains apart.

In the studies reviewed so far the particles were constraint to move in a plane; they were either resting on a surface or suspended by a thin wire but in all cases they were not free to move in all directions. Thus, the interaction between a collection of spheres in a three-dimensional systems is yet to be explored. In the remainder of this chapter we shall focus on the description of an experimental study of spheres suspended in a diamagnetic, vibrated fluid. A brief review on magnetic levitation can be found in Appendix A.

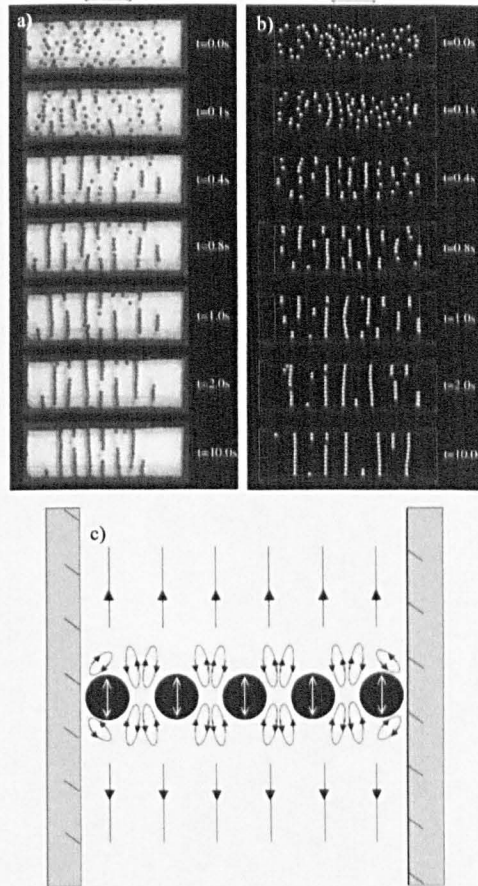


Fig. 4.7: Chain formation in an oscillatory fluid flow. a) Series of snapshots from experiments showing the evolution of a collection of spheres from an initial dispersed configuration to an ordered state. b) Snapshots taken from a simulation of the experimental system shown in a). The particles in the simulation undergo the same stages of evolution and the time scales are also comparable to those observed in the experiments. c) Schematic diagram of a short chain showing the streaming flow in the $x - y$ plane containing the centres of the spheres. All pictures were taken from Klotsa *et al.*, 2009.

4.3 Experimental Setup

In this section we describe the experimental array used in our study of collection of grains suspended in a vibrating, viscous fluid flow. The central piece of the experimental setup is the superconducting levitation magnet. A helium-cooled superconducting magnet specifically designed and manufactured

by Oxford Instruments was used to conduct levitation experiments. An image of the magnet is shown in figure 4.8.

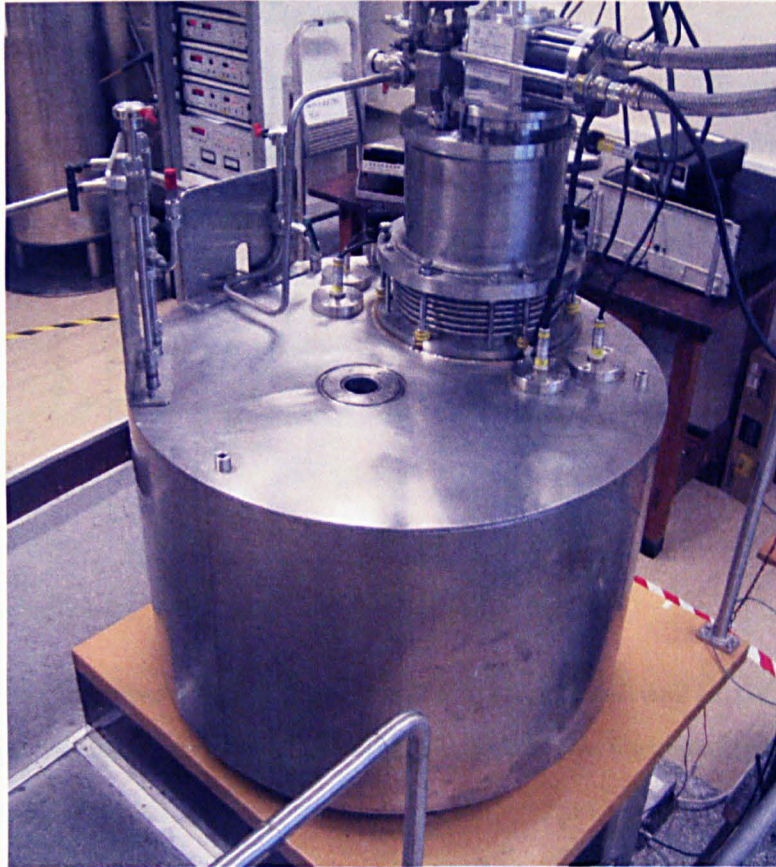


Fig. 4.8: The Helium-cooled superconducting magnet

The magnetic field was produced by superconducting coils which allowed the electric current to persist for long periods of time without the use of an external power supply. The coils were immersed in a liquid helium bath at a temperature of 4K. A closed-cycle cooling loop recovered the helium that had evaporated from the bath eliminating the need of replacing the helium periodically. Due to these features, the magnet is capable to produce fields of up to 16.5T for long periods of time.

The maximum value of the field is located at the centre of the magnet, around 18.8cm below the top plate of the magnet. The normalised profile of

the vertical component of the magnetic field is shown in figure 4.9, the origin $z = 0$ corresponds to the maximum field value. In figure 4.10 the normalised field-gradient product, $B dB/Dz$, is shown.

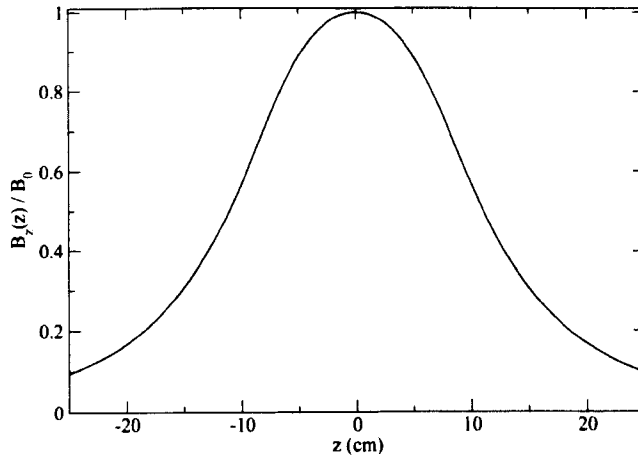


Fig. 4.9: The normalised profile of the magnetic field along the vertical axis of the levitation magnet. B_0 is the maximum value of the magnetic field, in this particular case $B_0 = 16.5T$.

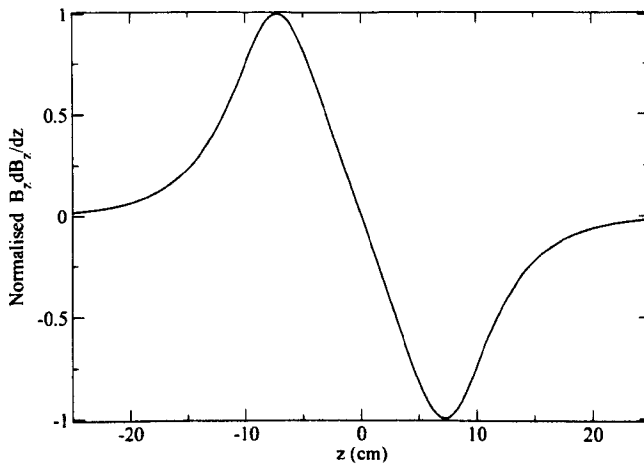


Fig. 4.10: Normalised profile of the axial field-gradient product $B dB/dz$.

The other major pieces of equipment can be divided in two groups; the

vibratory apparatus and the optics. In figure 4.11 a schematic representation of the complete experimental setup is shown.

The vibratory apparatus is similar to the one used in chapter 3, section 3.2. A long-throw electromagnetic transducer (8-inch loudspeaker by Peerless) was mounted facing upwards to a medium density fibreboard (MDF) box. A horizontal surface was created on top of the diaphragms using expanded polyurethane foam. A rigid, horizontal metal plate was fitted on top of this surface. A long aluminium rod was then attached to the metal plate and used to transmit the oscillation to the containers. The length of the aluminium rod could be adjusted to position the containers at the right height inside the bore of the magnet. The motion of the loudspeaker was monitored using a pair of capacitance cantilever accelerometers, Analog Devices ADXL105 and ADXL150, attached to the metal plate on top of the transducer. The accelerometers covered the ranges from $0 - 7g$ and $0 - 70g$ respectively, where g is the acceleration due to gravity.

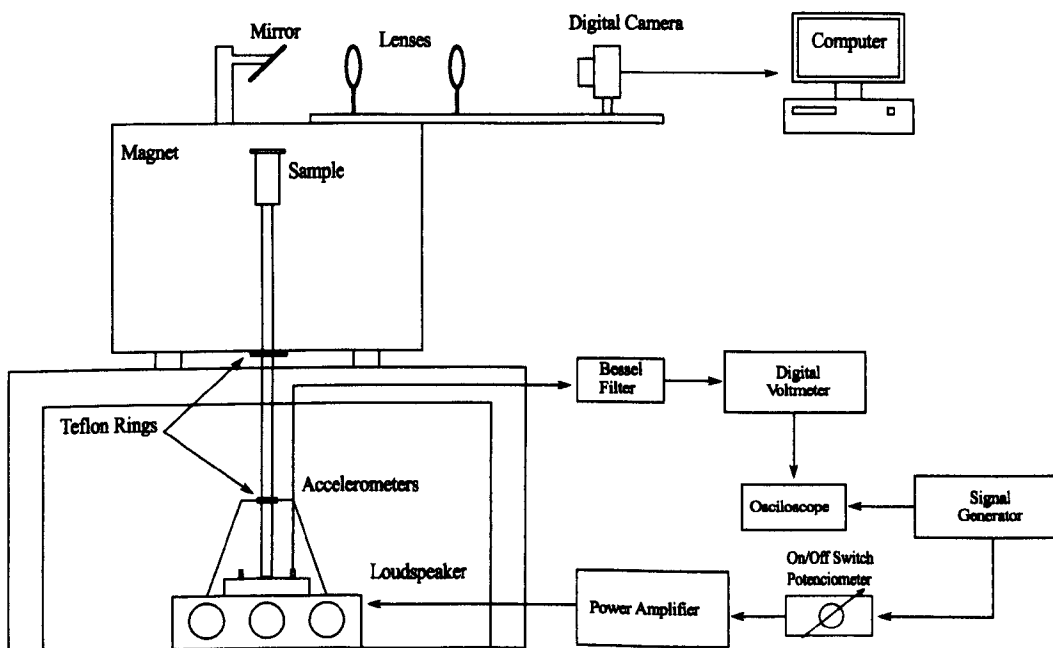


Fig. 4.11: Schematic representation of the experimental setup.

A continuous sinusoidal wave was generated to drive the transducer using a Signal Generator Model DS345 by Stanford Research Systems. The frequency and peak-to-peak voltage of the driving signal was adjusted to the desired values and sent through a device fitted with an on/off switch and a potentiometer to a custom-made power amplifier. The potentiometer allowed a finer control over the maximum voltage of the signal fed to the transducers hence controlling the maximum acceleration experienced by the apparatus. This acceleration was monitored by the pair of accelerometer described above. The signal from the accelerometers was sent through a 4-pole low-pass Bessel filter with a cut-off frequency of 800Hz . The output was displayed in a digital voltmeter which gain was calibrated so the voltages shown corresponded to the maximum dimensionless acceleration, Γ .

The experiments were monitored using a digital camera, Casio Exilim FX1. The image from the particles was projected towards the camera using a front-plated mirror at 45° with the horizontal placed directly above of the bore of the magnet. Two achromatic, biconvex lenses mounted on an optical rail were used to focus the image so it could be recorded by the camera which was placed at a distance $> 1\text{m}$ from the bore of the magnet to minimize the effects of the magnetic field on the electronics. The output of the digital camera was then visualized on a computer monitor.

Two containers, a cylindrical and a squared cross-section cell, were constructed out of PMMA for our experiments. The cylindrical container was 13cm in height with an inner diameter of 3.6cm. The top of this container could be removed, a feature that allowed us to easily fill the container with the viscous solution. The top was made out of optical class PMMA to prevent distortions on the images. Two access holes at the bottom of the cell were

used to remove air bubbles if case they form during experiments as well as to introduce, or change, the particles. The access holes were placed at the bottom of the cell to prevent obstructions with the field of view that were likely to occur if they were placed at the top of the cell.

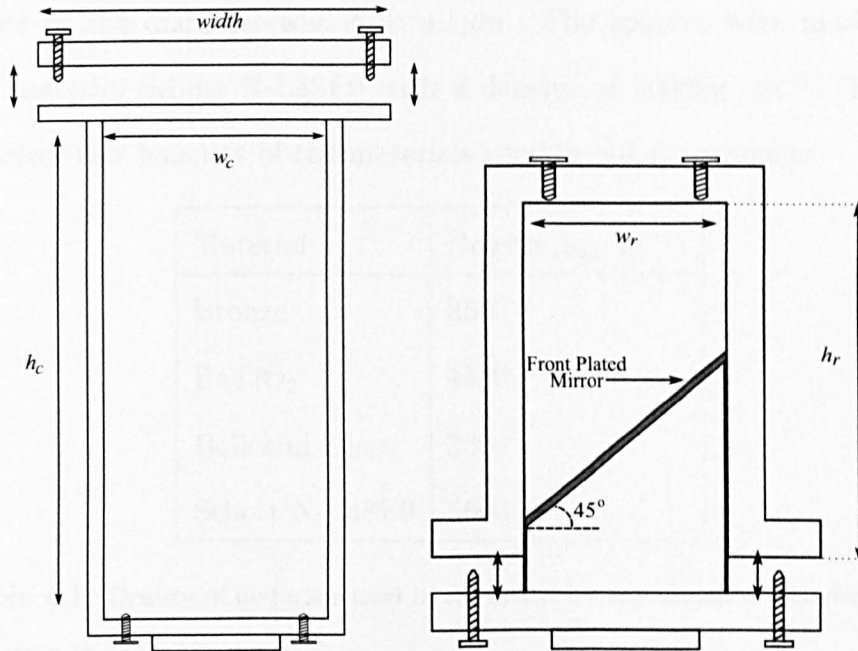


Fig. 4.12: Schematic view of the containers used in our experiments. The cylindrical container is shown on the left. The total width of this cell is 4.8cm. The inner diameter, w_c , is 3.6cm and the height of the cell is 12.0cm. The rectangular container with the mirror inset is shown on the right. The inner cross section of this container is squared and $w_r = 2.0$ cm. The height of the container, h_r , is 6.0cm.

The rectangular container had a squared cross-section of 2.0cm x 2.0cm and was 6.0cm in height. The base of this container could be detached. A special inset with a front-plated mirror at 45° with the horizontal could be placed inside the container to follow the vertical displacement of the particles. Two access holes were placed at opposite corner of the top face of the container to easily introduce or change particles in between experiments or to remove air bubbles. Figure 4.12 shows an schematic view of these containers.

Unless otherwise stated, the experimental results discussed in this chapter were obtained using ball lenses for diode lasers purchased from Melles Griot. The lenses are manufactured to have high-standard optical characteristics which translate in a homogeneous density and high sphericity. The tolerance in the diameter was $\phi = \pm 1\mu\text{m}$. The spheres were made of the optical material Schott N-LaSF9 with a density of $5600\text{kg} \cdot \text{m}^{-3}$. Table 4.1 summarizes the densities of the materials used in our experiments.

Material	Density($\text{kg} \cdot \text{m}^{-3}$)
Bronze	8500
BaTiO ₂	4500
Ballotini Glass	2500
Schott N-LaSF9	5600

Table 4.1: Density of materials used in the levitation experiments. The densities are given in $\text{kg} \cdot \text{m}^{-3}$

4.4 Levitated spheres

In our experiments, spherical particles are magnetically levitated inside a liquid-filled container. In most of the experiments an aqueous solution of glycerol and a paramagnetic salt was used. The solutions were prepared using a mixture of water, glycerol and $\text{MnCl}_2 \cdot 4\text{H}_2\text{O}$ salt from VWR International Ltd. The Mn^{2+} ion is strongly paramagnetic with 5 electrons in the half-filled 3d shell giving a spin $S = \frac{5}{2}$. For the majority of the experiments describe in this chapter a 0.18M solution of MnCl_2 was used. The ratio between water and glycerol was changed depending on the desired viscosity. The air dissolved

in the solution was pumped out using a rotatory vacuum pump to prevent the formation of bubbles inside the containers during experiments. Finally, the solution was cooled to a temperature close to that inside the bore of the magnet to avoid steep variations of temperature.

The container was filled with the solution and sealed. Special care was taken to prevent air bubbles getting trapped inside the container. The spheres were then introduced to the cell by removing one of the screws located at the bottom of the cylindrical container or the top of the rectangular container. The aluminium rod was attached to the container and both were slid into the bore of the magnet and then locked to the loudspeaker. Finally, a thermocouple was glued to the side of the container to monitor the temperature before and after each measurement.

4.4.1 Initial Observations

A collection of BaTiO_2 particles with an average diameter of $850\mu\text{m}$ were placed in the cylindrical container. Before switching on the vibration, the particles are observed to cluster at the middle of the cell around the levitation point. When the vibration is switched on the particles spread and formed a layer consisting of concentric rings. When the amplitude of vibration, controlled by the parameter Γ , was slowly increased or decreased the shape of the layer did not change. In fact, the formation of a layer could be observed for small values of Γ . However, for some combinations of Γ , f and viscosity, ν , the layer started to rotate in the plane containing the centres of the particles and perpendicular to the direction of vibration. Figure 4.13 shows a snapshot taken during one of these experiments. In this picture it is possible to observe the concentric rings that form the layer. This structure is similar to the one

observed by Voth *et al.* (2002) when spheres surrounded by fluid bounce on top of a vibrated surface in presence of gravity. However, the rotation of the layer was not reported in their study.

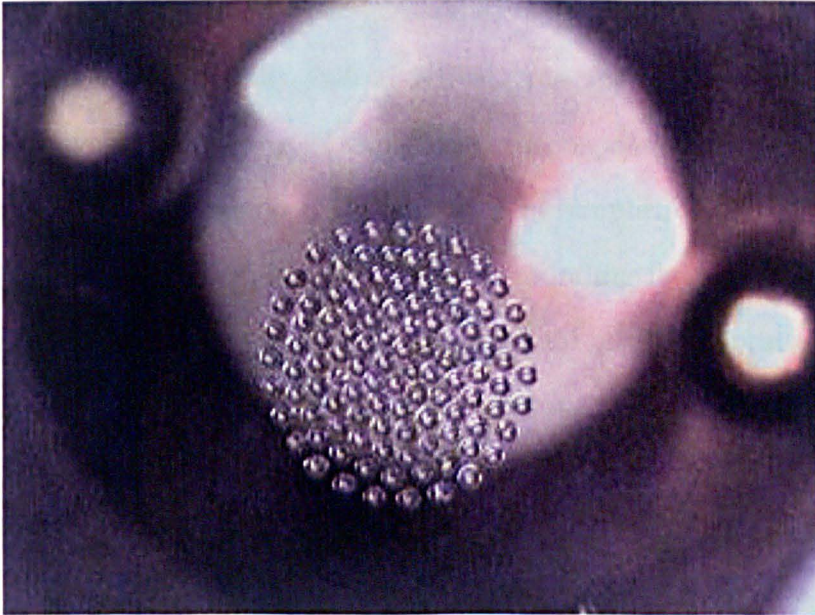


Fig. 4.13: BaTiO_2 particles form a monolayer when vertical vibration is applied. A collection of particles with average diameter $850\mu\text{m}$ were used in this experiment. The particles are levitated in a 0.1M solution of manganese chloride in a an aqueous solution of glycerol. For this particular picture the frequency is 20Hz and $\Gamma = 1$.

In order to understand the dynamics of the spheres in the fluid, we focussed our attention on two simpler systems; a single particle and two identical particles. In the following section we will describe in detail the experiments carried out to study the behaviour of these systems.

4.4.2 Dynamics of a single, levitated particle

The simplest system that could be studied is that of one sphere levitating in a viscous fluid. Although the particles are suspended in the fluid they are not neutrally buoyant. The amplitude of vibration of the container is

different to that of the particles suspended in the fluid due to the effective decoupling between the gravitational and the inertial mass. In previous studies (Wunenburger *et al.* 2002, Coimbra *et al.* 2004 and Klotsa *et al.* 2007) the amplitude of vibration of the particles relative to the surrounding fluid has been measured experimentally and analytical expressions have been proposed. The measurements were obtained using particles suspended inside the fluid by thin wires or sliding on top of a surface. The amplitudes and frequencies of vibration as well as the viscosity of the surrounding fluid were different to those explored in this chapter. Hence the analytical relations obtained in these studies are not applicable to our system due to its three-dimensional nature. Our aim is to obtain a gross approximation of the amplitude of oscillation of the particles relative to the oscillating fluid.

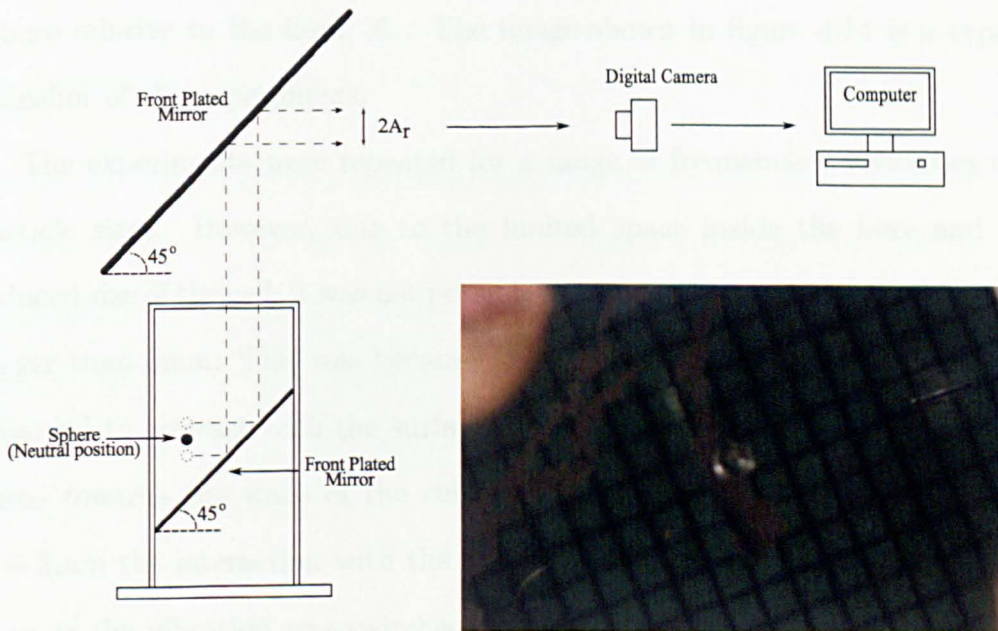


Fig. 4.14: Schematics of the experimental setup used to measure the motion of a single particles relative to the fluid. The neutral position of the particles (solid black circle) corresponds to the resting place of the sphere before turning on the vibration. The dotted circles mark the maximum displacement during a cycle.

To measure the relative amplitude a single glass particle was levitated at

the centre of the rectangular container sketched in figure 4.12. The container was prepared as described above and placed inside the bore of the magnet. The particle was observed to levitate above the mirror inside the cell and away from the other walls. The optical array consisting of a mirror and two biconvex lenses described in section 4.3 was used. A schematic of the experimental setup is shown in figure 4.14. For a given frequency, f , the amplitude of vibration was increased by adjusting Γ . The system was allowed to reach equilibrium and an image was taken using the digital camera. The exposure of the camera was chosen to allow several cycles to be captured. The resulting image showed the particle and its elongated image on the mirror. By measuring the elongated image it was possible to extract the distance travelled by the sphere, relative to the fluid, in a cycle which is twice the amplitude of vibration of a single sphere relative to the fluid, A_r . The image shown in figure 4.14 is a typical snapshot of the experiments.

The experiments were repeated for a range of frequencies, viscosities and particle sizes. However, due to the limited space inside the bore and the reduced size of the cell, it was not possible to obtain reliable data for amplitudes bigger than 5mm. This was because for bigger amplitudes the particles were observed to interact with the surface of the mirror or move in the horizontal plane towards the walls of the cell. Furthermore, for particles of diameter $d = 3\text{mm}$ the interaction with the mirror and walls was observed to start as soon as the vibration was switched on. Consequently, no experimental data could be acquired for this particular size of particle.

The images were analysed using Matlab. Each image was read by the code and presented on-screen. The size of the reflection was measured and the scale was calibrated by measuring the graph paper on the mirror. The experimental

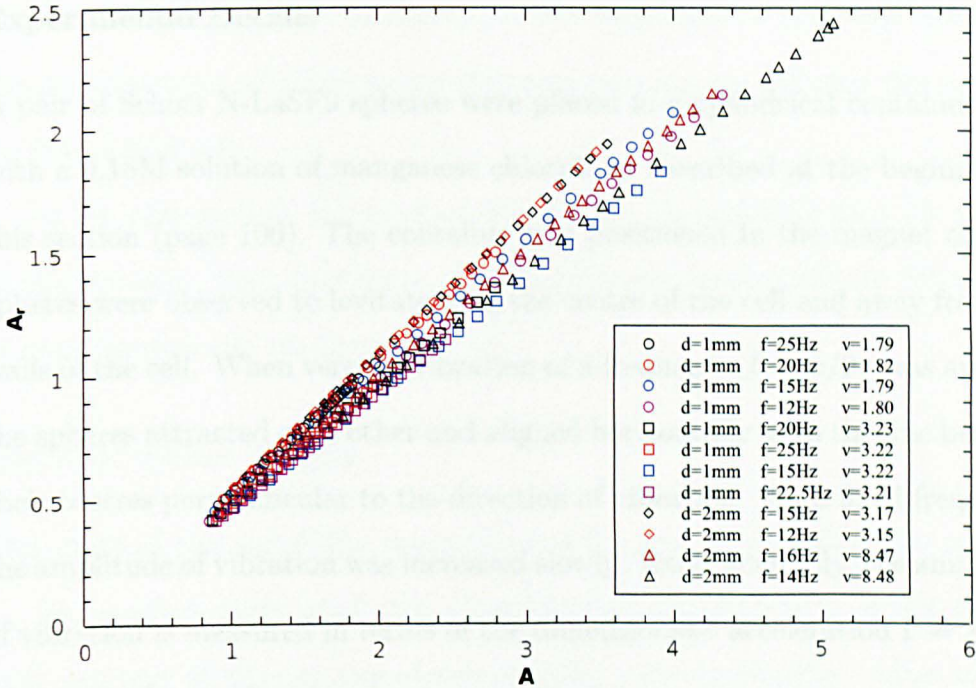


Fig. 4.15: The measured real amplitude of vibration as a function of the amplitude of vibration of the cell for three different combinations of particle size and viscosity. The experimental error (not shown for clarity) is of the same order of the data spread.

results for three different combinations of particles sizes and viscosities are plotted in figure 4.15. In this figure it is possible to observed that, as the amplitude of vibration of the container increases, A , the lines diverge. However, the experimental error of the measurements is of the same order of the resulting scattering and around $\pm 5\%$. Each data set can be fitted to a straight line of the form $A_r = cA$ with $c \simeq 0.5$.

4.4.3 Dynamics of two levitated spheres

In the following section the dynamics of a pair of identical spheres will be studied. When subjected to vertical vibrations hydrodynamical effects give rise to the onset of an instability which results in the spheres to orbit each other. The onset of the instability as well as the orbital velocity will be investigated.

Experimental Details

A pair of Schott N-LaSF9 spheres were placed in a cylindrical container filled with a 0.18M solution of manganese chloride as described at the beginning of this section (page 106). The container was positioned in the magnet and the spheres were observed to levitate near the centre of the cell and away from the walls of the cell. When vertical vibration of a frequency $f = \omega/2\pi$ was applied, the spheres attracted each other and aligned horizontally with the line between their centres perpendicular to the direction of vibration. For a fixed frequency, the amplitude of vibration was increased slowly. Experimentally, the amplitude of vibration is measured in terms of the dimensionless acceleration $\Gamma = A\omega^2/g$ where g is the acceleration due to gravity.

It was observed during our experiments that, as Γ was increased, the system reached a point where the spheres started to wobble around the vertical axis. This point indicates the onset of an instability. If the amplitude of vibration was increased, the spheres were observed to orbit each other, either clockwise or anti-clockwise.

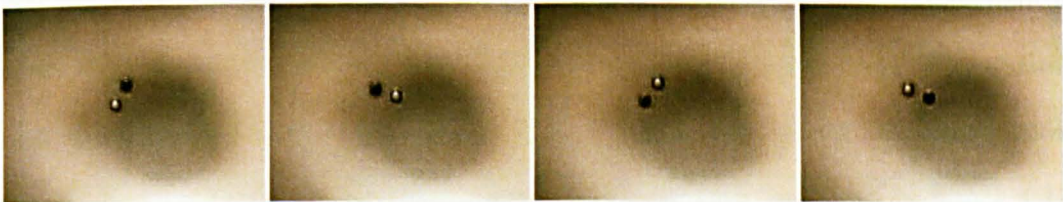


Fig. 4.16: Image composition of one period of rotation for two glass spheres levitated in a solution of MnCl_2 .

During the experiments it is possible to observe a well defined value of the amplitude of vibration for which the behaviour of the pair of spheres changes. This amplitude will be referred from now on as the critical value of the amplitude, A_c . For values of amplitude larger than A_c the particles orbit each other;

for lower values the rotation stops. As the amplitude is increased above A_c , the particles orbit at a faster rate and a gap can appear between the particles for high amplitude.

In the next section, the onset amplitude A_c , for orbital motion for a range of particle sizes, fluid viscosities, and vibration frequencies will be determined in order to quantify the instability.

Onset of orbital motion

The onset of the instability was measured by slowly decreasing the value of Γ . For a given value of f , the dimensionless acceleration Γ was increased until the pair of spheres was observed to be rotating steadily. After waiting some time for the system to stabilize, the value of Γ was decreased by a small amount and the system was allowed to reach equilibrium. This process was repeated until the spheres came to a complete stop. A second measure of the onset amplitude was obtained by increasing the amplitude until the motion started. The procedure was repeated increasing the time between changes in the amplitude until both measures of the onset agreed within experimental error. The instability shows very little hysteresis. The amplitude of vibration of the cell at the onset of the instability as a function of the viscous penetration depth, $\delta = (\nu/f)^{1/2}$, where ν is the kinematic viscosity, is shown in figure 4.17 for the range of particle sizes and viscosities explored in the experiments. The data appear to follow a straight line that intersect the origin.

If the transition is purely hydrodynamic the onset can only depend on three independent length scales: A , d , and the viscous penetration depth, δ . In figure 4.18 we plot the ratio A_c^*/d as a function of δ/d (both dimensionless quantities) for the range of parameters explored in our experiments. The

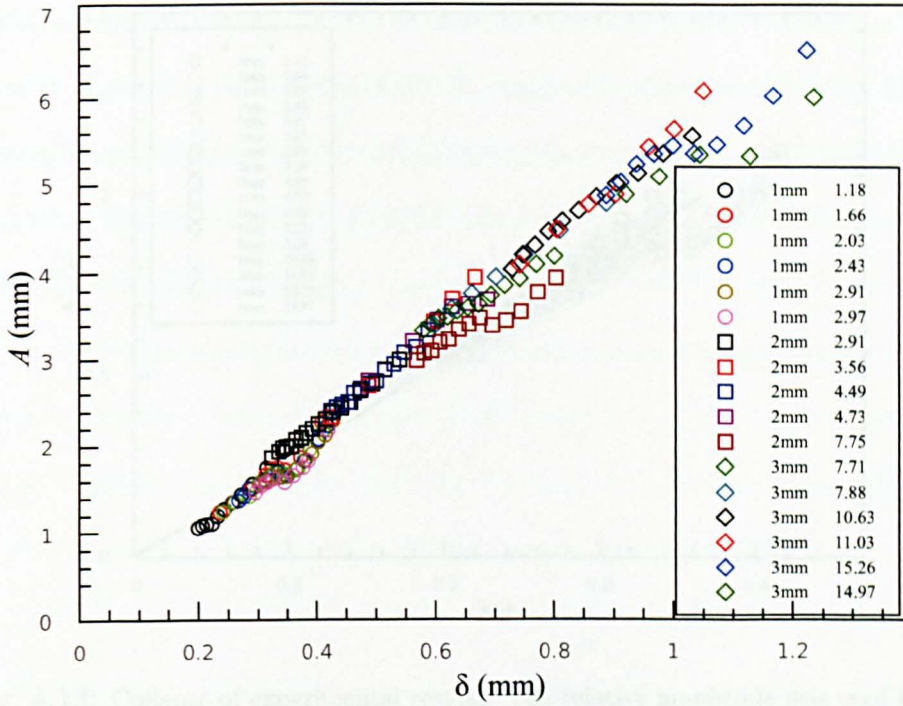


Fig. 4.17: The critical amplitude of vibration as a function of the viscous length for the three different particle sizes.

critical relative amplitude of vibration A_c^* is the amplitude of vibration of the particles relative to the fluid at the onset of the instability. In this case, the results of the previous section were taken into consideration and a value of $0.5A_c$ was used. It can be seen that there is a good collapse of the data onto a line for δ/d less than about 0.34. Within the scatter we can fit the data to a straight line to the origin. This line corresponds to a constant value of the streaming Reynolds number $Re_s = \frac{A^2}{\delta^2} = 74$ which is independent of the particle size.

For low values of A_c^*/d and δ/d there is no consistent rotational instability. The lower limit of our data for the onset of rotation corresponds to a particle Reynolds number $Re_p = \frac{Ad}{\delta^2} \simeq 120$, as shown in figure 4.19.

For δ/d greater than about 0.34 a gap opens up between the particles before the spheres start to orbit. The data in this region appears to collapse onto a

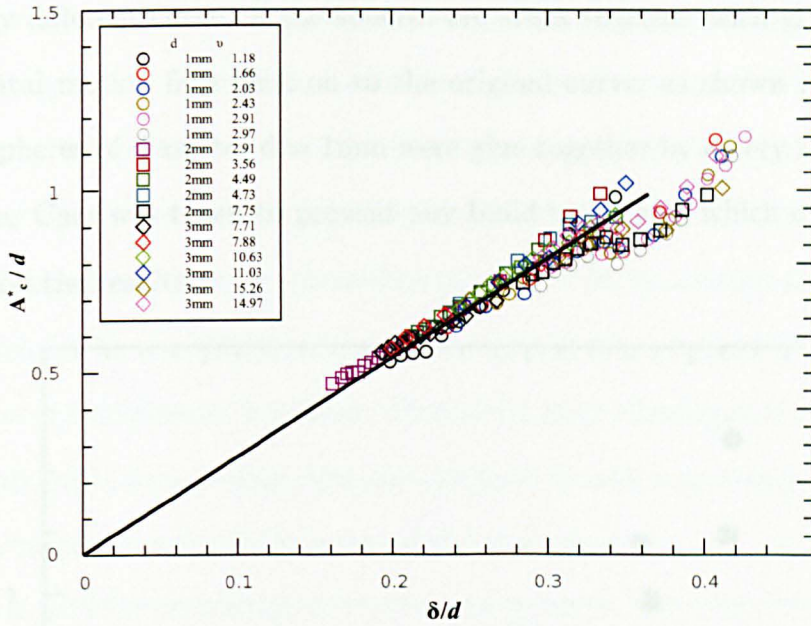


Fig. 4.18: Collapse of experimental results. The relative amplitude was used in this plot. The spread of the experimental data is of the order of the error in the measurements.

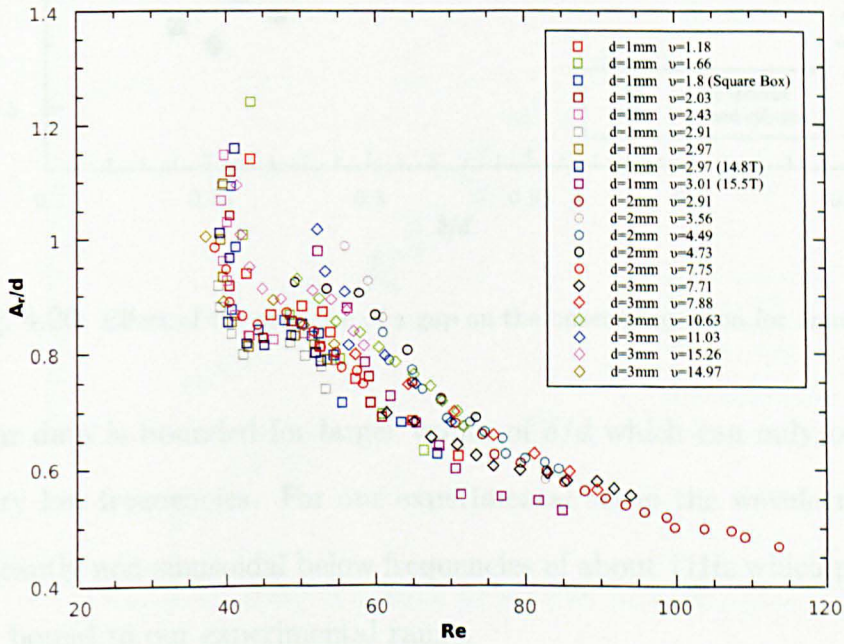


Fig. 4.19: The critical amplitude of vibration as a function of the particle Reynolds number $Re_p = A^*d/\delta^2$. The region for Re_p smaller than 50 corresponds to conditions where a gap between the particles is observed.

slightly different curve. If the spheres are stuck together with glue, the onset of orbital motion falls back on to the original curve, as shown in figure 4.20. Two spheres of diameter $d = 1\text{mm}$ were glue together by a very small amount of glue. Care was taken to prevent any build up of glue which could have an effect on the results.

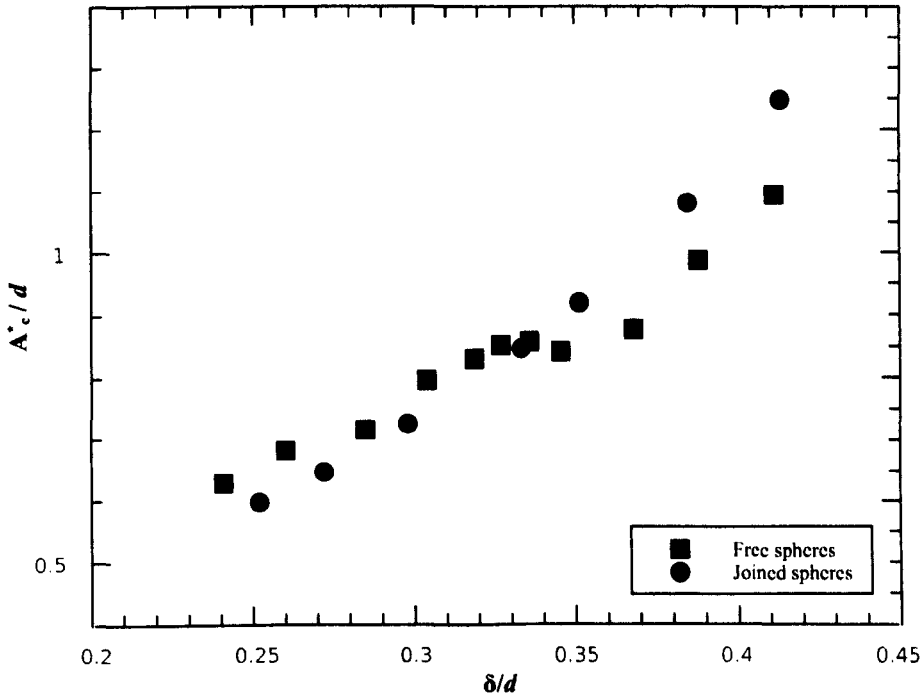


Fig. 4.20: Effect of the presence of a gap on the onset of rotation for 1mm spheres

Our data is bounded for larger values of δ/d which can only be achieved for very low frequencies. For our experimental setup the waveform becomes significantly non-sinusoidal below frequencies of about 11Hz which provides an upper bound to our experimental range.

Magnetic Effects

Although the collapse of the experimental data strongly suggest that the origin of the instability is purely hydrodynamic it is possible that other variables

could trigger the instability. It is conceivable that the magnetic field could be playing a role on the onset of orbital motion. There are two possible ways in which the magnetic field could affect the instability. Firstly, the fluid flow induced by the vibration may give rise to ionic currents in the manganese chloride solution which couple to the magnetic field, generating a Lorentz force on the fluid. To test this scenario, the experiments were repeated using bismuth shots in water/glycerol mixtures. Due to its large diamagnetic susceptibility, bismuth could be levitated without the need to add any manganese chloride to the liquid to enhance the buoyancy of the spheres.

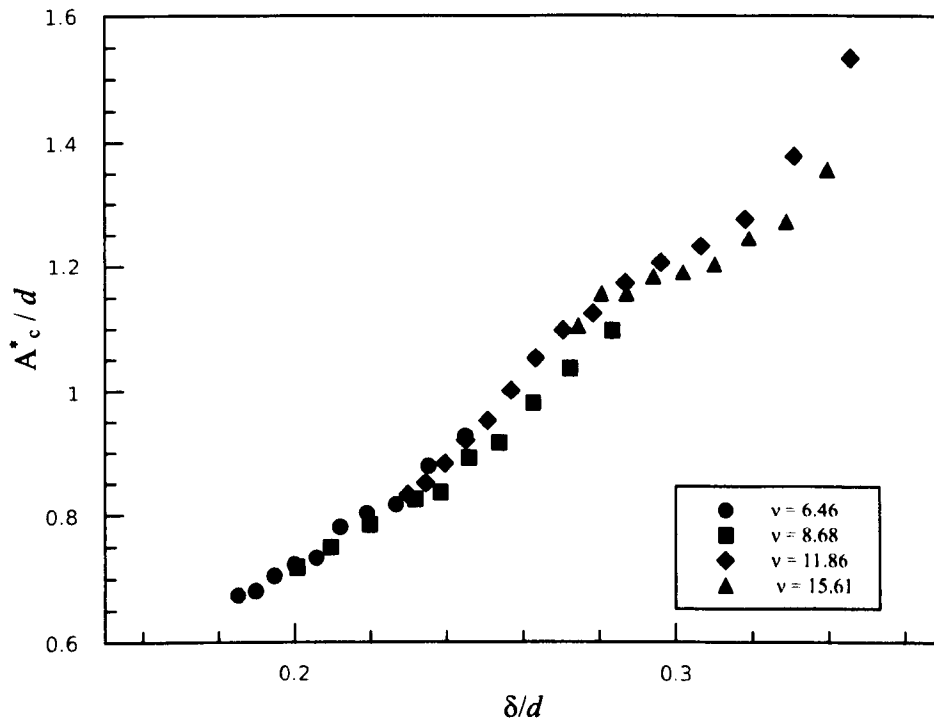


Fig. 4.21: Onset of rotation for $d = 2.8\text{mm}$ bismuth shoot.

The bismuth spheres behave in the same way as the glass spheres, giving a similar data collapse for the onset of the orbital motion. The similarity in the behaviour of the glass and bismuth experiments indicates that the magnetic Lorentz force, resulting from the motion of the ionic manganese chloride liquid

through the field, plays no significant role in the phenomenon.

Furthermore, the particles are kept suspended in the fluid inside a magnetic potential well (magnetic trap). The strength of the magnetic trap was measured and found to be equivalent to approximately 2% of the gravitational pull. The shape of the trap could have an effect on the onset of orbital motion. The strength of the magnetic field was varied which in turn changes the shape of the magnetic trap. For the lower value of the magnetic field the shape of the magnetic trap is elongated in the vertical direction and very narrow in the horizontal plane causing the particles to move towards the vertical axis of the magnet. For the intermediate value of the magnetic field the magnetic trap is shallower, with shorter vertical walls, resembling a bowl. The higher value of the magnetic field produces a very shallow trap with short vertical walls but strong in the horizontal plane.

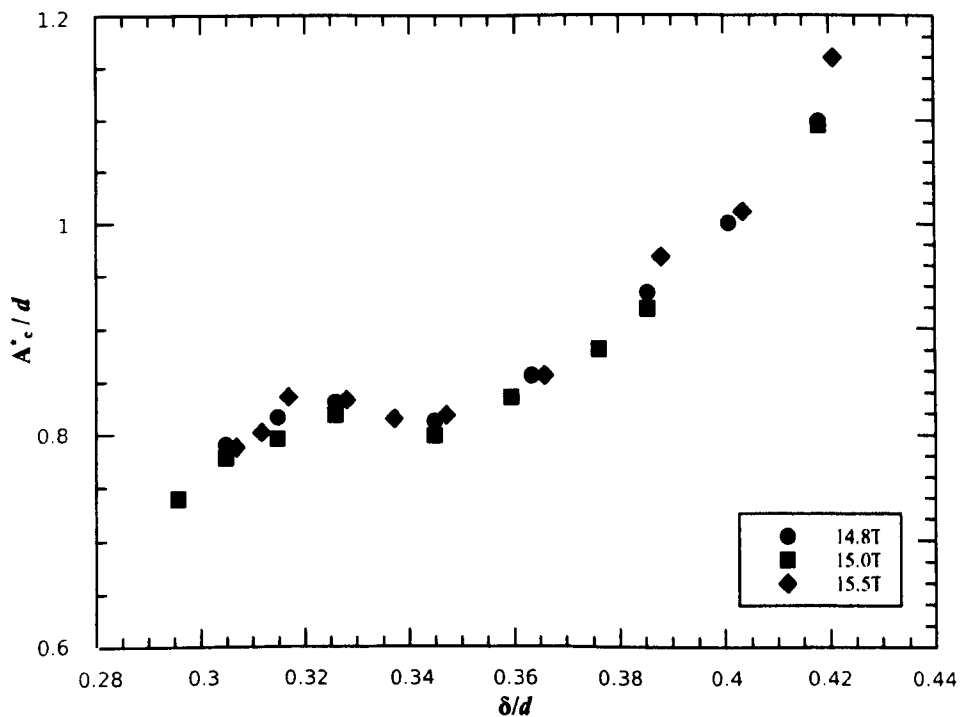


Fig. 4.22: Comparison of the onset of rotation for three values of the magnetic field for 2mm spheres.

For the lower magnetic field the particles levitated one on top of the other but as soon as the vibration was turned on they aligned on a horizontal plane. Figure 4.22 shows the onset of the instability for the three values of magnetic field. It is possible to observe that the change of shape of the magnetic trap has no effect on the onset of orbital motion.

Geometry Effects

The orbital motion of the spheres has a cylindrical symmetry which raises the question of whether the geometry of the container could be playing a part on the onset of the instability. To explore this possibility, the experiments were repeated in the rectangular container used in section 4.4.2. A pair of glass spheres of diameter $d = 1\text{mm}$ were placed inside the container in a 30% by volume mixture of water and glycerol. The concentration of Manganese chloride was 0.18M as in previous experiments. The critical amplitude for the onset was measured and compared with the results obtained for a system under the same conditions in the cylindrical cell. The results are shown in figure 4.23. It can be observed that the shape of the container has no measurable influence on the onset of orbital motion.

Speed of orbital motion

The container was filled with a 0.18M solution of MnCl_2 and two particles were placed inside. The cell was sealed and any remaining bubbles were removed through the access holes at the bottom of the cell. The container was placed inside the bore of the magnet and attached to the vibratory apparatus using the aluminium rod. The vibration was switched on and Γ was adjusted to a value where the particles were observed to rotate. The system was allowed

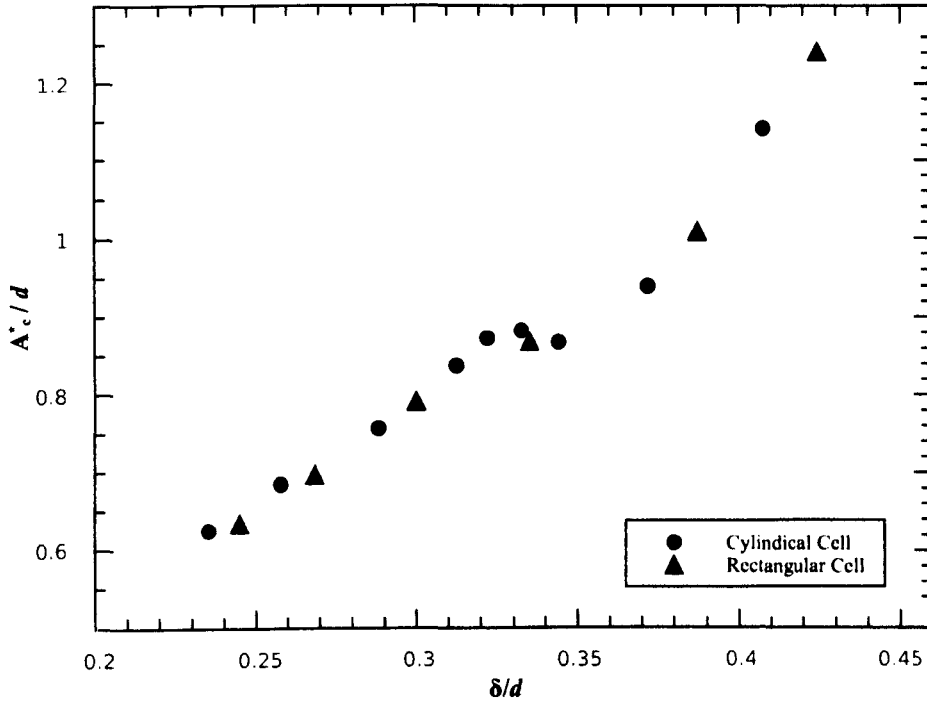


Fig. 4.23: Effect of the geometry of the container over the onset of rotation for 1mm spheres

to evolve in these conditions for a period of time, which will henceforth be referred to as the *settling time*, of 2 minutes to reach equilibrium. It was observed that measurements taken using a settling time as short as 20 seconds yielded the same results within the uncertainty of our measurements. The period of rotation was measured for several conditions. In a typical experiment a pair of particles were vibrated at a fixed frequency. The value of Γ was adjusted so the particles were rotating smoothly.

The system was left to vibrate under these initial conditions for a few minutes before starting the experiments. This *relaxation time* was allowed the system to stabilize. The period T for 5 cycles was recorded and the value of Γ decreased by a small amount, usually of the order of $\Delta\Gamma = 0.02$.

The experimental results for a range of viscosities, particle sizes and driving frequencies are shown in figures 4.24 to 4.28. In these figures the dimen-

sionless ration A^*/δ is plotted as a function of Ω/ω , where Ω is the orbital angular velocity of the spheres. It can be observed that the rotation rates are symmetric for the clockwise and anticlockwise directions, this being an indication of a broken symmetry at the onset of the orbital motion. As A increases the orbital angular velocity, Ω , increases too. Eventually, a gap between the particles opens up at high rotation rates and the orbital motion becomes unstable soon after. The rotation data cannot be collapsed in a simple way because the introduction of an orbital time scale introduces an extra length scale $l = (\Omega/\nu)^{1/2}$. In other words, there are three ratios of lengths, A/d , δ/d and l/δ . It is more obvious for the cases were there is a gap between the spheres. However, when there is no visible gap, the experimental data still diverges with increasing Γ and only when the amplitude of vibration is close to the critical value for the onset of the instability that the data converges.

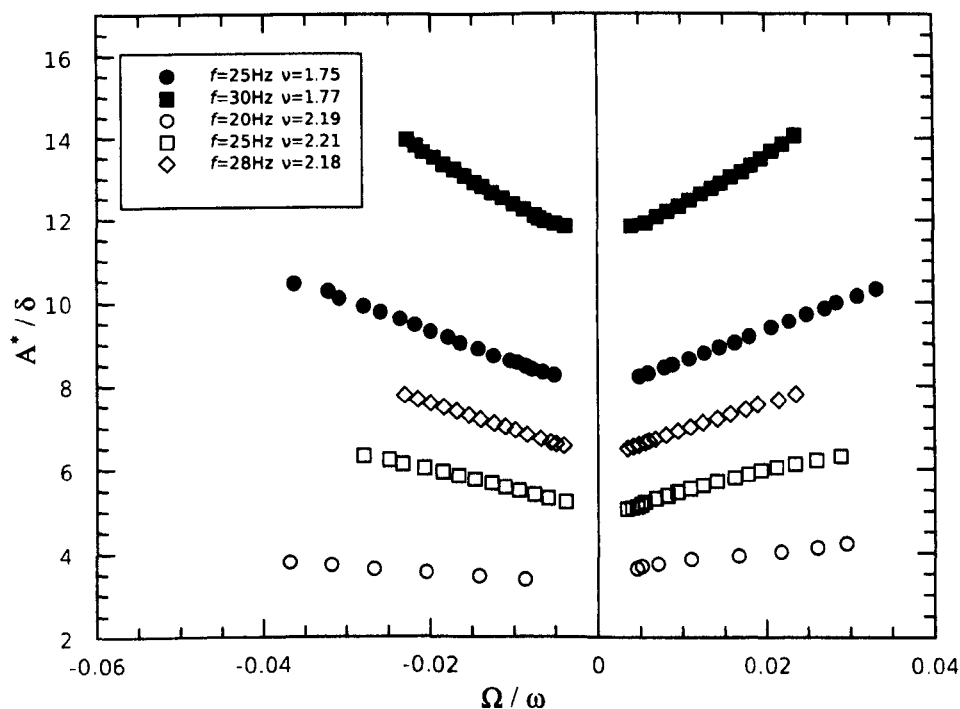


Fig. 4.24: Angular speeds measured for 1mm spheres when a gap is present.

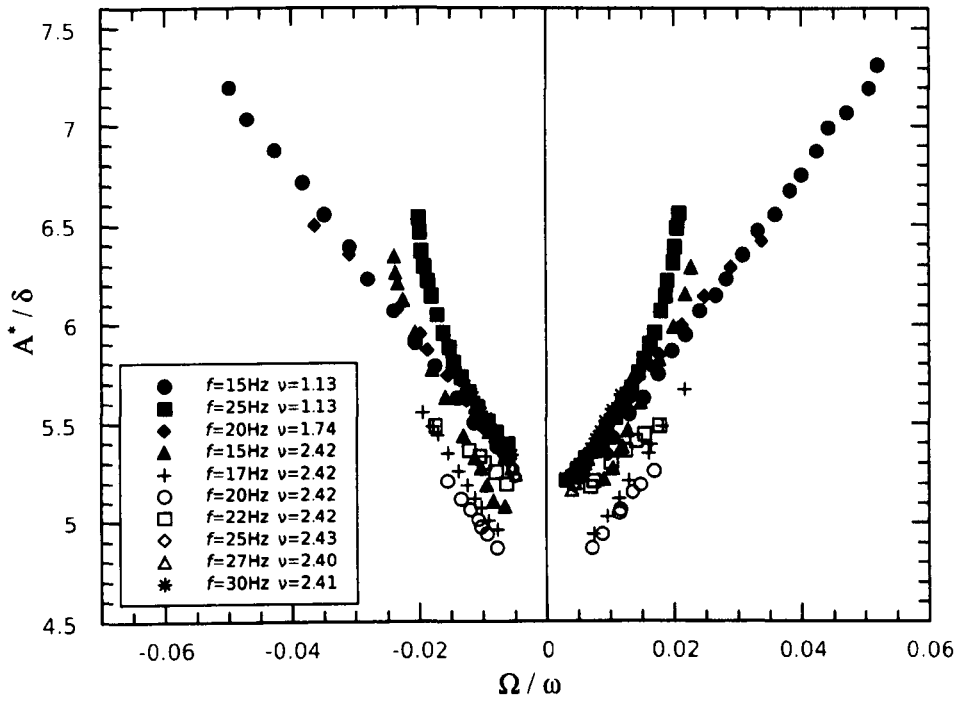


Fig. 4.25: Angular speeds measured for 1mm spheres when no gap is apparent.

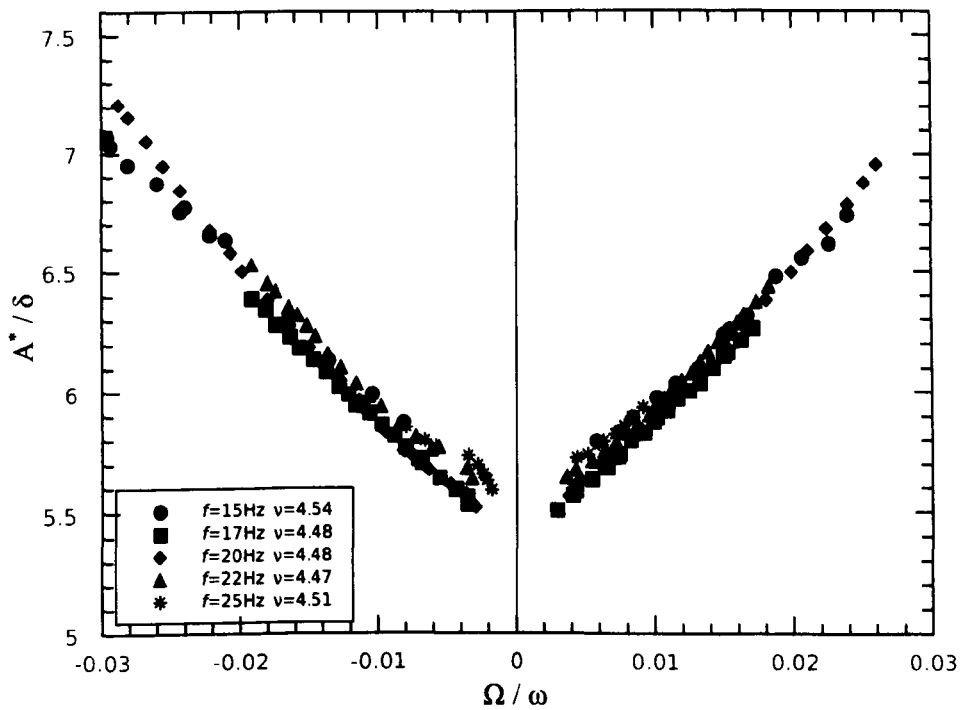


Fig. 4.26: Angular speeds measured for 2mm spheres in a viscous liquid. For this particular value of viscosity a gap do not develop over the values of amplitude an frequency explored.

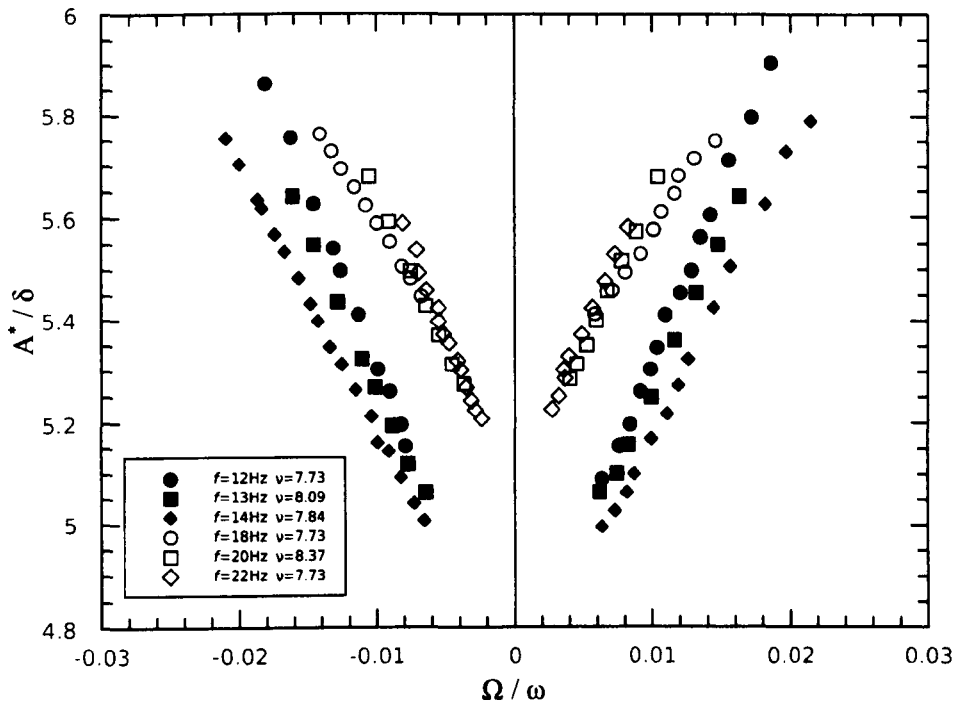


Fig. 4.27: Angular speeds for 2mm spheres. The apparition of a gap changes the scaling of the speeds.

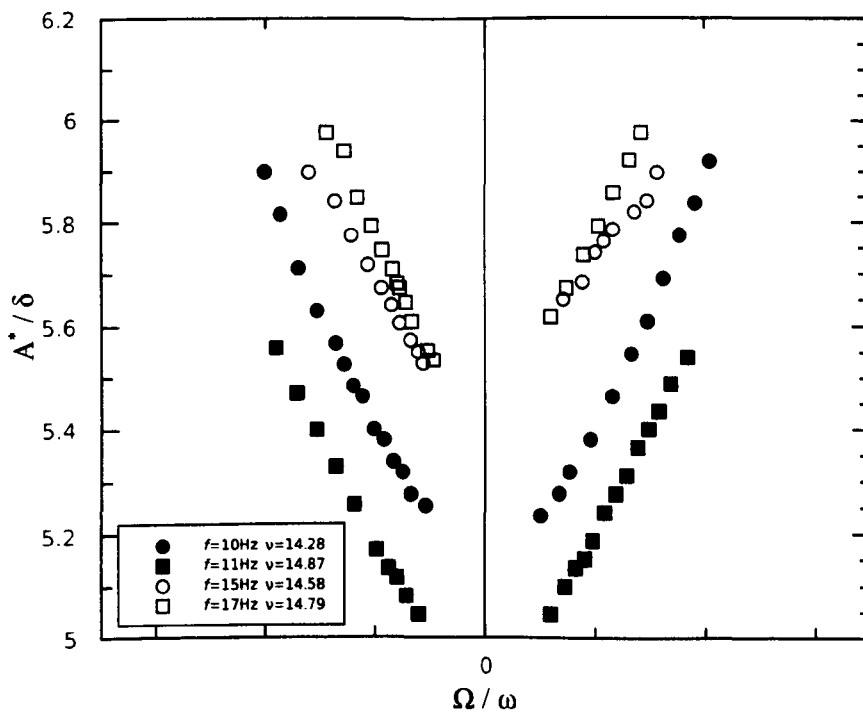


Fig. 4.28: Angular speeds for a pair of 3mm spheres. The same effect as 2mm 50 percent.

4.4.4 Streaming flow of levitated spheres

The onset of the instability and the symmetry of the speed of the orbital motion presented in the previous sections suggest that the phenomena observed in the system has its origin on hydrodynamic interactions; the streaming flows around the spheres should provide the driving forces causing the instability. To visualise the flows around two bismuth particles, bismuth powder was inserted into the cell. The powder levitates in the magnet at the same location as the bismuth spheres and, when the vibration is switched on, they follow the flow of the liquid around the spheres. Furthermore, bismuth powder has a high reflectivity which makes it a good material to use as tracer particles. The same technique could not be used in the experiments with glass spheres because bismuth and glass levitate under different magnetic field conditions.

The flows can be seen in figure 4.29. The image is a snapshot taken with a digital camera using long-time exposure. In this figure it is possible to observe the streaming flows induced by the vertical motion of the spheres relative to the fluid. However, the three-dimensional flow around the spheres cannot be visualised because of the confined space in the bore of the magnet.

In order to understand the streaming flows and the cause of the instability simulations based on the molecular-dynamics treatment of the particles coupled to a continuum, Navier-Stokes treatment of the fluid were carried out within our group. The details of the simulation method and its validation can be found in Klotsa *et al.* (2007) and Klotsa *et al.* (2009).

The simulations were performed using two different methods to excite the system. In the first method, the cell was vibrated and the response of the particles was recorded. In the second method, the particles were vibrated sinusoidally in a stationary container. Both methods yielded an onset of orbital

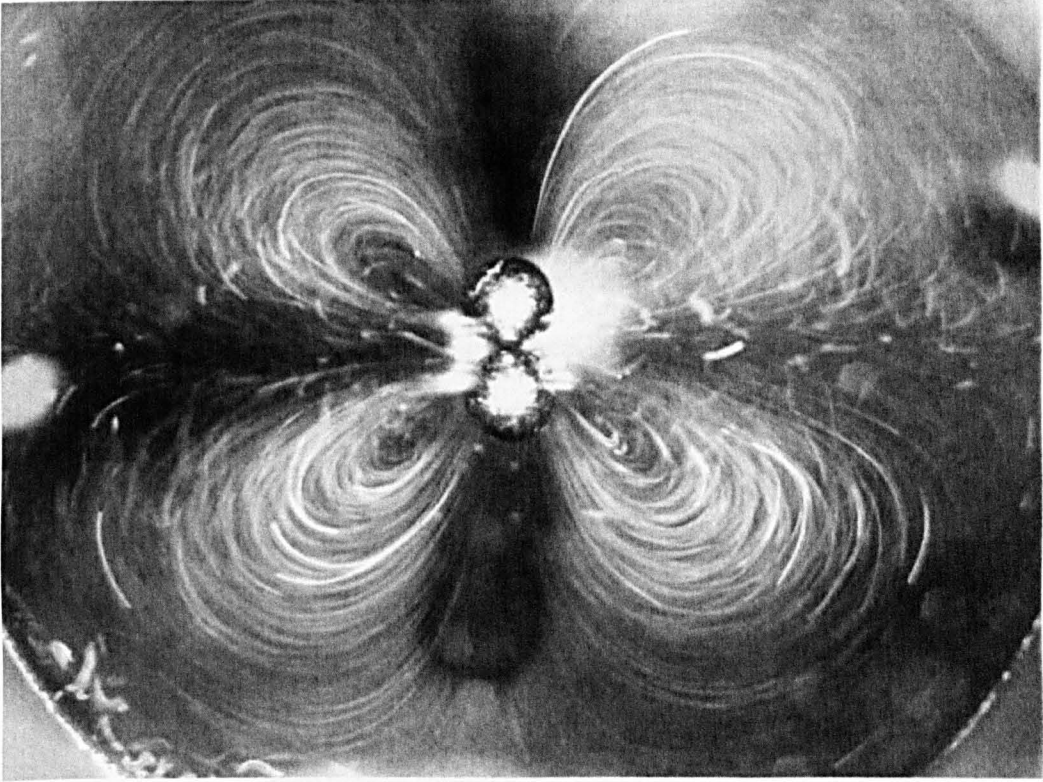


Fig. 4.29: Streaming flows for two bismuth spheres. The streaming flows in the plane containing the centres of the spheres can be observed. The image was taken using long-time exposure.

motion similar to that observed in the experiments.

The simulation parameters were chosen to match the experimental parameters as close as possible. The numerical noise was reduced by vibrating the particles in a static fluid. The amplitude of vibration of the particles relative to the fluid container was set to be a half of the driving amplitude used in the experiments.

The use of simulations allowed to investigate the full three-dimensional flow around the spheres and to determine the cause of the instability. The velocity field of the fluid flow was obtained and the curl of this field, the circulation, was calculated. The simulated flows are in good agreement with those found experimentally. In both experiment and simulation we observe that, in the

plane of the two spheres, there is an outward flow from the region between the two spheres and an inward flow elsewhere. This behaviour is completely different to that known for a single sphere where the equatorial flow is radially inward towards the sphere.

The streaming flows of a single sphere are shown in figure 4.30. On the left diagram, *Streamlines* have been drawn to show how the circulation forms closed loops at different positions around the sphere. The direction of the flows is obtained by using the right-hand rule in the same way as for current loops producing magnetic fields. For this case, the flow is away from the sphere and towards the sphere in the equatorial plane perpendicular to the direction of vibration. The equatorial flows are shown on the left diagram of figure 4.30

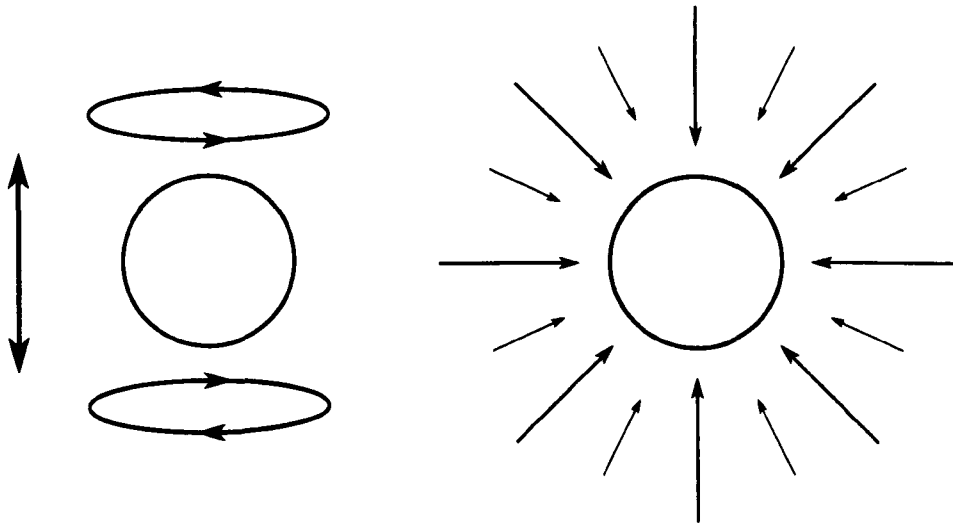


Fig. 4.30: Stream pattern for a single sphere. A single particle, as viewed from a direction perpendicular to the direction of motion, is shown on the left. The two rings are the stream lines of the flow which can be determined using the right hand rule. If the particle is vibrated vertically, the flow comes out from the top and the bottom of the sphere in the same direction of oscillation and returns towards the sphere in the plane horizontal plane containing the centre of the sphere. On the right side the same particle is depicted as viewed from above. The arrows point in the direction of the flow.

The streaming flows for two stationary spheres are shown in figure 4.31.

The circulation streamlines are sketched on the left diagram. Only three pairs of loops are shown for clarity. Above and below the spheres the flow is predominantly away from the spheres as in the case for a single sphere. Two side loops, one at the side of each sphere, indicate an inward flow at the outer point of the spheres. Note that this two loops connect the flow above and below the sphere. The small inner loops are responsible for the strong outward flow from the spheres. It is this complex vortex structure which gives rise to the strong outward, equatorial-plane flow from the gap between the spheres.

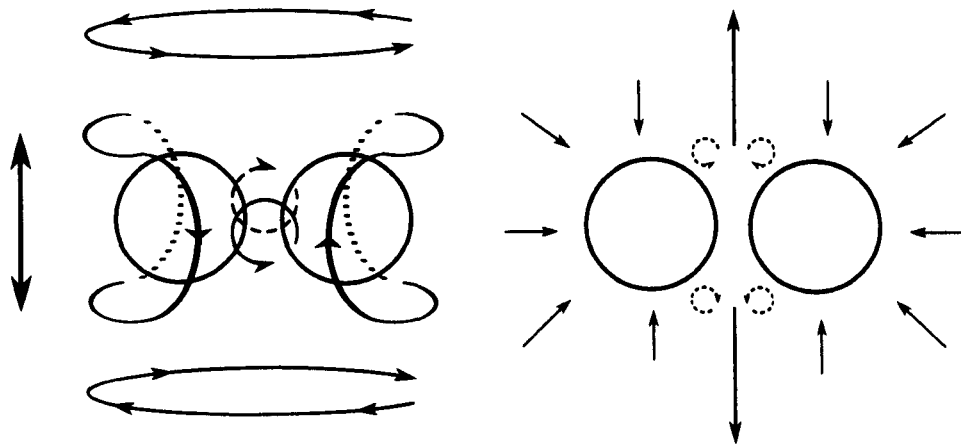


Fig. 4.31: Flow pattern for two spheres. A pair of spheres vibrating in the direction of the double arrow are shown in the image on the left. The outer streamlines, shown as the rings above and below the pair, resemble those observed in a single spheres which make a pair of spheres appear as a single particle from the distance. However, the steady streaming flow is more complex closer to the spheres. In the figure, two streamlines are shown. The flow associated with these streamlines can be observed in the image on the right which shows the pair of spheres as seen from the top. The steady streaming flow shown in this image occurs in the plane perpendicular to the direction of vibration that contains the centres of the particles. The flow comes out through the gap between the spheres and returns towards the particles elsewhere.

The equatorial fluid flow from simulation for the non-orbiting spheres at low amplitude is also shown in figure 4.31 (left diagram). When there is no orbital

motion the out flow in the equatorial plane emerges from the region between the spheres, as indicated by the arrows. The main flow is perpendicular to the line joining the centres of the spheres; there is symmetry in the flow pattern.

As the amplitude is increased the vortices generating the outward flow become unstable so that the outward flow is no longer perpendicular to the line through the centres of the spheres. The symmetry shown in figure 4.31(left) is broken resulting in the flow pattern shown in figure 4.32. It is the instability in the vortex structure which produces a net torque on the two spheres hence driving the orbital motion.

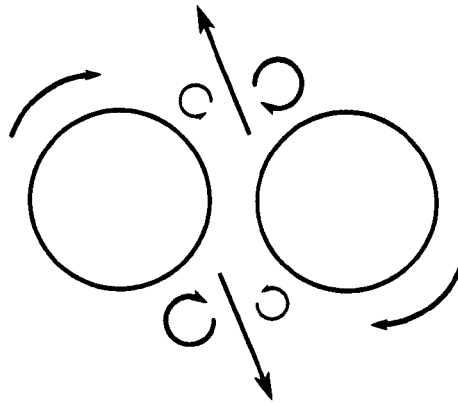


Fig. 4.32: Onset of orbital motion. The flows through the gap become unstable and provide the torque needed to spin the pair of spheres

4.5 Final Remarks

In this chapter the dynamics of spheres suspended in a fluid have been studied using magnetic levitation.

For a vibrating, single sphere, the amplitude of motion relative to the surrounding fluid was measured. It was found that, for the range of experimental parameters explored, the relative amplitude, A^* has a linear dependence on the real amplitude A . The main restriction to explore a wider range of parameters

was the limited space available inside the bore of the magnet which constricts the dimensions of the container.

When a pair of spheres were suspended in an oscillatory fluid flow, a novel hydrodynamic instability was observed. Under vertical vibration the spheres are attracted to each other and align perpendicularly to the axis of vibration. As the amplitude of vibration is increased the spheres were observed to break the cylindrical symmetry of the system by orbiting each other in the horizontal plane, either clockwise or anticlockwise. The parameters explored were the amplitude and frequency of vibration, the size of the particles and the viscosity of the fluid.

Simulations of the experimental system were also carried out within our Research Group. The simulations were found to reproduce the behaviour observed experimentally revealing the complex flow pattern responsible for the instability.

Chapter 5

Concluding Remarks

In the previous chapters, a description of the experimental studies carried out in three different granular systems were presented. In the present chapter, a review of the results of each study is given followed by suggestions for further studies.

5.1 Chapter review

Chapter 1 served as a general introduction to the field of Granular Matter. The ubiquitous presence of this type of materials in nature and industrial processes was underlined making emphasis on the important role they play in our everyday life. The introductory chapter was finished with the thesis outline describing the subjects that were to be discussed in the main body of the thesis.

Chapter 2 described the experimental and simulation results of our study of a vibrated monolayer of grains. The aim of this work was to determine if a two dimensional granular gas exhibits a long-range structure. To this end, the trajectories of single particles moving across a roughened surface

were characterised and the structure factor, $S(k)$, for a granular monolayer was measured experimentally. The chapter started with a review of previous studies focussing on the structural properties of granular gases. The current kinetic theories were introduced along with their predictions and we culminated with the introduction of the Random Force Model.

Our findings suggest that a collection of randomly-driven grains exhibit a behaviour that has not been reported before, namely, the existence of quasi long-range order. From our observations, a drag force is needed, along with the random force, to describe the trajectories of the particles and the features observed in the long-range structure of a 2-dimensional granular gas.

In **Chapter 3** we described the experimental work carried out to investigate some of the phenomena observed when a granular bed surrounded by fluid is subjected to vertical vibrations. In particular we studied the spontaneous migration of grains in a partitioned container and the influence of the presence of an incompressible fluid on the Brazil nut effect. The aim of these experiments was to provide a set of quantitative results to be compared with the predictions of the simulation models developed within our research group.

Our first aim was to investigate a new mechanism which can give rise to a spatial instability, namely, the interaction between fine grains and a background fluid. This process may be illustrated using a fluid immersed granular bed within a vertically-vibrating partitioned cell with two connecting holes, one at the top and one at the bottom of the cell. A gradual transfer of grains through the connecting hole at the base of the cell will result in the granular bed moving into just one of the columns.

From the experimental observations and the simulation results we proposed two mechanisms for the instability. Firstly, the resistance to fluid flow through

the bottom gap could be much bigger than the resistance through either bed. Under vibration each granular column is thrown independently and will develop an under-pressure proportional to its height. The pressure drop under the deeper bed early in flight will be greater than beneath the shallower bed causing grains to move in the direction of the deeper bed. Later in flight the changing pressure reduces the speed of the grains but it does not reverse the direction of grain motion. A second possibility is that the coupling between the two columns is such that the resistance to fluid flow through the lower hole is far less than that through either bed. Both columns experience a common under-pressure which can only be achieved if more fluid flows through the shallower bed rather than through the deeper bed. This fluid flow also transports grains towards the deeper granular column. Our results suggested that the migration of grains is the result of a greater flow of fluid through the shallower column of grains as the beds are thrown by the vibration.

In this chapter we also described an experimental study of the fluid-enhanced Brazil nut effect. This effect can be observed when the granular bed is fully immersed in a liquid. our experimental system consist of a bed of glass beads immersed in water and a large steel intruder. The motion of the steel intruder is closely monitored as the system is vibrated vertically. The experimental parameters are used to develop numerical simulations of this system to aid understanding of the rising mechanism. Our results showed that the intruder draws fluid and grains beneath it as it is thrown at the early stages of the cycle. Later in the cycle, the intruder lands on these particles increasing its vertical position. It is this fluid-enhanced ratcheting mechanism that causes the Brazil nut to rise rapidly through the bed.

Finally, in **chapter 4** we described a series of experiments aimed at study-

ing the behaviour of spherical grains immersed in an oscillatory fluid when the effects of gravity have been removed.

Making use of a 17T superconducting magnet we suspended grains in a fluid without the need of matching their densities to that of the surrounding liquid. This allows a relative motion between the fluid and the particles when their container is vibrated. Collections of grains with different properties were studied and many new behaviours were observed. For simplicity, our research focussed on the behaviour of a pair of identical spheres magnetically suspended on a viscous liquid. The observations shown an unexpected break of symmetry leading to orbital motion of the spheres. The onset of this break of symmetry was measured for different configurations. The results suggested that the effect is hydrodynamic. Streaming flows which result from the relative motion between spheres and fluid were shown to be behind the symmetry break causing the orbital motion.

5.2 Future Work

The results obtained in **Chapter 2** showed the existence of quasi long-range order in a randomly-driven granular monolayer. The particles in that system could be considered as self-propelled objects. This opens the possibility to explore systems of living organisms such as bacteria, flocks of birds or schools of fish and perhaps gain some insight on the way these collections living organisms organize.

The numerical simulation methods developed as a result of the work presented in **Chapter 3** do not make use of bed equations. As a result, they could be used to simulate systems where the current bed equations are not applicable such as systems with different species of grains or in systems were

there is a non-steady flow through the granular bed. Furthermore, the simulation techniques could be used as an independent method to test new bed equations.

The experimental technique described in **Chapter 4** opens the possibility to study a wider range of systems. For example, hydrodynamic interactions between particles are a known mechanism for inducing dynamic self-assembly. However, the current experiments are limited to two-dimensional ordering due to the presence of gravity on Earth. The current research considers either particles on a surface, confined between the interface of two immiscible liquids or suspended in the liquid by external means. The research on these systems could be enriched if the experiments were performed without the effects of gravity.

As an example, Wright *et al.* (2008) have studied the motion of asymmetric dimers in a horizontally-vibrated, fluid-filled, shallow cell. The dimers are observed to move in a direction perpendicular to the vibration with the smaller sphere at the front. However, when an asymmetric dimer is magnetically levitated using the technique described in this chapter, the trajectory of the dimer appeared to be a circumference contained in a plane perpendicular to the direction in which the vibration is applied. Furthermore, the orientation of the dimer is also different, with the smaller sphere now following the bigger one.

Appendix A

Magnetic Levitation

In this appendix we present a brief introduction to magnetic levitation, a technique that will be used in the experiments described in this chapter in the hope to observe the behaviour of particles suspended in an oscillatory fluid.

A.1 Magnetostatics

An external magnetic field produces a reaction upon any material. A magnetic field \mathbf{H} applied to a material will induce a magnetization \mathbf{M} . The direction and magnitude of \mathbf{M} depend upon the properties of the media and the applied magnetic field. In the simple situation of a linear, homogeneous and isotropic medium, the relation between \mathbf{H} and \mathbf{M} is given by the expression

$$\mathbf{M} = \chi\mathbf{H}, \quad (\text{A.1})$$

where χ is the dimensionless magnetic susceptibility of the medium. However, equation A.1 is only applicable to media that exhibit weak magnetism, this is, materials with $\chi \ll 1$. For the case of media with stronger magnetic properties, the susceptibility may depend upon the applied field.

The electromagnetic theory can be summarised with the Maxwell's equations. For magnetostatic problems, the relevant equations are

$$\nabla \times \mathbf{B} = \mu_0 \mathbf{J}, \quad (\text{A.2})$$

$$\nabla \cdot \mathbf{B} = 0, \quad (\text{A.3})$$

$$\nabla \cdot \mathbf{D} = \rho, \quad (\text{A.4})$$

where \mathbf{B} represents the magnetic flux density, \mathbf{J} is the current density, $\mu_0 = 4\pi \times 10^{-7} \text{V s}/(\text{A m})$ is the permeability of free space, \mathbf{D} is the electric displacement field and ρ is the total volume charge density. Equation A.2 allows the calculation of the magnetic field generated by an electric current. In the absence of currents, or in free space, the equation reduces to $\nabla \times \mathbf{B} = 0$. Equation A.3 states that there are no magnetic monopoles, since \mathbf{B} has no divergence. The unit of \mathbf{B} is T (Tesla), and $1\text{T} = 1\text{N A}^{-1} \text{m}^{-1}$.

In a magnetic solid we can relate the magnetic flux density \mathbf{B} to \mathbf{H} and \mathbf{M} as follows

$$\mathbf{B} = \mu_0(\mathbf{H} + \mathbf{M}). \quad (\text{A.5})$$

For weak magnetic materials, \mathbf{B} can be expressed as a function of \mathbf{H} if equation A.1 is substituted into equation A.5, giving

$$\mathbf{B} = \mu_0(1 + \chi)\mathbf{H} = \mu_0\mu_r\mathbf{H}, \quad (\text{A.6})$$

where $\mu_t = (1 + \chi)$ is the relative magnetic permeability of the material.

Traditionally, \mathbf{H} is referred to as the *magnetic field strength*, while \mathbf{B} is referred to as the *magnetic induction* or *magnetic flux density*. In vacuum, where $\mathbf{B} = \mu_0\mathbf{H}$, and in weak magnetic media such as the ones we will be working in, both vectorial magnitudes (\mathbf{B} and \mathbf{H}) are equivalent. Authors generally distinguish between \mathbf{B} and \mathbf{H} when working with strong magnetic

media, where the equations A.1 and A.6 are no longer valid. Since both quantities are proportional in the systems we work with, we will refer to both of them as the magnetic field. In general, and from now on, we will work with **B**.

A.2 Types of Magnetism

Depending on the way materials react to the application of an external magnetic field they can be classified as ferromagnetic, paramagnetic or diamagnetic materials.

The more commonly observed form of magnetism, observed in everyday life, is ferromagnetism. As a loose definition we can state that ferromagnetic materials present spontaneous magnetization even in the absence of external magnetic fields. Generally, the magnetic susceptibility of a ferromagnetic material depends on the magnetic field applied and the equations A.1 and A.6 are not applicable to describe their magnetization. Ferromagnets present hysteresis and, once the external field is removed, they are able to retain a certain degree of magnetization. Ferromagnetic materials are characterised by the Curie temperature, above of which their magnetic susceptibility becomes independent of the magnetic field applied and the equations mentioned earlier can be applied.

A paramagnetic material will only manifest its magnetic properties if it is under the presence of an external magnetic field. A material will be classified as paramagnetic if there are unpaired electrons within its atomic or molecular orbitals. These unpaired electrons act as permanent dipole magnetic moments. However, because these permanent moments tend to point in random direction due to thermal agitation, a paramagnetic material will not present any net

magnetization unless an external field is applied. When an external magnetic field is applied, the moments will tend to align themselves parallel to the magnetic field. Hence, paramagnetic materials have positive susceptibilities.

The susceptibility of paramagnetic materials depend upon the temperature and, at low magnetic fields, follows

$$\chi = \frac{C}{T}. \quad (\text{A.7})$$

This relationship is known as Curie's law and C is known as the Curie constant. When sufficiently high magnetic fields are applied, the magnetization tend to a constant value. It is then said that the material has reached its saturation point and cannot be magnetized any further since all its magnetic moments are aligned parallel to the external field and Curie's law is no longer valid.

As in the case of paramagnetism, diamagnetism is only exhibited in the presence of an external magnetic field. This is the weakest type of magnetism and it can be observed in all substances provided that they are exposed to a strong magnetic field. If a material exhibits paramagnetic or ferromagnetic tendencies, these will mask any diamagnetic behaviour. The origin of diamagnetism lies in the interaction between the electronic orbitals and the external magnetic field. According to Lenz's law, the presence of an external magnetic field acting on the electronic orbit of a single atom will cause the appearance of an electromotive force (e.m.f) and, as a result, a magnetic moment will be produce to oppose the external field. In other words, the magnetization of diamagnetic substances opposes the direction of the applied field, which means that $\chi < 0$ for diamagnetic materials.

Earnshaw's theorem states that no stationary object made of charges, magnets and masses can be held in space by any fixed combination of electric magnetic and gravitational forces. However, it does not apply to diamagnetic

materials since the magnetisation is induced by the external field and stable levitation is possible as it will be shown in the next section.

Common materials which are usually regarded as not having any kind of magnetic property are actually diamagnetic; water, NaCl, pure silicon, wood, paper and glass are examples of diamagnetic materials. The highest diamagnetic susceptibility is exhibited by bismuth with $\chi = -165 \times 10^{-6}$.

A.3 Diamagnetic levitation

As mentioned before, diamagnetic objects can be levitated when an appropriate vertical inhomogeneous magnetic field is applied. Let us consider a diamagnetic body of susceptibility χ , density ρ and volume V , placed at a position $\mathbf{r} = (x, y, z)$ where a magnetic field $\mathbf{B}(\mathbf{r})$ of magnitude B is being applied. Here, z will determine the vertical position, while x and y give the horizontal coordinates. Under such circumstances, the body achieves an induced magnetic dipole moment, $\mathbf{m} = \int \mathbf{M} dV$, given to a good approximation by

$$\mathbf{m}(\mathbf{r}) = \frac{\chi V \mathbf{B}(\mathbf{r})}{\mu_0}. \quad (\text{A.8})$$

By integrating the work $-d\mathbf{m} \cdot \mathbf{B}$ as the field is increased from zero to $\mathbf{B}(\mathbf{r})$, the total magnetic energy of the object can be obtained. If we also consider the presence of Earth's gravitational field, the total energy $E(\mathbf{r})$ of the body will be determined by

$$E(\mathbf{r}) = \rho V g z - \frac{\chi V}{2\mu_0} B(\mathbf{r})^2, \quad (\text{A.9})$$

where g is the magnitude Earth's gravitational acceleration ($g=9.81 \text{ m s}^{-2}$).

The object will float in equilibrium if the total vertical force vanishes. Thus

$$F_z = -\frac{\partial E(\mathbf{r})}{\partial z} = -\rho V g + \frac{\chi V}{2\mu_0} \frac{\partial B(\mathbf{r})^2}{\partial z} = 0. \quad (\text{A.10})$$

In our experiments the solenoid coils of the levitation magnet generates a field with rotational symmetry around the vertical axis z . Thus, if the object is considered to be placed on the vertical axis, the previous equilibrium condition can be written as

$$B(z) \frac{\partial B(z)}{\partial z} = \frac{\rho g \mu_0}{\chi}, \tag{A.11}$$

where we have written the field dependence as $B(z)$, ignoring the variation in the radial direction, given by x and y . In figure A.1 we can observe the forces acting on a levitated diamagnetic object.

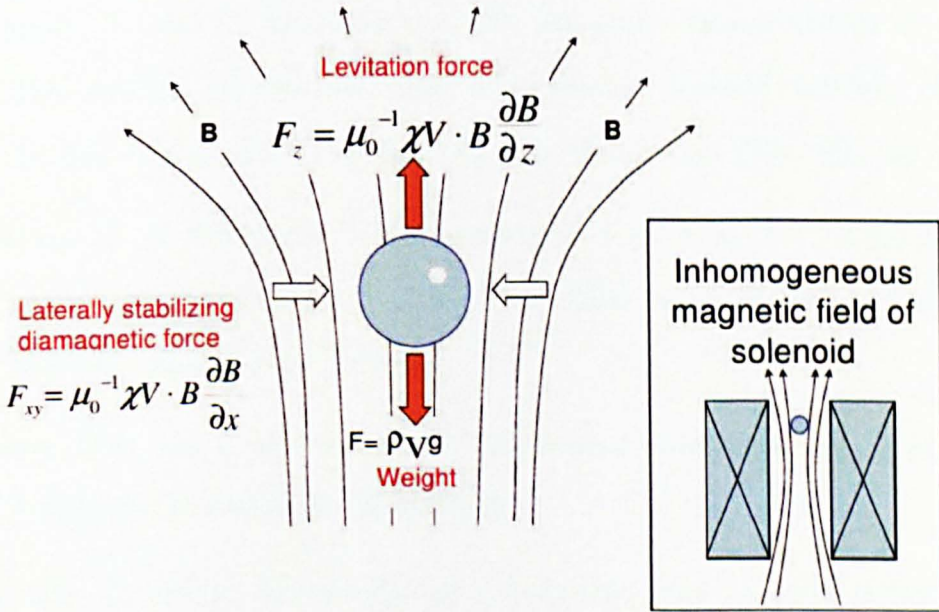


Fig. A.1: Schematic representation of the forces acting on an object levitating within an inhomogeneous magnetic field due to diamagnetic repulsion. The inset shows the position of the object with respect to the solenoid. The weight is balanced by the levitation force F_z but the lateral forces F_{xy} , indicated by the horizontal arrows, are essential to stabilize the object.

As a concept, diamagnetic levitation has been known since the times of Lord Kelvin but it was not until recently that it could be observed in the laboratory (Beaugnon and Tournier, 1991) when the technology to produce

the strong magnetic fields with large field-field gradient product required to produce levitation became available. More recent studies have made use of the so called magneto-Archimedes effect to separate minerals (Catherall *et al.*, 2005; Catherall *et al.*, 2007 and Lopez-Alcaraz *et al.*, 2007). These experiments introduced the technique of diamagnetic levitation to the study of granular materials.

Bibliography

- Akiyama, T. and T. Shimomura (1991). Investigation of wall shear stress in vibrating particle beds. *Powder technology* 66(3), 243-247.
- Akiyama, T. and T. Shimomura (1993, January). Measurements of wall shear stress in particle beds when vibrations are imposed vertically along the direction of shear. *Advanced Powder Technology* 4(2), 129-142.
- Akiyama, T., K. Shinmura, S. Murakawa, and K. M. Aoki (2001, August). A surface instability of granules under vibration in partitioned containers. *Granular Matter* 3(3), 177-183.
- Alassar, R. S. and H. M. Badr (1997). Oscillating viscous flow over a sphere. *Computers & Fluids* 26(7), 661-682.
- Andrade, E. (1931). Phenomena in a sounding tube. *Nature* 127(3203), 438-438.
- Andrade, E. and D. Smith (1931). The method of formation of sand figures on a vibrating plate. *Proceedings of the Physical Society* 43(3), 405-411.
- Anghel, D.-V., M. Strauss, S. McNamara, E. Flekkoy, and K. Maloy (2006, August). Erratum: Grains and gas flow: Molecular dynamics with hydrodynamic interactions [Phys. Rev. E 61, 4054 (2000)]. *Physical Review E* 74(2), 134302.

- Aranson, I. and L. Tsimring (2006, June). Patterns and collective behavior in granular media: Theoretical concepts. *Reviews of Modern Physics* 78(2), 641–692.
- Barrat, A., T. Biben, Z. Racz, and E. Trizac (2002). On the velocity distributions of the one-dimensional inelastic gas. *Journal of Physics A* 35, 463.
- Barrat, A. and E. Trizac (2003a). A molecular dynamics ‘Maxwell Demon’ experiment for granular mixtures. *Molecular Physics* 101(11), 1713–1719.
- Barrat, A. and E. Trizac (2003b, May). Random inelasticity and velocity fluctuations in a driven granular gas. *The European physical journal. E. Soft matter* 11(1), 99–104.
- Barrat, A., E. Trizac, and M. H. Ernst (2005, June). Granular gases: dynamics and collective effects. *Journal of Physics: Condensed Matter* 17(24), S2429–S2437.
- Beaugnon, E. and R. Tournier (1991). Levitation of organic materials. *Nature* 349(6309), 470–470.
- Belkin, M., A. Glatz, A. Snezhko, and I. Aranson (2010, July). Model for dynamic self-assembled magnetic surface structures. *Physical Review E* 82(1), 015301.
- Belkin, M., A. Snezhko, I. Aranson, and W.-K. Kwok (2009, July). Magnetically driven surface mixing. *Physical Review E* 80(1), 011310.
- Ben-Naim, E., S. Chen, G. Doolen, and S. Redner (1999, November). Shock-like Dynamics of Inelastic Gases. *Physical Review Letters* 83(20), 4069–4072.

- Ben-Naim, E. and P. Krapivsky (2000). Multiscaling in inelastic collisions. *Physical Review E* 61(1), R5.
- Ben-Naim, E., B. Machta, and J. Machta (2005, August). Power-law velocity distributions in granular gases. *Physical Review E* 72(2), 021302.
- Beysens, D., D. Chatain, P. Evesque, and Y. Garrabos (2008, May). Nucleation and growth of a bubble pattern under vibrations in weightlessness. *EPL (Europhysics Letters)* 82(3), 36003.
- Biswas, P., P. Sánchez, M. R. Swift, and P. King (2003, November). Numerical simulations of air-driven granular separation. *Physical Review E* 68(5), 050301.
- Blair, D. and A. Kudrolli (2001, October). Velocity correlations in dense granular gases. *Physical Review E* 64(5), 050301.
- Blair, D. and A. Kudrolli (2003a, February). Clustering transitions in vibrofluidized magnetized granular materials. *Physical Review E* 67(2), 021302.
- Blair, D. and A. Kudrolli (2003b, April). Collision statistics of driven granular materials. *Physical Review E* 67(4), 041301.
- Bordallo-Favela, R., A. Ramirez-Saito, C. Pacheco-Molina, J. Perera-Burgos, Y. Nahmad-Molinari, and G. Perez-Angel (2009, April). Effective potentials of dissipative hard spheres in granular matter. *The European physical journal. E, Soft matter* 28(4), 395–400.
- Bray, D., M. R. Swift, and P. King (2007, June). Velocity statistics in dissipative, dense granular media. *Physical Review E* 75(6), 062301.
- Brilliantov, N., C. Salueña, T. Schwager, and T. Pöschel (2004, September). Transient Structures in a Granular Gas. *Physical Review Letters* 93(13).

- Brinkman, H. (1947). A CALCULATION OF THE VISCOUS FORCE EXERTED BY A FLOWING FLUID ON A DENSE SWARM OF PARTICLES. *Applied scientific research. Section A* 1(1), 27–34.
- Burtally, N., P. King, and M. R. Swift (2002, March). Spontaneous air-driven separation in vertically vibrated fine granular mixtures. *Science (New York, N.Y.)* 295(5561), 1877–9.
- Catherall, A. T., P. López-Alcaraz, P. Sánchez, M. R. Swift, and P. King (2005, February). Separation of binary granular mixtures under vibration and differential magnetic levitation force. *Physical Review E* 71(2), 021303.
- Chen, W. and R. Wei (1998). A capillarity-like phenomenon in granular material under vertical vibration. *Physics Letters A* 244(5), 389–393.
- Cheng, N. (2008). Formula for the viscosity of a glycerol-water mixture. *Industrial & Engineering Chemistry Research* 47, 3285–3288.
- Ciamarra, M. P., A. Coniglio, and M. Nicodemi (2007, March). Phenomenology and theory of horizontally oscillated granular mixtures. *The European physical journal. E, Soft matter* 22(3), 227–234.
- Clement, C. P., H. A. Pacheco-Martinez, M. R. Swift, and P. King (2009, July). Partition instability in water-immersed granular systems. *Physical Review E* 80(1), 011311.
- Clement, C. P., H. A. Pacheco-Martinez, M. R. Swift, and P. King (2010, September). The water-enhanced Brazil nut effect. *EPL (Europhysics Letters)* 91(5), 54001.
- Clément, E., F. Malloggi, B. Andreotti, and I. S. Aranson (2007, August). Erosive granular avalanches: a cross confrontation between theory and

- experiment. *Granular Matter* 10(1), 3–11.
- Cody, G., D. Goldfarb, G. Storch, and A. Norris (1996). Particle granular temperature in gas fluidized beds. *Powder Technology* 87, 211–232.
- Coimbra, C. F. M., D. Lesperance, R. a. Lambert, J. D. Trolinger, and R. H. Rangel (2004, April). An experimental study on stationary history effects in high-frequency Stokes flows. *Journal of Fluid Mechanics* 504, 353–363.
- Cooke, W., S. Warr, J. Huntley, and R. Ball (1996). Particle size segregation in a two-dimensional bed undergoing vertical vibration. *Physical Review E* 53(3), 2812.
- Darias, J. R., I. Sánchez, and G. Gutiérrez (2010, September). Experimental study on the vertical motion of grains in a vibrated U-tube. *Granular Matter* 13(1), 13–17.
- Eggers, J. (1999). Sand as Maxwell's demon. *Physical Review Letters* 83(25), 5322–5325.
- Ennis, B., J. Green, and R. Davies (1994). The Legacy of neglect in the United-States. *Chemical engineering progress* 90(4), 32 – 43.
- Ergun, S. (1952). Fluid Flow Through Packed Columns. *Chemical engineering progress* 48(2), 89 –94.
- Eshuis, P., D. van der Meer, M. Alam, H. J. van Gerner, K. van der Weele, and D. Lohse (2010, January). Onset of Convection in Strongly Shaken Granular Matter. *Physical Review Letters* 104(3), 038001.
- Eshuis, P., K. van der Weele, D. van der Meer, and D. Lohse (2005, December). Granular Leidenfrost Effect: Experiment and Theory of Floating Particle Clusters. *Physical Review Letters* 95(25), 258001.

- Forchheimer, P. (1901). Water movement through the ground. *Zeitschrift des Vereines Deutscher Ingenieure* 45, 1781–1788.
- Gallas, J. A. C., H. Herrmann, T. Poschel, and S. Sokolowski (1996, January). Molecular dynamics simulation of size segregation in three dimensions. *Journal of Statistical Physics* 82(1-2), 443–450.
- Geng, J., E. Longhi, R. Behringer, and D. Howell (2001, November). Memory in two-dimensional heap experiments. *Physical Review E* 64(6), 060301.
- Goldhirsch, I. and G. Zanetti (1993). Clustering instability in dissipative gases. *Physical review letters* 70(11), 1619–1622.
- Gondret, P., M. Lance, and L. Petit (2002). Bouncing motion of spherical particles in fluids. *Physics of Fluids* 14(2), 643.
- Haff, P. (1983). Grain flow as a fluid-mechanical phenomenon. *Journal of Fluid Mechanics* 134, 401–30.
- Harwood, C. (1977). Powder segregation due to vibration. *Powder Technology* 16, 51–57.
- Herrmann, H. and S. Luding (1998, August). Modeling granular media on the computer. *Continuum Mechanics and Thermodynamics* 10(4), 189–231.
- Herrmann, H., S. Luding, and R. Caferio (2001, June). Dynamics of granular systems. *Physica A: Statistical Mechanics and its Applications* 295(1-2), 93–100.
- Hou, M., H. Tu, R. Liu, Y. Li, K. Lu, P.-Y. Lai, and C. Chan (2008, February). Temperature Oscillations in a Compartmentalized Bidisperse Granular Gas. *Physical Review Letters* 100(6), 068001.

- Huerta, D., V. Sosa, M. Vargas, and J. Ruiz-Suarez (2005, September). Archimedes principle in fluidized granular systems. *Physical Review E* 72(3), 031307.
- Jaeger, H., S. Nagel, and R. Behringer (1996). Granular solids, liquids, and gases. *Reviews of Modern Physics* 68(4), 1259–1273.
- Kang, W., J. Machta, and E. Ben-Naim (2010, August). Granular gases under extreme driving. *EPL (Europhysics Letters)* 91(3), 34002.
- Khain, E. and I. Aranson (2011, September). Hydrodynamics of a vibrated granular monolayer. *Physical Review E* 84(3), 031308.
- King, P., P. Lopez-Alcaraz, H. A. Pacheco-Martinez, C. P. Clement, A. J. Smith, and M. R. Swift (2007, March). Instabilities in vertically vibrated fluid-grain systems. *The European physical journal. E, Soft matter* 22(3), 219–26.
- Klotsa, D., M. R. Swift, R. M. Bowley, and P. King (2007, November). Interaction of spheres in oscillatory fluid flows. *Physical Review E* 76(5), 056314.
- Klotsa, D., M. R. Swift, R. M. Bowley, and P. King (2009, February). Chain formation of spheres in oscillatory fluid flows. *Physical Review E* 79(2), 021302.
- Knight, J. B., H. Jaeger, and S. Nagel (1993). Vibration-Induced Size Separation in Granular Media: The Convection Connection. *Physical review letters* 70(24), 3728–3731.
- Kohlstedt, K., A. Snezhko, M. Sapozhnikov, I. Aranson, J. Olafsen, and E. Ben-Naim (2005, August). Velocity Distributions of Granular Gases

- with Drag and with Long-Range Interactions. *Physical Review Letters* 95(6), 068001.
- Kotas, C. W., M. Yoda, and P. H. Rogers (2006, October). Visualization of steady streaming near oscillating spheroids. *Experiments in Fluids* 42(1), 111–121.
- Kudrolli, A. (2004, March). Size separation in vibrated granular matter. *Reports on Progress in Physics* 67(3), 209–247.
- Kuwabara, G. and K. Kono (1987, August). Restitution Coefficient in a Collision between Two Spheres. *Japanese Journal of Applied Physics* 26(Part 1, No. 8), 1230–1233.
- Lambiotte, R., J. Salazar, and L. Brenig (2005, August). From particle segregation to the granular clock. *Physics Letters A* 343(1-3), 224–230.
- Lane, C. A. (1955, November). Acoustical Streaming in the Vicinity of a Sphere. *The Journal of the Acoustical Society of America* 27(6), 1082.
- Leaper, M., A. J. Smith, M. R. Swift, P. King, H. E. Webster, N. Miles, and S. W. Kingman (2005, March). The behaviour of water-immersed glass-bronze particulate systems under vertical vibration. *Granular Matter* 7(2-3), 57–67.
- López-Alcaraz, P., A. T. Catherall, R. J. A. Hill, M. Leaper, M. R. Swift, and P. King (2007, October). Magneto-vibratory separation of glass and bronze granular mixtures immersed in a paramagnetic liquid. *The European physical journal. E, Soft matter* 24(2), 145–56.
- Maeno, Y. (1996). Numerical investigation of surface level instability due to a tube in a vibrating bed of powder. *Physica A: Statistical Mechanics and its Applications* 232(1), 27–39.

- Manna, S. (1999, August). Externally driven granular systems. *Physica A: Statistical Mechanics and its Applications* 270(1-2), 105–114.
- McNamara, S., E. Flekkoy, and K. Maloy (2000, April). Grains and gas flow: molecular dynamics with hydrodynamic interactions. *Physical review. E, Statistical physics, plasmas, fluids, and related interdisciplinary topics* 61(4 Pt B), 4054–9.
- McNamara, S. and M. Mareschal (2001, October). Origin of the hydrodynamic Lyapunov modes. *Physical Review E* 64(5), 051103.
- McNamara, S., P. Richard, S. de Richter, G. Le Caër, and R. Delannay (2009, September). Measurement of granular entropy. *Physical Review E* 80(3), 031301.
- McNamara, S. and W. Young (1994). Inelastic collapse in two dimensions. *Physical Review E* 50(1), R28–31.
- Mei, R. (2006, April). Flow due to an oscillating sphere and an expression for unsteady drag on the sphere at finite Reynolds number. *Journal of Fluid Mechanics* 270(-1), 133.
- Melby, P., F. Reyes, A. Prevost, R. Robertson, P. Kumar, D. A. Egolf, and J. S. Urbach (2005, June). The dynamics of thin vibrated granular layers. *Journal of Physics: Condensed Matter* 17(24), S2689–S2704.
- Michele, J., R. Patzold, and R. Donis (1977, May). Alignment and aggregation effects in suspensions of spheres in non-Newtonian media. *Rheologica Acta* 16(3), 317–321.
- Mikkelsen, R., D. van der Meer, K. van der Weele, and D. Lohse (2002, November). Competitive Clustering in a Bidisperse Granular Gas. *Physical Review Letters* 89(21), 214301.

- Milburn, R., M. Naylor, A. J. Smith, M. Leaper, K. Good, M. R. Swift, and P. King (2005, January). Faraday tilting of water-immersed granular beds. *Physical Review E* 71(1), 011308.
- Mobius, M., B. Lauderdale, S. Nagel, and H. Jaeger (2001, November). Size separation of granular particles. *Nature* 414(6861), 270.
- Moon, S., M. Shattuck, and J. Swift (2001, August). Velocity distributions and correlations in homogeneously heated granular media. *Physical Review E* 64(3), 031303.
- Naylor, M., M. R. Swift, and P. King (2003, July). Air-driven Brazil nut effect. *Physical Review E* 68(1), 012301.
- Nerone, N., M. Aguirre, A. Calvo, I. Ippolito, and D. Bideau (2000). Surface fluctuations in a slowly driven granular system. *Physica A: Statistical Mechanics and its Applications* 283(1), 218–222.
- Ohtsuki, T., D. Kinoshita, Y. Nakada, and A. Hayashi (1998). Surface level migration in vibrating beds of cohesionless granular materials. *Physical Review E* 58(6), 7650.
- Olafsen, J. and J. Urbach (1998). Clustering, order, and collapse in a driven granular monolayer. *Physical review letters* 81(20), 4369–4372.
- Olafsen, J. and J. Urbach (1999, September). Velocity distributions and density fluctuations in a granular gas. *Physical review. E, Statistical physics, plasmas, fluids, and related interdisciplinary topics* 60(3), R2468–71.
- Olafsen, J. and J. Urbach (2005, August). Two-Dimensional Melting Far from Equilibrium in a Granular Monolayer. *Physical Review Letters* 95(9), 098002.
- Onoda, G. Y. and E. G. Liniger (1990). Random Loose Packings of Uniform

- Spheres and the Dilatancy Onset. *Physical review letters* 64(22), 2727–2730.
- Otto, F., E. K. Riegler, and G. Voth (2008). Measurements of the steady streaming flow around oscillating spheres using three dimensional particle tracking velocimetry. *Physics of Fluids* 20(9), 093304.
- Pacheco-Vazquez, F., G. Caballero-Robledo, and J. Ruiz-Suarez (2009, April). Superheating in Granular Matter. *Physical Review Letters* 102(17), 170601.
- Pak, H., E. Van Doorn, and R. Behringer (1995). Effects of ambient gases on granular materials under vertical vibration. *Physical review letters* 74(23), 4643–4646.
- Peng, G. and T. Ohta (1998a, August). Scaling and Correlations in Heated Granular Materials. *Journal of the Physics Society Japan* 67(8), 2561–2564.
- Peng, G. and T. Ohta (1998b). Steady state properties of a driven granular medium. *Physical Review E* 58(4), 4737–4746.
- Perera-Burgos, J., G. Perez-Angel, and Y. Nahmad-Molinari (2010, November). Diffusivity and weak clustering in a quasi-two-dimensional granular gas. *Physical Review E* 82(5), 051305.
- Perez-Angel, G. and Y. Nahmad-Molinari (2011, October). Bouncing, rolling, energy flows, and cluster formation in a two-dimensional vibrated granular gas. *Physical Review E* 84(4), 041303.
- Petit, L. and P. Gondret (1992). Rectification Of An Alternating Flow. *Journal de physique. II* 2(12), 2115–2144.

- Poschel, T. and H. Herrmann (1995, January). Size Segregation and Convection. *Europhysics Letters (EPL)* 29(2), 123–128.
- Puglisi, A., A. Baldassarri, and V. Loreto (2002, December). Fluctuation-dissipation relations in driven granular gases. *Physical Review E* 66(6), 061305.
- Puglisi, A., V. Loreto, U. Marconi, and A. Petri (1998). Clustering and non-gaussian behavior in granular matter. *Physical review letters* 81(18), 3848.
- Puglisi, A., V. Loreto, U. Marconi, and A. Vulpiani (1999, May). Kinetic approach to granular gases. *Physical review. E, Statistical physics, plasmas, fluids, and related interdisciplinary topics* 59(5 Pt B), 5582–95.
- Ratkai, G. (1976). Particle flow and mixing in vertically vibrated beds. *Powder Technology* 15, 187–192.
- Raux, P., P. Reis, J. Bush, and C. Clanet (2010, July). Rolling Ribbons. *Physical Review Letters* 105(4), 044301.
- Reis, P., R. Ingale, and M. Shattuck (2006, June). Crystallization of a Quasi-Two-Dimensional Granular Fluid. *Physical Review Letters* 96(25), 258001.
- Reis, P., R. Ingale, and M. Shattuck (2007, May). Forcing independent velocity distributions in an experimental granular fluid. *Physical Review E* 75(5), 051311.
- Reis, P. and M. Shattuck (2007, April). Caging Dynamics in a Granular Fluid. *Physical review letters* 98(18), 188301.
- Reis, P., T. Sykes, and T. Mullin (2006, November). Phases of granular segregation in a binary mixture. *Physical Review E* 74(5), 051306.

- Reyes, F. and J. S. Urbach (2008, November). Effect of inelasticity on the phase transitions of a thin vibrated granular layer. *Physical Review E* 78(5), 051301.
- Riley, N. (1966). On a sphere oscillating in a viscous fluid. *The Quarterly Journal of Mechanics and Applied Mathematics* 19(4), 461.
- Riley, N. and E. H. Trinh (2001). Steady streaming in an oscillatory inviscid flow. *Physics of Fluids* 13(7), 1956.
- Rosato, A., K. Strandburg, F. Prinz, and R. H. Swendsen (1987). Why the Brazil Nuts Are on Top: Size Segregation of Particulate Matter by Shaking. *Physical review letters* 58(10), 1038–1040.
- Safford, K., Y. Kantor, M. Kardar, and A. Kudrolli (2009, June). Structure and dynamics of vibrated granular chains: Comparison to equilibrium polymers. *Physical Review E* 79(6), 061304.
- Sánchez, P., M. R. Swift, and P. King (2004, October). Stripe Formation in Granular Mixtures due to the Differential Influence of Drag. *Physical Review Letters* 93(18), 184302.
- Schlichting, F. (1932). The stability of the couette flow. *Annalen der Physik* 14(8), 905–936.
- Segur, J. (1951). Viscosity of glycerol and its aqueous solutions. *Industrial & Engineering Chemistry Research* 43(9), 2117–2120.
- Shattuck, M., R. Ingale, P. Reis, M. Nakagawa, and S. Luding (2009). Granular Thermodynamics. *AIP Conference Proceedings* 43(1), 43–50.
- Smith, A. J., M. Leaper, M. R. Swift, and P. King (2005, March). Traveling waves in a water-immersed binary granular system vibrated within an annular cell. *Physical Review E* 71(3), 031303.

- Snezhko, A., M. Belkin, I. Aranson, and W.-K. Kwok (2009, March). Self-Assembled Magnetic Surface Swimmers. *Physical Review Letters* 102(11), 118103.
- Sperl, M. (2005, December). Experiments on corn pressure in silo cells translation and comment of Janssen's paper from 1895. *Granular Matter* 8(2), 59–65.
- Swift, M. R., D. Klotsa, H. Wright, R. M. Bowley, P. King, M. Nakagawa, and S. Luding (2009). The Dynamics of Spheres in Oscillatory Fluid Flows. *AIP Conference Proceedings* 1039(1), 1039–1042.
- Tata, B., P. Rajamani, J. Chakrabarti, A. Nikolov, and D. Wasan (2000, April). Gas-liquid transition in a two-dimensional system of millimeter-sized like-charged metal balls. *Physical review letters* 84(16), 3626.
- Thomas, C. and J. Gollub (2004, December). Structures and chaotic fluctuations of granular clusters in a vibrated fluid layer. *Physical Review E* 70(6), 061305.
- Trejo Gonzalez, J. a., M. P. Longinotti, and H. R. Corti (2011, April). The Viscosity of GlycerolWater Mixtures Including the Supercooled Region. *Journal of Chemical & Engineering Data* 56(4), 1397–1406.
- van der Meer, D., K. van der Weele, and D. Lohse (2002, April). Sudden Collapse of a Granular Cluster. *Physical Review Letters* 88(17), 174302.
- van der Weele, K. (2007). Hysteretic clustering in granular gas. *EPL (Europhysics ...)* 328.
- Van der Weele, K. (2008, May). Granular gas dynamics: how Maxwell's demon rules in a non-equilibrium system. *Contemporary Physics* 49(3), 157–178.

- van der Weele, K., D. van der Meer, M. Versluis, and D. Lohse (2001). Hysteretic clustering in granular gas. *EPL (Europhysics Letters)* 53, 328.
- van Gerner, H. J., G. Caballero-Robledo, D. van der Meer, K. van der Weele, and M. van der Hoef (2009, July). Coarsening of Faraday Heaps: Experiment, Simulation, and Theory. *Physical Review Letters* 103(2), 028001.
- van Noije, T. P. C. and M. H. Ernst (1998). Velocity distributions in homogeneous granular fluids: the free and the heated case. *Granular Matter* 1, 57–64.
- van Noije, T. P. C., M. H. Ernst, E. Trizac, and I. Pagonabarraga (1999). Randomly driven granular fluids: Large-scale structure. *Physical Review E* 59(4), 4326–4341.
- van Zon, J. and F. MacKintosh (2004, July). Velocity Distributions in Dissipative Granular Gases. *Physical Review Letters* 93(3), 038001.
- van Zon, J. and F. MacKintosh (2005, November). Velocity distributions in dilute granular systems. *Physical Review E* 72(5), 051301.
- Viridi, S., M. Schmick, and M. Markus (2006, October). Experimental observations of oscillations and segregation in a binary granular mixture. *Physical Review E* 74(4), 041301.
- Visco, P., A. Puglisi, A. Barrat, F. van Wijland, and E. Trizac (2006, June). Energy fluctuations in vibrated and driven granular gases. *The European Physical Journal B* 51(3), 377–387.
- Voth, G., B. Bigger, M. Buckley, W. Losert, M. Brenner, H. Stone, and J. Gollub (2002, May). Ordered Clusters and Dynamical States of Particles in a Vibrated Fluid. *Physical Review Letters* 88(23), 234301.

- Wang, C.-Y. (1965, July). The flow field induced by an oscillating sphere. *Journal of Sound and Vibration* 2(3), 257–269.
- Welker, P. and S. McNamara (2009, June). What triggers failure in frictional granular assemblies? *Physical Review E* 79(6), 061305.
- Williams, D. R. M. and F. C. MacKintosh (1996, July). Driven granular media in one dimension: Correlations and equation of state. *Physical Review E* 54(1), R9–R12.
- Williams, J. (1976a). Continuous mixing of solids. A review. *Powder Technology* 15(2), 237–243.
- Williams, J. (1976b). The Segregation of Particulate Materials: A Review. *Powder Technol.* 15, 245–251.
- Wright, H., M. R. Swift, and P. King (2008, September). Migration of an asymmetric dimer in oscillatory fluid flow. *Physical Review E* 78(3), 036311.
- Wunenburger, R., V. Carrier, and Y. Garrabos (2002). Periodic order induced by horizontal vibrations in a two-dimensional assembly of heavy beads in water. *Physics of Fluids* 14(7), 2350.
- Wylie, J. J., Q. Zhang, H. Y. Xu, and X. X. Sun (2008, March). Drag-induced particle segregation with vibrating boundaries. *EPL (Europhysics Letters)* 81(5), 54001.
- Yan, X., Q. Shi, M. Hou, K. Lu, and C. Chan (2003, July). Effects of Air on the Segregation of Particles in a Shaken Granular Bed. *Physical Review Letters* 91(1), 014302.